THE STRUCTURE AND CONTROL
OF A
TURBULENT REATTACHING FLOW

Thesis by
Lorenz W. Sigurdson

In Partial Fulfillment
of the Requirements for the Degree of
Doctor of Philosophy

California Institute of Technology
Pasadena, California

1986
(Submitted 27 May 1986)

To Helga Julia Sigurdson, to the memory of Johann Straumford Sigurdson,
and to all members of my family

ACKNOWLEDGMENTS

I gratefully acknowledge the help of my advisor, Professor Anatol Roshko. His vast knowledge, broad point of view, and approach to conducting research have been enlightening. He suggested the initial research area and pointed the way to start in several instances. The patience and freedom of pursuit that he allowed me are appreciated.

Special thanks to Paul Schatzle for taking the time to listen to some of these ideas, and for being an excellent friend with whom to discover some of the more bizarre features of vortex motion, bizarre until understood. He was also an extremely helpful source of understanding and knowledge.

Thanks to Professor Tony Leonard for many useful discussions. Thanks to Professor Richard Feynman for inspirational conversation, books that encouraged a great deal of curiosity and excitement about life, and an approach to looking at nature at its simplest levels.

Thank you to my parents and all my family, especially my sister Sandra. In a situation that no one really understood, Sandra knew the most. Sometimes my family seemed the only reason to continue. Thanks as well to my extended family; you know who you are.

Thanks to Catherine Heising, Kathy Eriksen, Marcia Hudson and Jackie Beard for their secretarial help and friendship. Thanks to Clarence Hemphill, George Lundgren and Harry Hamaguchi for help with technical matters. Thanks to Greg Smedley, John Bruckner, Jim Cummings and Kiatt Chua for help in preparing some of the plots.

Financial support for this work was provided by the Office of Naval Research, contract number N00014-76-C-0260. The financial support by the California Institute of Technology is also gratefully acknowledged.

ABSTRACT

An unsteady and three-dimensional large-scale structure is proposed for the reattachment region of a separation bubble, based on a visualization study of the flow over a plate with a square leading edge and its axisymmetric counterpart, a flat-faced circular cylinder aligned coaxially with the free-stream. The initial free shear layer structures are primarily two-dimensional but evolve into boundary layer type structures as they near reattachment and interact with the wall. Some segments form "loops" which convect away from the wall and downstream, while spanwise adjacent parts convect toward the wall and upstream. The loops are sometimes clearly arranged in a staggered pattern. Their legs form a series of counter-rotating streamwise vortex pairs which bridge the reattachment zone. These observations reconcile apparently contradictory propositions concerning the fate of the structures as they encounter reattachment. The interaction between successive vortices at alternating spanwise locations is fundamental to several flows. The structure of turbulent wakes is also discussed.

An experimental study was made of the effect of a periodic velocity perturbation on the separation bubble downstream of the sharp-edged blunt face of a circular cylinder aligned coaxially with the free stream. Velocity fluctuations were produced with an acoustic driver located within the cylinder and a small circumferential gap located immediately downstream of the fixed separation line to allow communication with the external flow. The flow could be considerably modified when forced at frequencies lower than the initial Kelvin-Helmholtz frequencies of the free shear layer, and with associated vortex wavelengths comparable to the bubble height. Reattachment length, bubble height, pressure at separation, and average pressure on the face were all reduced. The effects on the large-scale structures were studied on flow photographs obtained by the smoke-wire technique. The

forcing increased the entrainment near the leading edge.

In both forced and unforced cases it was concluded that the final vortex of the shear layer before reattachment is an important element of the flow structure. There are two different instabilities involved, the Kelvin-Helmholtz instability of the free shear layer and the "shedding" type instability of the entire bubble. The latter results from an interaction with the image vortices due to the presence of the wall. A method of frequency scaling is proposed that correlates data for a variety of bubbles and supports an analogy with Karman vortex shedding.

New methods for approximating axisymmetric flows are presented. Transition of shear-layers and separation bubbles is also discussed.

TABLE OF CONTENTS

LIST OF FIGURES

LIST OF TABLES

LIST OF SYMBOLS

Symbol	Description
b	streamwise distance between vortices
C_{d_f}	coefficent of pressure drag on the face
C_p	coefficient of pressure
C_{p_s}	coefficent of pressure at separation
crit	critical
d	characteristic length
D	cylinder diameter
F	frequency
F_{ex}	frequency of excitation
F_{kh}	Kelvin-Helmholtz frequency
F_{kh_i}	initial Kelvin-Helmholtz frequency
F_{shed}	shedding frequency
h	bubble height or vertical spacing
hz	Hertz
H	shape factor
k	overshoot velocity = U_s/U_∞
l	eddy spacing
LIF	laser-induced-fluorescence
Re	Reynolds number
Re_D	Reynolds number based on D
St	Strouhal number = FD/U_∞
u'	rms velocity amplitude
U_c	convection velocity
U_∞	free-stream velocity
U_s	local velocity at separation
v	vertical velocity
v'	rms vertical velocity amplitude
X	downstream distance
X_r	reattachment location
Y	distance radially from cylinder surface
β	Falkner-Scan angle
δ	thickness
δ^*	displacement thickness

λ	wavelength
λ_{ex}	wavelength of forced structure
ν	kinematic viscosity
θ	momentum thickness

PART I UNFORCED REATTACHING FLOWS

Chapter 1
INTRODUCTION

Many incompressible flows can be thought of as a base potential flow with a superimposed distribution of line vortices. If the distribution of vorticity with time is known, then the kinematic qualities of the flow are known.

"It can be claimed that the problems of turbulence and transition are problems of the mechanics of vorticity, which is the fundamental dynamical quantity and constitutes the 'sinews and muscles of fluid motion'" (Saffman (1980), page 150).

The task of describing the motion of the vorticity is simplified by the recent observations of several researchers that it is often collected into large-scale structures (Roshko (1976)). These are essentially regions of concentrated vorticity. Saffman states that it is now proposed that turbulence be modelled as the creation, evolution, interaction and decay of these structures. It is supposed that each particular flow geometry will have a characteristic vortical structure. Its determination is not unlike the task in chemistry of determining the structure of a molecule once the constituent elements are known. With a few bits of knowledge about the behavior of the flow and use of the Biot-Savart law, much can be surmised.

How is one to go about discovering what the vortex dynamics are? Of several possible techniques, one of the most straightforward methods of obtaining FIELD measurements of the vortex trajectories is flow visualization. If the tracing dye is somehow placed in the cores of the vortices of interest early on in their evolution, then the motion of those vortex cores due to the convection of the cores can be observed. Following the dye trajectories cannot give much information about the viscous diffusion and perhaps resulting cancellation in the

case of interactions of opposite sign. In cases where this diffusion effect is small and the flow is dominated by convective transport of vorticity, the dye visualization can be quite informative.

In the following sections, on the basis of flow visualization, a characteristic three-dimensional vortex structure is proposed for the flow in the reattachment region of a separation bubble. (The term "region" is used, as opposed to the more commonly used term "point," because the actual reattachment occurs at an unsteady position, and the flow is quite three-dimensional.) The structure is shown to be consistent with results previously reported for this type of flow. The nature of the geometry is compared to other vortical flows. It has similarities to the structure observed in boundary layers. This is consistent with the observation that a reattaching flow is essentially a transition between a free shear layer and a boundary layer. Consequently, the free shear layer exhibits a largely two-dimensional structure, which changes to a three-dimensional boundary layer type structure as it nears the wall.

It is also used to hypothesize what may be occurring structurally in turbulent wakes, jets, vortex rings and possibly shear layers. Although these flows have marked differences, their similarities are stressed.

1.1. General Comments about Structure.

1.1.1. How High a Reynolds Number?.

One question that arises is "how high must the Reynolds number be to insure that the qualitative large-scale structure of the vorticity field is independent of an increase in Reynolds number?" Dimotakis et al. (1984) briefly address this question. For 2-D wakes, they point out the similarity in photographs of flows at Re = 10^8 and Re = 10^3. It is added here that the same qualitative vortex street structure exists down to a Re = 10^2. In each particular flow configuration the

question has to be addressed individually. One can consider some flow parameter (hopefully indicative of the large structure) and observe at what Reynolds number a constant value is reached. The qualitative structure of the large-scale vorticity field may be determined at a much lower Re than this. An example is the non-dimensional frequency of vortex shedding in the case of circular cylinder shedding.

The two-dimensional shear-layer vorticity is a simple example. The first instability that the laminar shear layer demonstrates as Re is increased, is a roll-up into discrete vortices. From Brown and Roshko (1971, 1974) it is clear that this discrete accumulation of vorticity is the basic structure of the fully turbulent case as well (although with higher order instabilities superimposed). Roshko (1976) points out that the large-scale processes and mean flow "seem to be very little affected by viscosity down to surprisingly small values of Reynolds number." The important effects "appear indirectly through the initial shear layer conditions and not through direct action of viscosity on the developing turbulent structure" (Roshko (1976), page 1354).

In the case of jets and wakes (Perry and Lim (1978); Perry, Lim and Chong (1980); Perry and Watmuff (1981) have carefully visualized and probed the characteristic structure. Although they studied at a Re of 350, the resultant smoke patterns are similar to those visualized by Taneda at a Re of 2.3×10^4. They concluded (Perry and Lim (1978)):

". . . many of these artificially produced structures have been observed in 'natural' situations even at Reynolds numbers well beyond the range used in the artificial flows." (In this case by "artificial" they are referring to their provision of a perturbation to "lock-in" the instability.)

Considering the validity of comparing water tunnel results of aircraft testing to what occurs at the much higher Reynolds numbers of full-scale flight, Erickson states:

"In general, at high angles of attack where large regions of separated flow exist (that is, when the flow field is vortex-dominated), the fundamental structure of the vortex flow field about wings and bodies is similar regardless of Reynolds number" (Erickson (1982), page 131).

The conclusion, for the general flow case, is that the Reynolds number at which the final Reynolds number independent structure qualitatively appears may be much lower than many researchers think. In the quest for each flow's structure, it would seem to be good investigative practice to study the Reynolds number regime where the flow first begins to be unstable, identify the large-scale motion, and then increase the Reynolds number until it is clear that the structure no longer changes qualitatively. The experimental results reported here were obtained with this in mind. When quantitative high Reynolds number data are desired, a good idea of the underlying structure will be quite helpful in designing the experiment.

1.1.2. Desirable Features of any Structure.

Desirable features of a proposed model of the vortex dynamics include the following:

1. a time-evolution description of how the vorticity got to its large-scale structure state from the geometry it was in when first created (as well as what that structure is);

2. a time-evolution description of how the structures change scale (if that is the nature of the flow, example: shear layer vortices pair, which allows growth of the shear-layer);

3. explanation of time-averaged results (an example: correlation results of Grant in the far wake of a cylinder suggested a pair of vortices, side by side, with axes approximately normal to the

plane of the wake. Roshko (1976) suggested that this may be due to a field of vortex loops);

4. agreement with flow visualization and any other observations;

5. agreement with conservation of momentum.

As an example, consider that if a point force is applied to the flow for a short time, a vortex ring must result, to represent the momentum that has been added to the flow. The ring must have its axis aligned with the direction that the force was applied. This is also true in the case of a continuous force on the flow. In that case, several rings may result, and only the axis direction averaged over all the rings must be consistent with the direction that the force was applied. The individual rings are not constrained so as always to be aligned with the direction of the force.

These features can be used as clues as to what the actual vortex structure is. Using the Biot-Savart law can give insight into items 1 and 2.

1.1.3. Basic Vortex Interactions.

In order to try to understand what sort of geometric evolution vorticity will exhibit, it is useful to consider a few basic interactions which are thought to occur. They can all be understood with the use of the Biot-Savart law, but once each is understood, they provide building blocks for understanding whole flows.

1. Vortex Pair of the Same Sign

They revolve around each other, which can be thought of as a vortex of twice the circulation.

2. Vortex Pair of Opposite Sign

If the diffusion time is much shorter than the convection time, cancellation can occur (in other words, at low Re).

More often, the Re is too high for much cancellation to occur, and the pair convects in a direction perpendicular to the pair. (Cancellation refers to the actual vorticity at a POINT being zero, as opposed to two strands of vorticity being in proximity and essentially appearing to the rest of the flow as if cancellation has occurred.) Convection has a chance to build a three-dimensional structure from an originally parallel pair of vortices. The result can be rings, due to the instability described by Crow (1970). This corresponds to a symmetric perturbation in the two cores. An asymmetric perturbation is also possible.

3. Loop in Free Space (far from any walls)

Swings up/down in a direction normal to the plane of the loop, depending on the sign of the vorticity.

4. Loop Near a Wall

Interacting with its image loop, and neglecting viscosity, the tip of the loop convects away from the wall, and the legs of the loop convect toward each other, or the tip convects toward the wall, and the legs convect away from each other (Willmarth (1975) (depending on the sign of the vorticity).

Chapter 2
EXPERIMENTS

2.1. Coaxial Cylinder.

2.1.1. Experimental Set-up.

Flow visualization experiments were performed in a low-speed water channel. Velocities were between 5 cm/s and 20 cm/s. Lucite models of various diameter were used, resulting in Reynolds numbers between 300 and 6300 (based on cylinder diameter). The flow configuration was that of coaxial flow about a circular cylinder with its axis aligned parallel to the flow direction. The end of the cylinder pointing into the flow was flat with a sharp corner. This insured separation would occur at the corner.

Cobalt dye was injected in two manners. In the first set of experiments, there were two dye ports on the face of the cylinder. They were placed diametrically opposite each other. In the second case, dye was injected along a circumferential slit immediately behind the separation point. The first configuration gave excellent side views of the flow, but not very much plan view information. (Figure I.2.1.1 is an example. This shows the initial onset of continuous instability of the bubble.) Later, it became clear that it was more desirable to have more plan view information, and the second technique was used.

35 mm still photographs were taken with a Pentax ME-Super camera, equipped with a Vivitar macro-zoom lens, using Tri-X and Ektachrome film. 16 mm movies were obtained with a Teledyne camera, using 4-X and Tri-X film and a Schneider 25 mm lens. In both cases, illumination was provided by back-lighting the flow with a bank of fluorescent lamps.

2.1.2. Results for the Laminar Bubble.

The bubble was observed to remain laminar up to Reynolds numbers of approximately 800. In this regime, the reattachment point (X_r) can be estimated from flow visualization photographs. When X_r/D is plotted against Reynolds number, a linear relation is seen to exist, Figure I.4.5.1. The backward facing step (Back and Roschke (1972)) and a forward facing blunt flat plate (Lane and Loehrke (1980)) also exhibit this linear relation. A simple argument assuming laminar growth is given in Back and Roshcke to explain why.

2.1.3. Mode I: Spanwise Phase Locked.

When the bubble first began to go unstable, it underwent periods of unsteadiness intermixed with the laminar behavior. With increasing Reynolds number the frequency of occurrence of unsteadiness increased until it was continuous at a Reynolds number of approximately 1100. It was observed that there was a certain Reynolds number range in which the instabilities formed in the separation bubble would apparently relaminarize downstream of the reattachment region. This implies that the Reynolds number (based on thickness) of the boundary layer was below the critical value. It is understandable that this can occur, since boundary layers have a higher critical Reynolds number than free shear flows. Above a Reynolds number of approximately 1000 it is felt that relaminarization no longer occurs. Much more careful experiments are needed to determine this. Similar relaminarization is observed in the wake of a circular cylinder, perhaps for the same reason (Cimbala (1984)). Presumably the wake Reynolds number is below the critical value (downstream), although the separated region immediately behind the cylinder is clearly unstable.

Figure I.2.3.1 illustrates the apparent quasi-periodic structure at a Reynolds number of 1097. Dye was injected on the cylinder face. It was clear that the shear layer vorticity was rolling up into large,

discrete vortices near the reattachment area. They then convected downstream. What is not as clear from the photograph is that the actual structure of this clump of vorticity is not axisymmetric, but actually in the shape of loops. It was not observed to be axisymmetric at any Reynolds number. Photographs of the same flow, but introducing dye through a circumferential slit, revealed the three-dimensional structure much better, Figure I.2.3.2. The qualitative shape of these loops is very similar to those visualized by Perry et al. (1981) in a perturbed boundary layer. The vortices were made more regular by oscillating a small rod in the flow. These vortices have long been of interest in boundary layers and have been given a variety of names. Here they will be referred to as "loops."

Figure I.2.3.3 provides plan and side views of the proposed vortical structure of the initial instability. The lines are representative of the regions of the highest concentration of vorticity, the "cores" of the structures. In actuality, the vorticity distribution is always changing due to diffusion, but it is not the intention to represent that in this figure. The plan view was constructed by taking the circumference of the cylinder and flattening it out for convenience. Two spanwise wavelengths are shown. At low Reynolds numbers it was surmised to be two for the entire circumference. (As far as the azimuthal periodicity is concerned, any integer would be satisfactory.) As the dye was injected only along a slit extending over one-half the circumference, even though the three-dimensionality quickly distributed it about the circumference, it was difficult to observe directly the structure on the far side of the model.

The figure illustrates what often occurred in the flow; however small modifications of this pattern also occurred. The sketch is an idealization to allow discussion of the vortex dynamics. Vortex 1 is the initial roll-up of the uniformly distributed vorticity in the shear layer into a discrete vortex. The plan view shows it undergoing a spanwise instability. This type of instability has been observed in

jets and in single vortex rings (Van Dyke (1982)). In the presence of a wall, the vortex dynamics are influenced by the no-slip condition and the necessity of image vortices to satisfy the zero normal velocity requirement. Willmarth (1975) reported that in two dimensions, a vortex pair near a wall will either convect toward each other and away from the wall, or away from each other and toward the wall. The direction is determined by the relative signs of the vorticity. This observation, along with consideration of what vortices preceding vortex 1 do, helps explain vortex 1's trajectory. The segments of vortex 1 which are farther downstream will have mutually induced velocities away from the wall. The pair of streamwise components of each segment convect toward each other. The segments of vortex 1 which are farther upstream have induced velocities toward the wall. The result is that the downstream segments find themselves in a faster moving region and get convected downstream, forming the loop vortices. The upstream segments become closer to the wall and get slowed down due to the no-slip condition. They go upstream, if they are caught upstream of the reattachment region. This is the configuration which vortex 2 represents. It is surmised that the streamwise portions of the segments convect away from each other, until a stable arrangement is reached. (Vortex 2 preceded vortex 1, and vortex 3 preceded vortices 2 and 3. Due to the periodicity, all phases of the dynamics can be surmised from this sketch.) Vortex 3 has been stretched out even farther, and in the side view its characteristic curl near the downstream tip of the loop can be seen.

Attention is drawn to the upstream traveling loops. They constitute a feedback to the initially rolling-up vortex 1. In the spanwise position (b) between the upstream loops, there is an induced velocity toward the wall. This draws part of vortex 1 toward the wall. Similarly, at positions (a) and (c) there is an induced velocity away from the wall, consequently convecting part of vortex 1 away from the wall. This provides an interaction which can sustain itself (above some critical Re) and also maintain a certain amount of steadiness of spanwise

phase. This gives insight as to why the first unsteadiness of the bubble comes in intermittent periods. Although it might be argued that these periods are tied to higher than normal periods of free-stream turbulence.

The steadiness of spanwise phase allows the streamwise vorticities from each vortex to line up and reinforce each other. The end view of Figure I.2.3.3 shows the streamwise vorticity. (In the sketch, vortex 2 and 3 are separate near the wall to allow distinction between them. It is thought that near the wall they merge.) Steadiness is important in order to be consistent with the flow visualization results obtained by Roshko and Thomke (1965). Their report indicates a surface flow pattern which suggests a number of streamwise vortex pairs passing right through the reattachment region. The oil flow visualization technique requires that their spanwise position must be steady over a reasonable length of time. This flow was a supersonic flow over a backstep. It is not proposed that the initial instability being discussed in this section is precisely what was occurring, but the features are similar. The higher order interaction described in the next section may be more applicable.

The upstream travelling loop's tip consists of vorticity of the opposite sign to that which is being generated at the wall. At low Reynolds number, some cancellation may occur. This is why the spanwise component of vorticity at the tip was not discussed as an important feature in the preceding paragraphs. This will not be the case in the next section.

A few last words about this section, which also have relevance to the following section. The suggested vortex dynamics are proposed to occur much of the time. However, the flow may also display some of the features described in the next section, even at the same Reynolds number. Also, the upstream travelling loop may continue downstream, instead of always being swept upstream. The relative scales in the

sketches are not necessarily accurate. Surface flow visualization has not been done in this flow configuration (to the author's knowledge) and is suggested as a method of confirming the structure proposed here. This is quite important, since the flow structure near the wall is largely surmised.

2.1.4. Mode II: Spanwise Phase Offset by π.

When the Reynolds number was increased, the nature of the instability changed slightly. Figures I.2.4.1 and I.2.4.2 (Re_D=2750) are prints made by enlarging the color slides. The dye consequently appears darker than the surroundings. Figure I.2.4.2 appears to be at a slightly later phase than Figure I.2.4.2. The initial wavy appearance of the first roll-up is quite clear in Figure I.2.4.2. A close look at the next vortex downstream indicates that the azimuthal wave on it is approximately half a wave-length out of phase with the upstream vortex. This observation is the crux of the proposed vortex structures to follow, a key to unlock several turbulent flow structures. In the next instant, the upstream segment of the vortex will pair with the downstream segment of the upstream vortex. This is shown in Figure I.2.4.2. The resulting vortex segment will convect downstream as a loop. The adjacent segments of the upstream vortex will follow shortly as loops, and then the cycle repeats. The fate of the vortex segments between these two loops will be discussed shortly.

Figure I.2.4.3 is an idealized sketch of the resulting vortex structure for this type of interaction. Patience is requested of the reader in interpreting this figure. The essential features of the structure are the same as those in the mode I interaction, Figure I.2.3.3. The major difference is that as a result of the spanwise half-wave phase shift, the wavelength of the periodicity in the streamwise direction (λ_{st}) has doubled. Note that this has been achieved with no change in the frequency of the initial vortex roll-up. It is simply a result of the pairing nature of the mode II instability.

There are still only two spanwise loops at any streamwise location, but if they catch up to each other, it can appear that there are actually four. The number of streamwise vortex pairs at the wall jump from two to four. The number of "streaks" consequently jumps from four to eight. Where vortices of the same sign are close together, they have been sketched individually in order to allow distinction of their origin. The hypothesis is that they merge.

The feedback that maintains the instability is stronger in this case than in the mode I interaction. The upstream travelling segments of vortex 3 at positions (b) and (c) do not remain close to the wall but pair with the vortex above them, vortex 2. (Once again, the number of the vortex can be thought of as an indication of the "age" of the vortex.) The reason for this qualitative change in behavior might be explained by the following observations. As the velocity increases, the approximate streamwise wavelength of the resulting vortex near the reattachment region is approximately the same. Therefore, its circulation is increasing linearly with velocity. This leads to stronger induced velocities between the vortices. Also, the viscous region near the wall becomes thinner and less likely to cancel the circulation of the upstream travelling loop.

As in the mode I interaction, the segments of the vortices which are joining the loops get strained into streamwise vorticity. The spanwise steadiness allows the streamwise vorticity to line up and reinforce each other, resulting in a steady spanwise pattern of vortex pairs close to the wall and passing across the reattachment region. Once again, the loops occur over areas where the streamwise vortices are inducing an upward velocity (spanwise positions a, b and c). The "streaks" may extend farther upstream than sketched. Mode II is more likely to describe the events occurring in the backstep flow of Roshko and Thomke (1965) discussed earlier. The streaks observed by Gai and Sharma (1984) in the reattachment zone behind a backward-facing step may also be explained this way. The cross-sectional view shows the

streamwise vortices near the wall. Where vortices of the same sign are close together, they have been sketched individually in order to allow distinction of their origin. In actuality, they can be thought of as one vortex with twice the circulation of the individual vortices.

As mentioned in the previous section, the structure near the wall is largely surmised (from consideration of the induced velocities of the outer observed structure). However, if the streamwise vortices do not come as close to the wall as supposed, they may actually convect downstream. Surface flow visualization would be valuable in clarifying this.

2.1.5. Higher Reynolds Numbers.

On the basis of movies at Reynolds numbers of 22,000, and the photographs shown in Figure I.2.5.1, it is felt that the loop is an integral part of the Reynolds number independent flow. Figure I.2.5.1 depicts the flow at a Reynolds number of 6300. The dye patterns strongly suggest the presence of loops. The dye in Figure I.2.5.1 a is injected at one point on the face, and yellow dye is injected upstream. In Figure I.2.5.1b yellow dye is injected upstream of the model, and blue dye is injected near the time averaged reattachment region from a small port in the wall.

How high must the Reynolds number be before the observed structure is qualitatively the final one? In this case, a look at the C_{p_s} (coefficient of pressure at the separation point) and time averaged reattachment distance (X_r/D) versus Reynolds number would be useful. Both reach a constant value above a Reynolds number of approximately 6000. This would imply that the structure of the flow does not vary much above that Reynolds number. It must reach the same qualitative structure at Reynolds numbers somewhere below 6000.

2.2. Blunt Flat Plate.

2.2.1. Introduction.

The flow over a blunt flat plate was investigated. It is the two-dimensional counterpart of the blunt-faced cylinder aligned with the free-stream. This was to allow better visualization of the loop structures previously seen on the cylinder, emerging from the reattachment zone. It was also to test the hypothesis that the existence of the azimuthal instability in the coaxial case is not a result of the axisymmetry, but would also occur when the geometry of the boundaries was two-dimensional rather than axisymmetric. This hypothesis was confirmed.

Still photography and a video cassette recording system were used to acquire data. Dye was introduced along a slit immediately behind the separation line. Back-lit cobalt blue dye gave a good indication of the overall geometry of the structure. Fluorescein dye was illuminated with a sheet of laser light in two ways: parallel to the wall and perpindicular to both the wall and the free-stream.

2.2.2. Confirmation of Three-dimensional Structure.

The loops seen in the coaxial case were observed to also occur in the flow over the plate geometry. At the first stages of transition in the bubble, the loops were often arranged in a staggered pattern, as shown in the reproductions of two video frames in figure I.2.2.2.1 (flow is right to left) or the 35 mm photograph in figure I.2.2.2.2 (flow is bottom to top). At higher Reynolds numbers, this pattern became more chaotic, but is certainly not primarily two-dimensional as the free shear layer is considered. Dye motion released from the wall at the reattachment zone indicates a series of streamwise counter-rotating vortex pairs passing through the reattachment zone near the wall. These were predicted by the vortex structure model suggested for the coaxial case.

2.2.2.1 Cobalt Blue Dye Results.

Photographs were taken with blue dye intoduced from a slit located upstream (X/D=5.0) of the reattachment region (X/D=6.1). This was to confirm the hypothesis of a series of streamwise counter-rotating vortex pairs passing through the reattachment zone. Figure 2.2.2.1.1 is a photograph that was taken shortly after the dye was introduced. The accumulation of dye into streaks is consistent with the hypothesis. Figure 2.2.2.1.2 is a photograph taken approximately one shedding cycle later. It is included to show that the spanwise position of these streaks is not rapidly varying. The suggested feedback in the instability keeps them occurring very close to the same location from cycle to cycle.

The wavelength was estimated from these photos to be $\lambda_{sp}/D=1$, which compares well with the measured wavelength from the sectional views discussed in the next section. This supports the vortex model's connection between these streaks and the loop structures observed downstream of reattachment.

2.2.2.2 Laser Induced Fluorescence Results.

X_r/D was measured at a Reynolds number based on plate thickness (Re_D) of 852. It was determined by observing the direction of the motion of the dye in the video-taped images, and choosing the time-averaged location where the direction of travel changed sign, some dye going upstream, and some downstream. It was determined to have a value of 6.1. This concurred with the location estimated from the LIF still photographs, of which Figure 2.2.2.2.1 is an example. These are two new methods of locating the reattachment region.

The spanwise wavelength (λ_{sp}/D) was estimated by counting the number of streamwise vortex pairs in Figures 2.2.2.2.2 and 2.2.2.2.3. At the downstream locations X/D = 8.3 and 16.6, λ_{sp}/D was 1.2 and 2.3,

respectively. At X/D = 8.3, this compares well to the value of λ_{sp}/D = 1.0 measured in the previous section. As stated then, this confirms the connection between the streamwise vortices passing through the reattachment zone, and the loops.

Clearly, an amalgamation of the loop structures emerging from the reattachment region had occurred by X/D = 16.6 . An amalgamation resulting in approximately double the λ_{sp}/D as compared to X/D = 8.3 . It should be noted that the larger scale stuctures appeared to be composed of three or more of the original streamwise vortex pairs. If the structure of the flow remains self-similar in a staggered pattern, a doubling of scale means a QUADRUPLING of the previous structures. The plan view in Figure 2.2.2.2.4 suggests that this is what happens. The λ_{st} clearly increases with X, and approximately doubles between X/D = 8.3 and 16.6. The structures in the figure have a diagonal symmetry, making a 45 degree angle with the free-stream direction. The photograph indcates a continuous transition of scale with increasing distance downstream.

2.2.2.3 LIF Upstream Views.

Videos looking upstream at a spanwise laser sheet indicate that spanwise coherence exists in the sense that the loops tend to come through the plane all at the same time. This is followed by a gap of only dye near the wall, and then the next set of loops coming through. It is the spanwise location of the loops that changes from one set to the next.

Chapter 3
DISCUSSION

3.1. The Controversy in the Back-step Flow Case.

The flow over a backward-facing step has many similarities to the forward-facing case. They both have definite separation lines and reattach onto a flat wall. The major differences are that the initial shear-layer is strongly curved in the forward-facing case, and the boundary layer at separation is generally much thinner.

Eaton and Johnston (1981) review the research on subsonic turbulent reattachment. They point out that there exists a controversy concerning what happens to the large vortices as they near the reattachment region (they refer to them as "eddies"). The fate of these is thought to be important to explain the decay of turbulent stresses in the reattachment region.

"Perhaps the most poorly understood part of a reattaching flow is the rapid decrease of the Reynolds stresses in the reattachment zone. A correct understanding of this decrease is necessary in order to correctly predict the redevelopment of the downstream boundary layer" (Eaton and Johnston (1981), page 1099). The conclusions of previous researchers will be discussed in the following paragraphs.

Bradshaw and Wong (1972) define the larger eddies as bodies of fluid whose dimension in each direction is at least as large as the correlation length scale. They conclude:

"Since the dividing streamline is not too far from the line of maximum shear stress or turbulence intensity in the shear layer prior to reattachment, the large eddies that extend over most of the flow and

produce much of the shear stress are roughly torn in two. The result is a rapid decrease in turbulent shear stress and there is strong indirect evidence that the turbulent length scales also decrease markedly" (Bradshaw and Wong (1972), page 134).

Chandrsuda and Bradshaw (1982) measured second- and third-order mean products of velocity fluctuations. They noted that rapid changes in turbulence quantities occur in the reattachment region. They report that the intermittency does not behave as would be expected if large eddies moved alternately upstream and downstream at reattachment. They also maintain that reversals of slow moving flow near the surface (as observed by Kim, Kline and Johnston (1978) using tufts) are not incompatible with splitting, rather than alternation, of large eddies as suggested by Bradshaw and Wong.

Kim et al. (1978) concluded that the unsteady movements of tufts and the structure of d/dt(u'v') downstream of reattachment support the hypothesis of alternating eddies. Also "it is unlikely that the splitting is the only phenomenon that takes place at reattachment" (Kim et al., page 308). McGuiness (1978) studied the structure behind an orifice at the entrance to a pipe. The techniques used included spectral analysis of the velocity and wall static pressure, as well as flow visualization. He tentatively concluded that some of the eddies went downstream and some upstream.

Eaton and Johnston (1981) reported that in crude flow visualization experiments of their own, there was no evidence of large eddies going upstream.

These observations seem to cover all the possibilities:

1. eddies are split,

2. eddies alternately go upstream and downstream (or at least some go each way),

3. eddies all go downstream,

4. eddies all go upstream (the one exception).

Assuming that these flows are similar to the forward-facing Assuming in the reattachment region, the vortex structure described in previous sections is quite useful. The vortices are in a sense "split," since a portion of a vortex goes downstream, but a portion of the same vortex goes upstream. In the mode II instability, at a fixed spanwise location (such as position a in Figure I.2.4.3), it would be observed that alternate vortex segments head upstream and downstream, providing that this was done very carefully, since the upstream travelling segment convects toward the wall and is difficult to observe. The downstream travelling vortex segments are much easier to observe since they convect away from the wall, and because they have probably paired with another segment, making them larger. This is perhaps why Eaton et al. (1981) observed only downstream travelling eddies.

The terminology should be clarified here. In previous sections, the term vortex is used to describe an accumulation of vortex lines. If the term eddy refers to the resulting largest scale vortex in the reattachment region, then in the mode II interaction it might be concluded that all the eddies go downstream. If the term eddy includes the groups of vortex lines which go upstream at reattachment, then it would be concluded in the mode II case that the eddies go alternately upstream and downstream.

Regardless of the terminology, it is proposed that the vortex structure described in the mode II case explains how the apparently contradictory conclusions discussed above can be reconciled.

Chapter 4
THEORETICAL CONSIDERATIONS

4.1. Introduction.

In order to calculate the boundary layer quantities on the face of the cylinder using Thwaite's method, a velocity distribution as a function of radial position is necessary. This distribution can be inferred through the pressure measurements on the face made by Koenig at a high Reynold's number. However, to estimate the boundary layer quantities at lower Re or with the separation bubble manipulated by excitation, this distribution will not be accurate. Under these conditions, the pressure at separation, as well as the shape of the separation bubble, is different. In two dimensions, the notched hodograph theory (Roshko (1954)) allows an approximation of the velocity about a plate normal to the flow as a function of the pressure at separation, C_{p_s}. This can be converted to a velocity overshoot parameter $k = Us/U_\infty$. This section discusses an effort to use the notched hodograph to approximate the axisymmetric flow as a function of C_{p_s}.

4.2. The Transformation.

On page 54 of Koenig (1978) he describes a skillful argument by Roshko, which relates C_{p_s} to the ratio of bubble diameter maxima (D2) to the cylinder diameter (D1). This argument is also described in Koenig and Roshko (1985). Conversely, if C_{p_s} is given, D2/D1 can be found. This reasoning is the basis for the procedure, with a modification made to account for the blockage: in the force balance the non-zero drag on a semi-infinite body with blockage is used. (The argument holds exactly only for inviscid flow, where the only forces involved are pressure forces. In the real flow, there are also shear forces. This changes the argument in two ways; the drag on the semi-infinite

body is no longer known, and neither are the forces on the free-streamline. Consequently, the higher the shear stresses in the flow, the less accurate the theory is likely to become.) Note that it is unrealistic to directly use the axisymmetric k in the hodograph equations. The hodograph results may also be compared in the shape of the separating streamline, as in figures I.4.2.2.1, I.4.2.2.2 and II.4.4.2. Ota has measured the time-averaged streamlines in the bubble for both two-dimensional and axisymmetric flows. Using the respective C_{p_s} measured by Ota, the associated free streamlines were plotted to compare with the measured time-averaged streamlines. The two-dimensional results compare well. The axisymmetric bubble reaches its maximum height much sooner and is much smaller all around, compared to that calculated. These are the steps in the procedure:

1. Calculate the diameter ratio from the measured C_{p_s}.

2. Calculate what two-dimensional C_{p_s} in the notched hodograph would result in this diameter ratio.

3. Use this two-dimensional C_{p_s} to calculate the velocity distribution from the hodograph.

4. Normalize this velocity distribution to give the necessary C_{p_s}.

The idea is quite simple. Once the diameter ratio is known, choose the two-dimensional flow that gives that shape of bubble. Then use the shape of the resulting velocity distribution as the shape for the desired axisymmetric flow, by normalizing it. Consider the velocity distributions on the surface of some well known bodies in potential flow:

1. Both the circular cylinder and the sphere have a cosine distribution of tangential velocity. They differ only in amplitude. Application of the approach outlined above would yield a perfect comparison.

2. The flow about both a wedge and a conical body have a power of x velocity distribution. As an example, for a half-angle = 90 degrees, velocity is proportional to x to the first power, for both wedge and cone. For other angles the similarity is close but not exact.

A comparison of this technique for velocity calculation with the measured distribution of Koenig (1978) is shown in figure I.4.2.2.3.

4.3. The Boundary Layer on the Face.

The axisymmetric Thwaites method (White (1974)) can be used to calculate the boundary layer on the face. The velocity distibution input into the method is the one developed in the previous section. The results are shown in figures I.4.3.1 and I.4.3.2. The conclusion is that the thickness becomes very small at separation.

The Motives for Doing the Calculations:

1. Knowledge of θ at the separation point is desirable in order to estimate the most unstable wavelength of the free shear layer. (It turns out that the estimation is often more difficult since the shear layer is not immediately unstable at low Reynolds numbers.) This is necessary to compare experimentally observed wavelengths and also to know what frequencies of excitation the shear layer will amplify.

2. The local Reynolds number based on thickness at separation is important to whether or not the shear layer will be immediately unstable. Ko and Lessen (1969) have calculated the critical Reynolds number for the free shear layer. To this author's knowledge, this result has never been experimentally verified. Regardless of the comparison, the growth of the boundary layer and shear layer along the free streamline is important to understanding the problem of critical Reynolds number. The boundary layer thickness at separation is needed to estimate the virtual origin of the laminar shear layer. This allows approximation of the growth of the layer using the computed solutions of Lock (1951).

3. Knowledge of the development of the boundary layer is necessary to determine its stability characteristics, in particular, whether, it becomes turbulent before reaching the separation point.

4.3.1. Stability of the Boundary Layer.

Once the shape factor (H) is known from the Thwaites calculation, the equivalent Falkner-Skan included angle (β) can be found from Smith (1954). He provides a table correlating the two. The minimum in Thwaites' table is an H = 2, and the minimum in Smith's table is H = 2.155, corresponding to β = 2. The calculation exceeds the limit of Thwaites' table at separation, therefore H is less than two there. The maximum β is 2 however, which corresponds to an infinite exponent (M), where $U(x) = c\ x^M$ is the external velocity field. (The flow is one going in and out of an infinitely thin slit.) The wisdom of comparing the boundary layer to a Falkner-Skan equivalent is consequently suspect.

The stability calculations of Wazzan, Okamura and Smith found in White (1974) page 405, provide a $Re_{\theta_{crit}} = 5{,}636$ for $\beta = 1$. With the knowledge that the $Re_\theta/Re_\delta^{1/2} = .0713$ at the separation point, this means that the Re_δ must be greater than six billion

for any instability to occur. This is a lower limit. Consequently, the boundary layer is most certainly laminar for the experimental magnitudes of Re_δ reported here.

For comparison, it is interesting to note that the Blasius boundary layer has a critical Reynolds number based on displacement thickness (Re^*_δ) of 520. The critical Reynolds number based on momentum thickness (Re_θ)) is 201. As the shear layer is in general more unstable than the boundary layer, it might be expected that the associated critical values are less.

The boundary layer has a critical Re^*_δ of 520 from stability analysis, but the actual value for transition to turbulence in a low external disturbance flow over a flat plate does not occur until Re^*_δ approaches 2900 (White, 1974). This is a six-fold increase in the critical value. Estimates from shear layer experiments suggest a critical Re_θ of 49 (at most). Ko and Lessen (1969) calculate a critical Reynolds number based on $\delta = \sqrt{(\nu\ x/U)}$ of 10.2. θ is approximately 1.147 times δ; therefore, this corresponds to a critical Re_θ of 11.7 . The experimentally estimated critical Re_θ is 4.18 times this value.

4.4. Free Shear Layer Transition.

4.4.1. Overview.

Previous calculations allow estimation of the separated-shear-layer growth up to the location of transition. Figures 4.4.1 and 4.4.2 show the normalized results for laminar growth. (The position is measured from the stagnation point on the face.) The Mangler transform is used to account for the axisymmetry. Coupled with stability theory, the results indicate that the boundary-layer and the shear-layer at separation are stable up to a surprisingly high Re_D. This is due to the extremely favorable pressure gradient upstream of separation.

4.4.2. Mangler Transformation.

Mangler found a transformation that transforms the axisymmetric boundary layer equations into the two-dimensional boundary layer equations. These equations apply to thin shear layers as well; only the boundary conditions are different. The transformation provides an easy way to calculate the shear layer discussed here, because it has an approximately constant external velocity. Consequently, the axisymmetric shear-layer maps into a two-dimensional free shear layer with constant external velocity. This 2-D flow has been calculated by Lock. The crucial requirement for the success of this approach is the constant external velocity. If this was not the case, one would have to solve the problem of a two-dimensional layer in a pressure gradient, which has not been done to this author's knowledge. There is not an equivalent method to the Thwaites method for laminar boundary layer growth in an arbitrary pressure gradient.

4.4.2.1 The Transformation and Its Inverse.

1. The radius used in the calculation is generated using free-streamline theory. It is therefore an approximation but has been verified to be a good one. It represents not the dividing streamline of the shear layer, but the dividing streamline with an added displacement thickness. This is because the free streamline is an inviscid result.

   For this calculation, it is assumed that the displacement thickness is a negligible addition to the radius.

2. This calculation is expected to overestimate the momentum thickness. The actual shear layer does not have the low speed side with zero velocity, but probably an initially zero velocity, increasing along the shear layer. Therefore, the velocity difference across the layer decreases, and the growth rate is reduced.

For more advanced modelling, the flow inside might be modelled as the flow inside a wedge.

3. The use of the axisymmetric boundary layer equations assumes that $\delta^* << R$.

This puts a minimum limit on the Reynolds number for which this calculation is valid.

4. The free-streamline shape varies with Reynolds number for Reynolds numbers based on diameter less than roughly 5000. This calculation was done for the resulting final shape at higher Reynolds numbers, corresponding to k = 1.265. Applicability to lower Reynolds numbers depends on how close the shape compares to this one.

5. Consideration of a small axisymmetric volume element suggests that:

$$\frac{\delta^*_{actual}}{\delta^*_{2\text{-}D}} = \frac{Ro}{Ro + \delta R} \quad ,$$

where Ro is the radius of the cylinder. The maximum delta R is the bubble height, roughly .5 Ro. Therefore, one would expect that the shear-layer thickness to be roughly sixty-six percent as thick as 2-D theory predicts. However, while the continuity requirement narrows down, the shear-layer the resulting increased velocity gradient enhances the diffusion of vorticity. The result is a smaller reduction in the thickness. (Note: this result comes from consideration of a small area element dxdy. U(s) is constant along the layer, so that dx is expected to remain unchanged. Thus Dy must become smaller to conserve the volume of the ring element, $2*\pi*R * dx * dy$.)

6. The virtual origin is virtually zero, for growth of the shear-layer.

4.5. Bubble Transition.

For the shear-layer, experimentally observed transition locations appear to be consistent with the stability theory. In particular, $X_{tr}/D = 2000Re_D^{-1}$ is an estimate of the transition distance (X_{tr}) as a function of diameter (D) and Reynolds number based on diameter (Re_D); this is obtained from photographs. This relation also predicts the transition from a wholly laminar separation bubble to a turbulent one for both the axisymmetric and the two-dimensional blunt flat plate (Figure 4.5.1). If the reattachment distance is less than this X_{tr}, the bubble remains laminar, otherwise the bubble becomes turbulent. Thus, the initial instability of the bubble has transition characteristics similar to those of the free-shear-layer.

Chapter 5
DISCUSSION

5.1. 'Explanation' of the Instability.

5.1.1. Introduction.

In order to describe what fluid with a particular set of boundary conditions will do, there are several mathematical approaches There are also many levels of explanation. The first is to set up the problem rigorously and attempt to find a solution, or approximate a solution using numerical methods. Even if the solution may be found, which is rare if not unheard of in turbulence problems, this approach still requires a careful interpretation of the result to make sense of them. Having the solution is not enough. If it is understanding the researcher is after, he must try to get a heuristic "feel" for what causes this behavior that the solution dictates. As an example, we could consider the Kelvin-Helmholtz instability. When the linearized problem of the interface of two streams is considered, the solution indicates an exponentially growing wave at the interface. This instability is understood by considering that, should an infinitesimal wave initially exist at the interface, the peaks will grow since the pressure as dictated by Bernoulli's Theorem will be lower on the convex side than on the concave side of the interface, as a result of the higher velocity one expects on the convex side. But does this explain periodicity? This "ad hoc" "explanation" involves taking two concepts previously understood which together help in understanding the driving forces for the instability. These are the idea that flow speeds up near obstructions (continuity equation) and that pressure drops when flow speeds up (momentum equation).

The second approach is to formulate the problem as in the first approach but to make simplifying assumptions which allow easier solution. Once the solution is found however, the problem of interpretation still remains. Examples of this include the boundary layer equations and von Karman's discrete vortex modelling of the vortex street behind a cylinder.

The third approach is that employed often in the field of turbulence. The equations are too complex to solve, so the only understanding which can be obtained is an ad hoc pasting together of previously understood fluid behavior. This is coupled with numerous empirical investigations, which usually come first, to be closely followed by the ad hoc explanation.

The other possibility is that empirical laws may be formed for which there is no good understanding whatsoever. An example is the logarithmic law for turbulent boundary layers.

The thing about ad hoc explanations is that they are not unique. One person's explanation may be quite different from, but just as good as, someone else's.

One of the most outstanding problems of present-day turbulence is vortex shedding behind a cylinder. The steady, laminar wake profile has been analyzed for instabilities, but how the instability actually works immediately behind the cylinder is a mystery. In the following text an ad hoc explanation of cylinder shedding and the unsteady separated flow over a two-dimensional semi-infinite slab will be dis-

cussed.

5.1.2. Outline of Explanation. The basic concepts to be used in the argument are:

1. large scale vortices in free shear layers convect with a velocity (a celerity) of approximately the average of the upper and lower irrotational streams.

2. in boundary layers these structures tend to move at approximately eighty percent of the free-stream velocity. (These could perhaps be thought of as structures in free shear layers with a nonzero velocity stream between them and the wall.)

3. when structures find themselves in a situation where their celerity is decreasing with distance (negative celerity gradient), they merge.

4. when structures find themselves in a positive celerity gradient, they are stable and maintain their identity.

The structures in the free-shear-layer near separation initially have a positive celerity gradient because the recirculating flow beneath them is speeding up with increasing distance downstream. As the structures continue downstream the velocity beneath them decreases as the flow is actually reversed there as the structures encounter the reattachment zone. This results in a decreasing celerity with increasing X, or a negative celerity gradient. This is put forth as an explanation of why the vortices merge to form a characteristic final structure in the reattachment zone.

In the unsteady case, the Biot-Savart law would give an indication of the induced velocities experienced by the various structures. A structure in the reattachment zone will begin to speed up downstream,

while its induced velocity on upstream vortices will cause them to encounter a negative celerity gradient and begin to pair to form another characteristic final structure, and so on in a periodic manner. The same kind of explanation could be applied to Karman vortex shedding.

5.1.3. Free Shear Layer Approach.

Brown and Roshko (1974) have found the distribution of eddy spacings in a two-dimensional shear layer to be $l/X = 0.31$ where l is the spacing between the eddies, and X is the distance downstream from the apparent origin of the mixing layer. The frequency of formation of these eddies is then $F = U_c/l$ where U_c is the convective velocity, which is equal to the average of the two velocities on either side of the shear layer. For axisymmetric flow over a cylinder,

$$U_s = U_\infty(1 - C_p)^{1/2},$$

where C_p is approximately -0.7 as found by Ota (1975). Setting $U_c = U_s/2$, one gets for the frequency

$$F = \frac{(1/2)U_s}{0.31X} = 2.2\,\frac{U_\infty}{X}.$$

For a reattachment distance of $X/D = 1.6$, the frequency has the form $FD/U = 1.4$. This number gives an indication of the "shedding" frequency discussed in Part II.

5.2. Ubiquity of Structure.

5.2.1. Introduction.

Some of the research into flows containing three-dimensional structures was reviewed and compared to the present results. Perry et al. (1981) proposed a similar geometry to the mode II interaction, but for the generation of turbulent spots (Perry's paper was found after

the present Mode II was proposed). Savas (1979) found an apparent "preference" for a staggered array of spots in the boundary layer. A figure from Batill and Mueller (1981) indicates that the separation bubble on a wing may have a mode II interaction at work, although it was not mentioned. A possible evolution to a three-dimensional structure in the far wake of cylinders is provided by the mode II idea.

The idea of interaction between successive vortices at alternating spanwise locations is thought to be fundamental to a wide variety of large-scale structures.

5.2.2. Turbulent Boundary Layer.

In the turbulent boundary layer literature there exists some controversy regarding the origin of the streamwise vorticity near the wall (the "streaks"). It is noted that in this case of a reattaching flow, the origin of the streaks appearing in the boundary layer downstream of reattachment is clearly accounted for by the vorticity coming from the separation point.

5.2.3. Wakes of Finite Axisymmetric Bodies.

5.2.3.1 Structure. Figure I.5.2.2.1.1 depicts an idealization of the wake of an axisymmetric body ascertained by Perry et al. (1980). This basic structure is in agreement with Taneda (1978) but not with Achenbach (1974)(this discrepancy will be discussed later, Section 5.2.3.2). Perry's original figure illustrates where smoke, initially placed in the entire wake, eventually ends up. The more important question is:" Where is the vorticity ?". Figure I.5.2.2.1.1 is meant to illustrate where the highest concentrations are. It is seen that the wake can be idealized as an interconnected chain of vortex rings, inclined to the free stream and with self-induced convection velocities in the upstream direction.

The evolution of this type of structure can be understood with the observation that it is basically a mode II interaction. However, interaction is at only one azimuthal position, as opposed to several as discussed earlier. In more straightforward terms, it might be useful to observe that this pattern of rings is qualitatively the same one that an aircraft would make while undergoing a maneuver of alternately climbing and diving, due to the alternating sign of the tip vortices as the lift on the wing changes sign. Similarly, armed with the knowledge that there is an oscillating lift on the sphere, one could deduce the ring structure of the sphere wake.

In the two sectional views provided in Figure I.5.2.2.1.1, it is seen that there is a symmetric as well as an asymmetric aspect to the proposed structure. There are two spacing ratios necessary to describe the geometry of the structure, h/b and hs/bs, referring to the asymmetric and symmetric aspects, respectively. In a similar manner to the 2-d wake, it might be thought that there are preferred values for these ratios. They might be deduced using a stability analysis as employed by Von Karman and Rubach (1912), but for a chain of rings instead of point vortices. The ratio of h/b can be estimated from the photographs of Perry et al. (1978) to be roughly .5 for wakes and .6 for jets, hs/bs is not shown clearly. This is considerably higher than the h/b = .28 usually associated with 2-d wakes.

5.2.3.2 Sensitivity of Azimuthal Phase. Perry et al. (1978) found that the structure of the wakes and jets was quite strongly influenced by buoyancy; asymmetries in the vertical direction were quite pronounced. It is suggested that the sketch of the sphere wake deduced by Achenbach from dye flow visualization indicates that negative buoyancy of the dye was a factor.

It is proposed that asymmetries in tunnel blockage are a factor in the azimuthal phase of the rings. In a totally unblocked flow, the orientation of the chain of rings is expected to change slowly in time.

However, if there are asymmetries in the boundary conditions, they might lock the structures into a preferred orientation. Taneda's (1978) experiments were conducted with a 33 cm sphere in a wind tunnel section which was 200cm high and 400 cm wide. The overall blockage is quite low, but the blockage in the side-to-side direction was much lower than in the up-and-down direction. It is suggested that this locked the large side-to-side motion into the diagonal direction of the tunnel, where blockage was the least.

A similar effect may be at work in the case of shedding behind a sphere in a stratified flow. Up-and-down motion is suppressed, and the dye visualization indicates a staggered vortex street in the horizontal plane (Tritton (1977), page 187). This visualization suggests that the rings are being shed with their side-to-side motion locked in the horizontal plane.

5.2.4. Wakes of Two Dimensional Cylinders.

5.2.4.1 Comparison to the 2-D Blunt Flat Plate. The blunt flat plate has an instability similar to vortex shedding behind a cylinder. Hints of this instability are provided in the results of Parker and Welsh, Welsh and Gibson (1979), Lane and Loehrke (1980), and Kiya, Sasaki and Arie (1982). The present results for the axisymmetric case discuss the instability in detail. The deviation of the structure from that found behind a cylinder is due to the no-slip and zero normal velocity conditions at the wall.

When the vortex dynamics of the problem is considered a system of image vortices is required to satisfy the zero normal velocity condition on the wall. Satisfying the no-slip condition requires another system of vortices nearer the wall, and their associated images, but are not important to this particular discussion and will be neglected. Together with their images, the vortices form a symmetric vortex street, Figure I.5.2.3.1.1 . The cylinder wake is free to be either symmetric or asymmetric, but the asymmetric mode is usually the one

observed. Perhaps the asymmetric mode has greater amplification and therefore dominates. In the far wake it might be present along with the asymmetric mode. The symmetric mode is observed when the cylinder is vibrated laterally, Taneda (1965). The frequency of forcing is one-half the natural frequency, and hs/bs=.4 .

5.2.4.2 Possible Evolution of Proposed Structure. The evolution of the structure described in this section is derived by assuming that the interactions occur initially between the vortices of the same sign. Assume that the same type of interaction occurs as described in the mode II instability, but since there is not a no-slip boundary condition, the trailing segments of the vortices don't get stretched as much. The structure resulting from this consideration is sketched in Figure I.5.2.3.2.1b . The upper vorticity is represented by the solid lines. The next assumption is that the lower vorticity will follow the same pattern, but out of streamwise phase by half a wavelength. This will provide the familiar staggered pattern of the usual two-dimensional vortex street. The lower vorticity is represented by the broken lines.

Chapter 6
CONCLUSIONS

An unsteady and three-dimensional large-scale structure is proposed for the reattachment region of a separation bubble, based on a visualization study of the flow over a plate with a square leading edge and its axisymmetric counterpart, a flat-faced circular cylinder aligned coaxially with the free-stream. The initial free shear layer structures are primarily two-dimensional but evolve into boundary layer type structures as they near reattachment and interact with the wall. Some segments form "loops" which convect away from the wall and downstream, while spanwise adjacent parts convect toward the wall and upstream. The loops are sometimes clearly arranged in a staggered pattern. Their legs form a series of counter-rotating streamwise vortex pairs which bridge the reattachment zone. These observations reconcile apparently contradictory propositions concerning the fate of the structures as they encounter reattachment. The interaction between successive vortices at alternating spanwise locations is fundamental to several flows, such as turbulent wakes and jets. The loop structure can be seen in turbulent vortex rings.

A result of this interaction is that cancellation between two signs of vorticity does not often occur. Instead they often pinch off to effectively form closed loops. The Reynolds number at which the flow exhibits its characteristic structure is often not much greater than the value at which the first instabilities appear.

New methods of approximating axisymmetric flows are presented. The shape of the separating streamline, height of the separation bubble, and velocity on the face of the body can be obtained from transformation of the results for the two-dimensional free streamline theory to account for the axisymmetry.

Boundary layer calculations indicate that the boundary layer is stable up to Re of the order of billions based on cylinder diameter. Shear layer calculations indicate that the separating shear layer is actually stable at separation, and does not exceed the the critical Re until it has thickened with downstream distance. Above a $Re_D \tilde{} 10,000$ it is expected to be unstable at the line of separation. This stability is unusual as most shear layers studied in detail have been unstable at separation.

PART II FORCED REATTACHING FLOW

Chapter 1
INTRODUCTION

Previous investigators of free-shear layers have discovered that organized vortical structures play an important role in the dynamics of the flow (Brown and Roshko (1974) and Winant and Browand (1974)) . It was also found that periodic forcing of these structures could modify their development and consequently the growth of the shear layer (Oster and Wygnanski (1982)). The purpose of our investigation was to study the effect of a periodic velocity perturbation on a separation bubble, where the separated shear flow begins its development as a free-shear layer but undergoes interaction with the wall at reattachment and ultimately becomes a boundary layer flow farther downstream. A study was made of the effect of a periodic velocity perturbation on the separation bubble downstream of the sharp-edged blunt face of a circular cyinder aligned coaxially with the free stream. It is part of a larger research effort to characterize the structure of reattaching flows in general. Preliminary results were reported by Sigurdson, Cimbala, and Roshko (1981) .

The effects of forcing on forebody drag, bubble length and pressure distribution were investigated. The effects on the bubble structure and, especially, on the turbulent structures of the free-shear layer, were studied in flow photographs obtained by the smoke-wire technique in a wind tunnel. The laser-induced fluorescence technique was used in water for the unforced case.

Chapter 2
EXPERIMENTAL APPARATUS

Figure II.1.1 is a schematic of the flow mean streamlines and a cross-sectional view of the flat-faced cylinder. The forcing technique is to produce acoustic waves inside the cylinder by oscillation of the speaker located there. These are communicated to the flow through a small circumferential gap located just downstream of the separation line. This allows velocity fluctuations to be superimposed on the external flow.

The main cylinder was 16.5 cm in diameter (D) with 0.64 cm thick walls and was constructed out of plexiglas. The front face was 1.27 cm thick plexiglas connected to the main body of the cylinder by three 0.32 cm diameter bolts. A 0.64 cm gap was left between the face plate and the main body of the cylinder.

A 12.7 cm woofer acoustic speaker was mounted within the cylinder. It was driven by a power amplifier with a sinusoidal output of controllable frequency and amplitude. Due to a number of resonant frequencies in the forcing system, the voltage amplitude to the woofer had to be carefully controlled. A calibration was performed to keep the velocity perturbation measured at the gap constant over a range of frequencies. The rms amplitude of the velocity perturbation (u') through the gap was measured using a hot-wire with the wind tunnel flow off. A biasing flow over the hot-wire was provided to avoid the rectification problems associated with flows with zero average velocity. In this way the necessary voltage to drive the woofer could be determined for each frequency. It was found that, at a fixed frequency, the velocity perturbation was linear with voltage. The hot-wire was also used to select frequencies at which harmonics were not present.

When comparing the results of this experiment to other forcing experiments where the velocity perturbation amplitude is controlled, one should keep the following in mind. The u' measurement in this experiment was taken right in the middle of the gap behind the leading edge. If there were no reflections from the tunnel walls, the amplitude of perturbation would be expected to decrease with radial distance (r) from the gap slightly faster than 1/r, which would occur for a 2-d source. Consequently, as opposed to experiments with free shear layers where the entire free stream is perturbed, the forcing amplitude in this case dropped off very rapidly away from the separation line. This makes it difficult to compare amplitudes.

The mean pressure in the cavity ahead of the speaker was measured with a Barocel electronic manometer and was used to calculate the pressure coefficient C_{p_s} at the separation line. The dynamic pressure was measured upstream of the model with a pitot static tube. Time-averaged reattachment location X_r was measured by visual inspection of tufts attached to the model. It was judged to occur where the oscillating tufts spent equal time pointing upstream and downstream. This allowed accuracy to better than 0.1 diameters.

Flow visualization was achieved with a smoke-wire illuminated by a General Radio Stroboscope. The electronic synchronizing controller for their operation was built at the Illinois Institute of Technology where the technique was perfected. For further details see Corke et al. (1977) .

The experiment was conducted in an open-return, low-turbulence wind tunnel with a flow velocity variable from 0.5 m/s to 12 m/s. The rms turbulence intensity of the free stream was measured to be 0.4% at U_∞ = 2 m/s. The test section was 2 m long and 0.51 m square resulting in a model blockage of 8.3% based on the cylinder cross-sectional area. No attempt has been made to correct the measurements for blockage. The

measured effects of forcing are for this particular geometry.

Chapter 3
EXPERIMENTAL RESULTS

3.1. Pressure, Drag and Reattachment Length.

C_{p_s} and X_r are both reduced with forcing. It is notable that they were never observed to increase under the effects of excitation. Figure II.3.1 shows the distribution of negative C_p as a function of downstream distance from the leading edge, X, normalized by the cylinder diameter D. The non-dimensional frequency or Strouhal Number ($St = F_{ex}D/U_\infty$) of excitation was 3.1. These data were measured on an earlier version of the experiment and are included here only to give a qualitative impression. It demonstrates that C_{p_s} becomes more negative and the length of the bubble is decreased with excitation. Tufts indicated that X_r/D decreased from 1.4 to 1.2.

Results from the present experiment are given in Figure II.3.2. The Reynolds number based on D (Re_D) was fixed at 132,000 which corresponded to free-stream velocity (U_∞) of 12 m/s. Two different rms amplitudes of excitation (as measured in the gap) were used (u'/U_∞): 3.9 and 7.8 percent. An estimate of the pressure drag on the cylinder face (C_{d_f}, which is the same as the average C_p on the face) could be made from the measured C_{p_s} and empirical relations representing the drag on circular disks. This technique is discussed in Koenig (1978) on page 53 (also Koenig and Roshko (1985)). The relation used here was:

$$C_{d_f} = 0.80 + 0.20\ C_{p_s} \quad .$$

The change in C_{d_f} normalized by the unforced value in percent is plotted in Figure II.3.2 as a function of forcing frequency (F_{ex}).

There is a minimum in both curves for values of F ranging between 150 and 200 hz, which have corresponding values of $F_{ex}D/U_\infty$ ranging between 2 and 3, forming a " drag bucket ". The magnitude scales with the excitation amplitude: a 3.2% drag reduction for 3.9% forcing amplitude, and a 6.4% reduction for 7.8% forcing. The corresponding effect on C_{p_s} was stronger, a reduction of 10% and 17% for the two cases, respectively.

The same data are replotted in Figure II.3.3 but normalized with the maximum drag reduction and plotted versus $F_{ex}D/U_\infty$. It is interesting that the curves collapse very well for $F_{ex}D/U_\infty$ less than that for minimum drag, but diverge for the $F_{ex}D/U_\infty$ greater than that for the minimum. This suggests that the flow responds linearly to the lower frequencies but nonlinearly to the higher ones.

The results were very sensitive to the presence of harmonics in the excitation. Everything else held constant, the drag reduction was usually greater with harmonics present. Figures II.3.2 and II.3.3 contain measurements at frequencies preselected for their absence of observed harmonics.

X_r/D was reduced a maximum of 31% and 19% for the 7.8% and 3.9% forcing amplitudes, respectively. It behaved monotonically with C_{d_f}; as the drag was lowered the bubble became shorter. The reattachment length for the unforced case was $X_r/D = 1.2$. This is less than the value of 1.6 found by Ota (1975) for a cylinder in a flow with less blockage. The higher blockage in the present case accounts for both the shorter bubble length and the lower value of $C_{p_s} = -1.05$ for the unexcited case, as compared to -0.6 from Ota.

3.2. Flow Visualization Results.

A series of smoke-wire photographs (Figure II.3.2.1) were taken at $F_{ex}D/U_\infty$ = 0 (no excitation), 20, 12, 8, and 4, with all other parameters fixed: (U_∞ = 4 m/s, Re_D = 42,400, and u'/U_∞ = 23%). The conditions were at a lower Re_D and higher u'/U_∞ than the C_{d_f} data but in the same $F_{ex}D/U_\infty$ range to give a qualitative idea of the response of the flow to excitation. The smoke-wire was located 0.6 cm ahead of the cylinder face, and on the centerline. If the smoke-wire is placed farther ahead of the model, its wake becomes a problem as it encounters the stagnation region. Therefore, it must be located either very close to the model, so that the wake is weak due to the lower stagnation velocities, or very far, so that the wake has had time to diffuse.

The wavelength λ_{ex} of the vortices corresponding to the forcing should scale as follows:

$$\lambda_{ex} = U_c/F_{ex}$$

where U_c is the convection velocity of the vortices. Figure II.3.2.1 demonstrates this result. For these values of $F_{ex}D/U_\infty$ and u'/U_∞, the frequency of the initial structures in the shear layer follows the forcing frequency identically. This conclusion was checked with a hot-wire anemometer. At this Re_D the initial Kelvin-Helmholtz instability of the shear layer has a frequency (F_{kh_i}) located in a broad band around 500 hz. The photos indicate that the initial structures lose their clarity within two or three wavelengths downstream of separation, suggesting that an amalgamation has occurred.

Figure II.3.2.2a and II.3.2.2b show flows with no excitation and with excitation at $F_{ex}D/U_\infty$ = 1.64, u'/U_∞ = 12%, respectively. Both have U_∞ = 2 m/s and Re_D = 22,000. The free streamlines calculated with a semi-empirical theory using the measured C_{p_s} are plotted over the photographs. They will be discussed in a following section.

The value of $F_{ex}D/U_\infty = 1.64$ is near the range of 2 to 3 where the minimum in C_{d_f} was measured (Figure II.3.3). The resulting vortex wavelength associated with this forcing frequency (λ_{ex}) is now so large that the vortex interacts with the wall almost immediately as it rolls up. Near separation, U_c can be approximated by $U_s/2$, where

$$\frac{U_s}{U_\infty} = (1 - C_{p_s})^{1/2}$$

is obtained using Bernoulli's equation. The result is

$$\frac{\lambda_{ex}}{D} = \frac{1}{2} \frac{U_s}{U_\infty} (F_{ex}D/U_\infty)^{-1} \quad .$$

For the conditions in Figure II.3.2.2b, λ_{ex}/D was calculated to be 0.46, which describes the structure located between X/D = 0.4 and 0.9 reasonably well.

The large structure farthest downstream in the photograph has more than twice the wavelength of the initial structures corresponding to F_{ex} and is surmised to result from an amalgamation. Much smaller vortices can be seen near the separation line, with a wavelength associated with the initial Kelvin-Helmholtz instability. U_∞ was too low to use the tufts to measure X_r/D, but it would be 0.8 if X_r/D is assumed to scale linearly with the maximum height of the free streamline (h) plotted in Figure II.3.2.2b.

3.3. How C_{d_f} is Reduced.

The streaklines toward the top of the pictures in Figures II.3.2.2 a and b indicate that the interference from the presence of the model is reduced in the excited case. They are much more curved and more inclined in the unexcited case. In the excited case, it appears from the pictures that the large forced structures cause a large increase in entrainment close to the separation line. The increased entrainment

(and correspondingly higher Reynolds stress) draws the irrotational flow closer to the model, resulting in time-averaged streamlines with a smaller radius of curvature near the separation line. The smaller radius maintains a higher radial pressure gradient; consequently, C_{p_s} and C_{d_f} are reduced (mainly from the increased suction on the edge of the face).

The reduced reattachment length is consistent with the increased growth rate of the shear layer. For backward-facing steps, Eaton and Johnston (1980) point out that X_r is determined by the growth rate of the shear layer and its curvature toward the wall. In this case, the growth rate is increased, and the height of the bubble is decreased, so that the shear layer does not have to grow as much before reaching the wall.

Chapter 4
DISCUSSION

4.1. Why $F_{ex}D/U_\infty$ has an Optimum Value.

As pointed out in the previous section, the drag is reduced due to the increase in entrainment near the leading edge. There appear to be two important factors for the optimum drag reduction: there should be an increase in entrainment and it should occur close to separation. Consequently, the faster the shear layer can be made to grow, the smaller the drag will be. The growth rate will depend on how well the excitation is amplified and where the amplification occurs.

In trying to understand the mechanics of these effects, it was concluded that an important element of the flow structure is the final vortex of the shear layer before reattachment. The scales of this vortex are more closely tied to the overall dimensions of the separation bubble than to those of the initially separating shear layer. In this it has similarities to the cavity flow problem, the cylinder shedding problem and the "preferred mode" of the circular jet. An important conclusion is that there are two fundamentally <u>different</u> instabilities involved, the Kelvin-Helmholtz instability of the free-shear layer, and the "shedding" type instability of the entire bubble. These are different but not uncoupled. The basic difference is that the free shear layer vorticity interacts with itself, while the "shedding" instability results from interaction of the vorticity with the wall. This is an interaction with vorticity of the opposite sign, the image vorticity resulting from the presence of the wall. It is hypothesized that the greatest drag reduction results from forcing at frequencies which are amplified by both the Kelvin-Helmholtz and the "shedding" instability. Figure II.3.2.2b shows structures that are clearly interacting with the wall, and the value of $F_{ex}D/U_\infty = 1.64$ is near the optimum range of 2 to 3.

This two instability approach to the problem was prompted by some observations made in the unforced bubble (although it is well established in the case of cylinder shedding and the the "preferred mode" of the circular jet). Figure II.4.1.1 is a laser induced fluorescence photograph of the unforced flow in a water channel. Dye was introduced far upstream ahead of the contraction, so that probe interference was minimized. The cylinder was made of plexiglas to allow the laser sheet to pass through it and cause the dye to fluoresce where the sheet and dye intersect. The dye impinging on the face of the cylinder acted as a tracer for the vorticity being generated there. Although its motion accounts only for the convective redistribution of vorticity and not the viscous diffusion (due to the high Schmidt number of water), locations of high dye concentration are indications of the highest vorticity concentration.

The striking conclusion from Figure II.4.1.1 is that there is a large quasi-periodic structure emerging from the bubble. This is the "terminating" vortex which results from earlier amalgamations that ceases when the vortex has grown to a size where its interaction with the wall becomes dominant and the flow "reattaches". The "terminating" vortex of the shear layer at reattachment convects downstream. The final vortex of the shear layer becomes the first structure in the attached turbulent boundary layer. Further amalgamations of this boundary layer structure may occur downstream but at a much slower rate than in the preceding shear layer. An unsteady three-dimensional structure for this reattaching zone and boundary layer has been proposed by Sigurdson and Roshko (1984) and is discussed in Part I.

Large-scale vortices shed downstream of the separation bubble have been reported recently for the blunt flat plate, the two-dimensional analog of the geometry discussed here (Cherry, Hillier and Latour (1983) and Kiya and Sasaki (1983)). It is expected that the cylinder flow is not qualitatively different, as the separation bubble height is only 20% of the diameter, or 7% of the circumference.

4.2. Regimes of Forcing $F_{ex}D/U_\infty$.

The concept of two different instabilities suggests four regimes for $F_{ex}D/U_\infty$:

I. $F_{ex} >> F_{kh_i}$

II. $F_{kh_i} > F_{ex} > F_{shed}$

III. $F_{ex} \simeq F_{shed}$

IV. $F_{shed} >> F_{ex}$

(Where F_{shed} is the most amplified frequency of the shedding instability and F_{kh_i} is the initial Kelvin-Helmholtz frequency).

Forcing in the first regime has little effect on C_{d_f} or X_r/D , as there is no instability to amplify the excitation. Forcing in the second regime is amplified by the shear layer. Oster and Wygnanski (1982) showed that the frequency of excitation determines the downstream location of amplification. The layer can amplify a broad band of frequencies lower than F_{kh_i} but limited by the available length before reattachment. In region III, the shedding instability is being driven and the maximum effect is observed. In region IV, the shedding instability can no longer amplify the forcing, and its effect is decreased. For values of Re_D discussed in this experiment, F_{kh_i} is always much greater than F_{shed}.

4.3. Proposed Scaling for F_{kh_i}.

Freymuth (1966) demonstrated that F_{kh_i} scales with velocity divided by the momentum thickness θ at separation:

$$\frac{F_{kh_i}\theta}{U_c} = \text{constant} \quad .$$

Assuming that U_c scales with U_s and that the boundary layer on the cylinder face is laminar, the result is:

$$\frac{F_{kh_i}D}{U_\infty} \quad \alpha \quad \frac{U_s}{U_\infty} Re_D^{1/2} \quad .$$

This accounts for the effect of changing U_s on U_c, but not for the effect on θ resulting from the altered velocity distribution on the cylinder face. With forcing, U_s increases and the velocity as a function of radius on the cylinder face is modified; therefore, even if the Re_D is unchanged, θ at separation will be altered.

4.4. Proposed Scaling for F_{shed}.

The basic hypothesis behind the proposed scaling for F_{shed} (for the axisymmetric geometry as well as for the blunt flat plate) is that the instability is like cylinder shedding, but the vortex interaction is with image vortices due to the wall rather than actual ones. (It is different in that it is symmetric rather than asymmetric.) This suggests that a scaling similar to that used by Roshko (1955) for cylinders of differing cross-sectional shape may apply. Figure II.4.4.1a shows a schematic of the modified free streamline theory that was used. The measured C_{p_s} was used to give U_s, and the corresponding separating streamline was calculated to give h, which for that case was the half width of the wake. It was found that although FD/U_∞ has values of 0.21 for a circular cylinder, 0.18 for a 90 degree wedge, and 0.14 for a bluff plate, $F_{shed}h/U_s$ had a universal value of 0.08 for all

cases.

Figure II.4.4.1b shows how h should be chosen for the present situation. In analogy to cylinder shedding, h represents the half distance between the vorticity and its corresponding image of opposite sign. The technique used to approximately calculate the separating streamlines in Figure II.3.2.2 was developed using the two-dimensional theory of Roshko (1955) and the analysis reported in Koenig (1978) to relate the bubble height with C_{p_s} for an axisymmetric body. That analysis has been extended to accommodate blockage. Figure II.4.4.2 is included to show how well the theory predicts the free streamline shape when blockage is low.

The expected result is that:

$$\frac{F_{shed}h}{U_s} = \text{constant}$$

therefore:

$$\frac{F_{shed}D}{U_\infty} \alpha \frac{D}{h}\frac{U_s}{U_\infty} .$$

The non-dimensional shedding frequency is only an indirect function of Re_D through its effects on h/D and U_s/U_∞, effects that are relatively weak when compared to the linear Re_D dependence of $F_{kh_i}D/U_\infty$.

4.5. Results of the Scaling.

There are two main uses for the proposed scaling. It allows some understanding of the effects of varying the frequency of excitation. It also correlates the "shedding" frequency range which occurs for a variety of geometries and is discussed in the next section.

For the structures in Figure II.4.1.1, FD/U_∞ can be estimated from their wavelength, $\lambda/D = 1.0$, assuming that $U_c = 0.5\ U_\infty$ (measured by Kiya and Sasaki (1983)). The result is $FD/U_\infty = 0.5$ and with $h/D = 0.23$ and $U_s/U_\infty = 1.27$, the value of $Fh/U_s = 0.09$. This is close to the value of 0.08 reported in Roshko (1955) for the Karman vortex street. This is somewhat surprising because, although they are both generically similar phenomena, Karman vortex shedding is unsymmetrical, whereas here symmetry is imposed by the reflection condition.

For the forcing conditions shown in Figure II.3.2.2b, the value of $F_{ex}h/U_s = 0.16$, twice the expected value of $F_{shed}h/U_s = 0.08$. The pairing implied by the photograph suggests that the resulting structure shed from the bubble has $Fh/U_s = 0.08$. This observation is reinforced by the photograph in Figure II.4.5.1, which has the same $F_{ex}D/U_\infty$ as Figure II.3.2.2b but with a higher amplitude of excitation, $u'/U_\infty = 21\%$. The distinct structures downstream of reattachment have a value of λ corresponding to half the value of F_{ex}.

These observations suggest that F_{ex} for minimum C_{d_f} is up to four times higher than the most amplified shedding frequency. The $F_{ex}D/U_\infty$ range of 2 to 3 in Figure II.3.3 for minimum drag corresponds to $F_{ex}h/U_s = 0.26$ to 0.32 . This is consistent with the hypothesized requirement for minimum drag, that the entrainment be increased near the separation line. It may also be due to the diminution of the imposed excitation with distance from the leading edge, resulting in better amplification at higher F_{ex} which can amplify closer to the origin of excitation.

The dependence of the most amplified frequency on h/D and U_s/U_∞ has a complicating consequence. When exciting the bubble, both of these quantities change, so that it cannot be stated a priori what the optimum forcing F will be.

The equation given earlier for λ_{ex}/D can be rewritten to give:

$$\frac{\lambda_{ex}}{h} = \frac{1}{2} (F_{ex}h/U_s)^{-1} \quad .$$

For the minimum drag range of $F_{ex}h/U_s$ of 0.26 to 0.32, this results in values of λ_{ex}/h from 1.9 to 1.6 . Therefore, the minimum drag corresponds to values of λ_{ex} comparable to the bubble height.

4.6. More Experiments.

Six experiments were conducted at various Re_D and u'/U_∞. The experimental conditions are listed in table II. Values of u'/U_∞ ranged from 3.9 to 23.6 percent. Figure II.4.6.1 plots drag reduction versus F_{ex}. Figure II.4.6.2 plots drag reduction versus $F_{ex}D/U_\infty$, and shows a trend for the minimum in the drag to occur at higher and higher $F_{ex}D/U_\infty$ for higher values of u'/U_∞. Note also that in this figure the two curves for u'/U_∞ = 11.8 percent collapse despite the large Re_D difference, indicating that the Re_D is not important at these high values of Re_D. The reason that the minimum swings to higher $F_{ex}D/U_\infty$ is that the natural bubble "shedding" frequency is getting higher due to reduced h and increased U_s. Figure II.4.6.3 shows how plotting versus Fh/U_s brings the minima of the curves to occur at the same value of Fh/U_s. Figure II.4.6.4 indicates that the maximum drag reduction possible at any u'/U_∞ is a linear function of u'/U_∞. The data can be reduced one more step by normalizing the drag reduction with the maximum possible drag reduction at that particular value of u'/U_∞. This result is plotted in figure II.4.6.5. The data collapse for values of Fh/U_s less than that for maximum drag reduction, indicating a linear response to the forcing. The "shedding" instability is being forced in that regime. For values of Fh/U_s greater, the curves do not collapse indicating that the free-shear-layer response is non-linear.

4.7. Comparison with Other Geometries.

The proposed scaling also appears to apply to separation bubbles occurring in other geometries. In studying the effect of an oscillating flap on the reattaching flow behind a two-dimensional wedge, Koga, Reisenthal and Nagib (1984) found that the most effective reattachment control occurred near values of $F_{ex}h/U_\infty$ of about 0.075 . They also noted that "control" could be achieved by the generation of vortices with sizes that are on the order of the separation height.

For the blunt flat plate Cherry et al. (1983) obtained a value of $FD/U_\infty = 0.14$, which corresponds to $Fh/U_s = 0.06$ (using their measured value of C_{p_s}, which gives $U_s/U_\infty = 1.3$ and thus $h/D = 0.51$ from the two-dimensional theory). For the backward-facing step Eaton et al. (1980) found a spectral peak near reattachment with $Fh/U_\infty = 0.07$. This needs no renormalization to be consistent with the present scheme, since $U_\infty = U_s$ for the step and h is equal to step height.

Mabey (1972) reported that the spectra of pressure fluctuations near the reattachment line are similar for bubbles caused by leading-edge separation on wings, forward-facing steps, rearward-facing steps, sudden enlargements in pipes, and cavities, if non-dimensionalized with the bubble length. Peak pressure fluctuations occurred for values of FX_r/U_∞ between 0.5 and 0.8 . A typical value of X_r/h is 7, which results in values of Fh/U_∞ between 0.07 and 0.11 . The broadness of this range might be reduced if U_s was used in the normalized frequency rather than U_∞.

Levi (1983) proposed a universal "Strouhal Law" for the relationship between the frequency of oscillation, U_∞, and a typical width (d) of the "fluid body" for a wide variety of fluid phenomena. These included wakes, jets, shock waves, cavitation, wing auto-rotation, vortex breakdowns, and surface and internal waves. The value of $Fd/U_\infty = 0.16$ was claimed for all cases, which corresponds to a value of Fh/U_∞

= 0.08, since d = 2h.

4.8. What Effect Does Forcing Have on the 3-D Structure?.

Films of the forced and unforced cylinder flow were taken using the Teledyne movie camera. They give an indication of the effect of forcing on the 3-D structure. The unforced flow shows strong asymmetry between the structure of the top and the bottom reattachment zones of the cylinder. When forcing is applied, this lack of symmetry remains the same. The flow does not become noticeably more two-dimensional at reattachment. (although at separation symmetry is evident) Smoke comes out of the plane of the streaklines in the potential flow in both forced and unforced cases, indicating the presence of 3-D loops.

4.9. Potential Flow Region.

The quality of the upstream flow is very good, and is demonstrated in the films. The smoke-wire is located two feet upstream of the model, yet the steaklines are rock steady. The stagnation point is stationary on the face of the cylinder. This is an indication that the turbulence does not induce velocities there.

4.10. Stability of Shear Layer During Sucking and Blowing.

Many sequences indicate that when the excitation is sucking, small Kelvin-Helmholtz waves appear on the shear layer closer to the separation line than when blowing. As the sucking stops and blowing begins, these structures get carried away from the separation line. As U_c decreases when sucking and increases when blowing.

4.11. Comparison to a Rankine Body.

Attempts have been made to learn more about the effects of excitation on the flow by analyzing the streakline photographs. The slope (v/u) of the streaklines has been measured as a function of radial distance (R) from the axis of symmetry, figure II.4.11.1. This was compared to the results predicted from the exact solution for a Rankine body with a final diameter equal to that predicted by the free

streamline theory. If the slopes were measured at the same downstream location as the source in the Rankine body, for large values of R the slopes decayed as the inverse of R squared, as the theory predicted. The excited case also had values of v/u less than those for the unexcited case, consistent with the drag reduction in the excited case. The values of slope agreed with those for the Rankine body within 30% for radial distances greater than one diameter (D), for the unexcited case. With excitation, the discrepancy was much less.

There are two primary reasons for disagreement. The strongest reason is that the theory does not account for the actual free streamline shape. The second is the flow unsteadiness in the photographs. Both of these effects are reduced with increased radial distance, and the agreement between theory and experiment is consequently improved. Similarly, agreement is better for the excited case since the body is smaller, therefore the distance from the surface of the body is relatively larger.

Chapter 5
CONCLUSIONS

The flow is considerably modified when forced at frequencies for which associated wavelengths are comparable to bubble height. At high Reynolds number these wavelengths are greater, and the forcing frequencies are lower than those of the initial Kelvin-Helmholtz frequencies of the separating free shear layer. Forcing then increases entrainment in the early part of the shear layer; as a result, reattachment length, bubble height, pressure at separation, and drag on the face are all reduced. Table III summarize the maximum change in these quantities. Larger effects were observed under less controlled circumstances.

In the unforced flow there is a natural "shedding frequency," analogous to that in wakes of bluff bodies and to the "preferred frequency" in the early axisymmetric jet. There are two fundamentally <u>different</u> instabilities involved, the Kelvin-Helmholtz instability of the free shear layer and the "shedding" type instability of the entire bubble which is controlled by interaction with the wall.

The method of frequency scaling proposed ($F_{shed}h/U_s$), based on an analogy with cylinder vortex shedding, correlates frequency data for separation bubbles occurring in a variety of geometries which reattach on walls, and results in values of $F_{shed}h/U_s$ near 0.08, the value for cylinder shedding. This is surprising because, although they are both generically similar phenomena, Karman vortex shedding is unsymmetrical, whereas separation bubbles that reattach on walls have symmetry imposed by the reflection condition.

The minimum drag occurs over a $F_{ex}D/U_\infty$ range of 1 to 3, which corresponds to a range of 0.16 to 0.32 in $F_{ex}h/U_s$, between two and four times the expected most amplified "shedding" frequency. This suggests that the minimum occurs when the initial shear layer is used to

amplify the forcing, creating structures that amalgamate to form a final structure with $F_{shed}h/U_s = 0.08$. The three-dimensional nature of the "shedding" instability discussed in Part I may explain why the F_{ex} must be greater than the first harmonic of F_{shed}, since each shed structure consists of two shear layer structures.

The dependence of the most amplified "shedding" frequency on h/D and U_s/U_∞ makes it difficult to predict what the optimum forcing F will be. The use of free streamline theory simplifies this problem by relating these quantities to the measured value of the pressure coefficient at separation.

REFERENCES

Abbott, D.E. and Kline, S.J. 1962. "Experimental investigation of subsonic turbulent flow over single and double backward facing steps," Trans. of the ASME, JBE, Sept., 317-325.

Abbott, D.E., Smith, C.R. and Walker, J.D.A. 1982. "Theoretical and experimental investigation of coherent structure in the turbulent boundary layer," AFOSR-TR-82-0684.

Achenbach, E. 1974. "Vortex shedding from spheres," J. J. Fluid Mech. 62, part 2, 209-221.

Achenbach, E. 1976. "Remarks on the wake behind spheres," Symp. Presented by General Motors Res. Lab., Warren, MI, Sept.

Ahuja, K.K., Whipkey, R.R. and Jones, G.S. 1983. "Control of turbulent boundary layer flows by sound," AIAA 8th Aeroacoustics Conference, paper no. AIAA-83-0726.

Amini, J. and Lespinard, G. 1982. "Experimental study of an 'incipient spot' in a transitional boundary layer," Phys. Fluids 25, Oct., 1743-1750.

Ashurst, W.T. 1983. "Large eddy simulation via vortex dynamics," Presented at the AIAA Sixth Computational Fluid Dynamics Conference, Danvers, MA, July 13-15, paper no. AIAA 83-1879-CP.

Back, L.H. and Roschke, E.J. 1972. "Shear-layer flow regimes and wave instabilities and reattachment lengths downstream of an abrupt circular channel expansion," J. Applied Mech. 677-681, Sept.

Batill, S.M. and Mueller, T.J. 1981. "Visualization of transition in the flow over an airfoil using the smoke-wire technique," AIAA J. 19, no. 3, 340-345, March.

Bernal, L.P. 1981. "The coherent structure of turbulent mixing layers: I. Similarity of the primary vortex structure. II. Secondary streamwise vortex structure," Ph.D. Thesis, Calif. Institute of Tech., Pasadena.

Bradshaw, P. and Wong, F.Y.F. 1972. "The reattachment and relaxation of a turbulent shear layer," J. Fluid Mech. 52, part 1, 113-135.

Breidenthal, R. 1980. "Response of plane shear layers and wakes to strong three-dimensional disturbances," Phys. Fluids 23, no. 10, Oct., 1929-1934.

Breidenthal, R.E. 1978. "A chemically reacting turbulent shear layer," Ph.D. Thesis, Calif. Institute of Tech., Pasadena.

Browand, F.K. and Laufer, J. 1975. "The role of large-scale structures in the initial development of circular jets," Proc. 4th Symp. on Turb. in Liquids, Univ. of Missouri, Rolla.

Brown, G.L. and Roshko, A. 1974. "On density effects and large structure in turbulent mixing layers," J. Fluid Mech. 64, no. 4, 775-816.

Brown, G.L. and Roshko, A. 1971. "The effect of density difference on the turbulent mixing layer," AGARD-CP-93, paper no. 23q.

Chandrsuda, C. and Bradshaw, P. 1981. "Turbulence structure of a reattaching mixing layer," J. Fluid Mech. 110, 171-194.

Cherry, N.J., Hillier, R. and Latour, M.E.M.P. 1983. "The unsteady structure of two-dimensional separated and reattaching flows," J. Wind Engineering and Industrial Aerodynamics 11, 95-105.

Cimbala, J.M. 1984. "Large structure in the far wakes of two-dimensional bluff bodies," Ph.D. Thesis, Calif. Institute of Tech., Pasadena.

Corke, T., Koga, D., Drubka, R. and Nagib, H. 1977. "A new technique for introducing controlled sheets of streaklines in wind tunnels," IEEE Publication 77-CH 1251-8 AES.

Crow, S.C. 1970. "Stability theory for a pair of trailing vortices," AIAA J. 8, no. 12, Dec., 2172-2179.

Desruelle, D. 1983. "Beyond the Karman vortex street," Master's Thesis, Mechanical Engineering, Illinois Institute of Tech., Chicago, May.

Dimotakis, P.E., Miake-Lye, R.C. and Papantoniou, D.A. 1984. "Structure and dynamics of round turbulent jets," Phys. Fluids; also GALCIT Report FM82-01, Calif. Institute of Tech., Pasadena.

Dinkelacker, A., Hessel, M., Meier, G.E.A. and Schewe, G. 1977. "Investigation of pressure fluctuations beneath a turbulent boundary layer by means of an optical method," Phys. Fluids 20, no. 10, part II, S216-S224 (Proc. IUTAM Symp. on Structure of Turb. and Drag Reduction).

Driver, D.M., Seegmiller, H.L., and Marvin, J. 1983. "Unsteady behavior of a reattaching shear layer," AIAA paper no. 83-1712, July.

Dyment, A. 1981. "The development of vortices in a mixing Layer," Unsteady Turbulent Shear Flows, IUTAM Symposium, Toulouse, France.

Eaton, J.K. and Johnston, J.P. 1982. "Low frequency unsteadiness of a reattaching shear layer," Turbulent Shear Flows 3, Bradbury et al., eds., Springer-Verlag:,pp. 162-170.

Eaton, J.K. and Johnston, J.P. 1981. "Research on subsonic turbulent flow reattachment," AIAA J. 19, no. 9, 1093-1100, Sept.

Eaton, J.K. and Johnston, J.P. 1980. "Turbulent flow reattachment: An experimental study of the flow and structure behind a backward-facing step," Thermosciences Div., Dept. of Mech. Eng., Stanford Univ. Report MD-39, June.

Erickson, G.E. 1982. "Vortex flow correlation," AIAA Aircraft Systems and Technology Meeting, ICAS paper no. 82-6.6.1, Seattle, Wash., Aug. 22-27.

Freymuth, P. 1966. "On transition in a separated laminar boundary layer," J. Fluid Mech. 25, part 4, 683-704.

Fuchs, H.V., Mercker, E. and Michel, U. 1978. "Large scale coherent structures in the wake of axisymmetric bodies," DFVLR-FB 78-28, Berlin.

Gad-el-Hak, M., Davis, S.H., McMurray, J.T., and Orszag, S.A. 1983. "On the stability of the decelerating laminar boundary layer," Submitted to J. Fluid Mech.

Gai, S.L. and Sharma, S.D. 1984. "Subsonic turbulent flow over a rearward facing segmented step," Phys. Fluids 27, no. 3, 544-546, March.

Gerrard, J.H. 1978. "The wake of cylindrical bluff bodies at low Reynolds number," Phil. Trans. Roy. Soc. 288, 351.

Gerrard, J.H. 1965. "A disturbance-sensitive Reynolds number range of the flow past a circular cylinder," J. Fluid Mech. 22, part 1, 187-196.

Ginoux, J.J. 1960. "The existence of three-dimensional perturbations in the reattachment of a two-dimensional supersonic boundary layer after separation," AGARD Report 272, April.

Glezer,A. 1981. "An experimental study of a turbulent vortex ring," Ph.D. Thesis, Calif. Institute of Tech., Pasadena.

Goldstein, R.J., Eriksen, V.L., Olson, R.M. and Eckert, E.R.G. 1970. "Laminar separation, reattachment, and transition of the flow over a downstream-facing step," Trans. of the ASME, JBE, 732-731, Dec.

Hama, F.R. 1957. "Three-dimensional vortex pattern behind a circular cylinder," J. Aero. Sci., Feb.

Hama, F.R. 1963. "Progressive deformation of a perturbed line vortex filament," Phys. Fluids 6, no. 4, 526-534, April.

Hama, F.R. and Nutant, J. 1963. "Detailed flow-field observations in the transition process in a thick boundary layer," Proc. of the 1963 Heat Transfer and Fluid Mech. Inst., 77-93.

Hernan, M.A. and Jimenez, J. 1982. "Computer analysis of a high-speed film of the turbulent mixing layer," J. Fluid Mech. 119, 323-345.

Hillier, R. and Cherry, N.J. 1981. "The effects of stream turbulence on separation bubbles," J. of Wind Engineering and Industrial Aerodynamics 8, 49-58.

Hirata, M.,and Kasagi, N. 1979. "Studies of large-eddy structures in turbulent shear flows with the aid of flow-visualization techniques," in Heat Transfer Studies, T.F. Irvine, Jr. et al., eds., Hemisphere:, pp.163.

Kataoka, K., Kamiyama, Y., Hashimoto, S. and Komai, T. 1982. "Mass transfer between a plane surface and an impinging turbulent jet: The influence of surface-pressure fluctuation," J. Fluid Mech. 119, 103.

Kelvin, Lord. 1880. "Vibration of a columnar vortex," Proceedings of the Royal Science of Edinburgh, March 1.

Kim, J., Kline, S.J., and Johnston, J.P. 1978. "Investigation of separation and reattachment of a turbulent shear layer: Flow over a backward-facing step," Stanford Univ. Report MD-37.

Kiya, M. and Sasaki, K. 1983. "Structure of a turbulent separation bubble," J. Fluid Mech. 137, 83-113, Dec.

Kiya, M., Sasaki, K. and Arie, M. 1982. "Discrete-vortex simulation of a turbulent separation bubble," J. Fluid Mech. 120, 219-244.

Ko, S. and Lessen, M. 1969. "Low Reynolds number instability of an incompressible half-jet," Physics of Fluids 12, no. 2, 404-440.

Koenig, K. 1978. "Interference effects on the drag of bluff bodies in tandem," Ph.D. Thesis, Calif. Institute of Tech., Pasadena.

Koenig, K. and Roshko, A. 1985. "An experimental study of geometrical effects on the drag and flow field of two bluff bodies separated by a gap," J. Fluid Mech. 156, 167-204.

Koga, D.J., Reisenthal, P. and Nagib, H.M. 1984. "Control of separated flowfields using forced unsteadiness," IIT Fluids and Heat Transfer Report R84-1, January.

Kosmicki, J.J. 1973. "Experimental study of the separation and reattachment in a partially confined jet," Aeron. Engineer's Thesis, Calif. Institute of Tech., Pasadena.

Kotsovinos, N.E. 1977. "Plane turbulent buoyant jets. Part 2. Turbulence structure," J. Fluid Mech. 81, part 1, 45-62.

Lane, J.C. and Loehrke, R.I. 1980. "Leading edge separation from a blunt plate at low Reynolds number," J. Fluids Eng. 102, 494-496, Dec.

Laufer, J. and Jia Xiang Zhang. 1983. "Unsteady aspects of a low mach number jet," Phys. Fluids 26, no. 7, 1740-1750, July.

Lessen, M. and Ko, S. 1966. "Viscous instability of an incompressible half-jet flow," Phys. Fluids 9, no. 6, 1179-1183.

Levi, E. 1983. "A universal Strouhal law," J. Eng. Mech. (ASCE), 109, no. 3, 718-727, June.

Levi, E. 1983. "Oscillatory model for wall-bounded turbulence," J. Eng. Mech. (ASCE), 109, no. 3, 728-740, June.

Liepmann, H.W. 1979. "The rise and fall of ideas in turbulence," American Scientist 67, no. 2, 221-228, March-April.

Lock, R.C. 1951. QJAMM 42, 63.

Long, M.B. and Chu, B.T. 1981. "Mixing mechanism and structure of an axisymmetric turbulent mixing layer," AIAA J. 19, no. 9, 1158-1163.

Mabey, D.G. 1972. "Analysis and correlation of data on pressure fluctuations in separated flow," J. Aircraft 9, no. 9, 642-645, Sept.

Magarvey, R.H. and MacLatchey, C.S. 1964. "The disintegration of vortex rings," Can. J. Phys. 42, 684-689, April.

Matsui, T. 1982. "Flow visualization studies of vortices," in Surveys in Fluid Mechanics, R. Narasimha and S. M. Deshpande, eds., Indian Academy of Sciences: Bangalore, pp. 145-163.

McGuiness, 1978. Ph.D. Thesis, Cambridge, England.

Moussa, Z.M., Trischka, J.W. and Eskinazi, S. 1977. "The near field in the mixing of a round jet with a cross-stream," J. Fluid Mech. 80, part 1, 49-80.

Mumford, J.C. 1982. "The structure of the large eddies in fully developed turbulent shear flows. Part 1. The plane jet," J. Fluid Mech. 118, 241-268.

Mumford, J.C. 1983. "The structure of the large eddies in fully developed turbulent shear flows. Part 2. The plane wake," J. Fluid Mech. 137, 447-456.

Munk, M. 1952. "Mechanism of turbulent fluid motion," Aero Digest, 32-46, June.

Nagabhushanaiah, H.S. 1967. "Separation flow downstream of a plate set normal to a plane boundary," Ph.D. Thesis, Colorado State Univ.

Okabe, J. and Inoue, S. 1961. "The generation of vortex rings II," Reports of Res. Inst. for Appl. Mech. IX, no. 36.

Okabe, J. and Inoue, S. 1961. "Shedding of vortices from vortex rings," Reports of Res. Inst. for Appl. Mech. IX, no. 34.

Oshima, Y. and Asaka, S. 1975. "Interaction of two vortex rings moving side by side," Natural Science Report 26, no. 1, 31-38, Ochanomizu University.

Oster, D. and Wygnanski, I. 1982. "The forced mixing layer between parallel streams," J. Fluid Mech. 123, 91-130.

Ota, T. 1975. "An axisymmetric separated and reattached flow on a longitudinal blunt circular cylinder," J. Applied Mechanics (ASME) 311-315, June.

Ota, T. and Motegi, H. 1980. "Turbulence measurements in an axisymmetric separated and reattached flow over a longitudinal blunt circular cylinder," J. of Applied Mechanics (ASME) 47, 1-6, March.

Ota, T. and Itasaka, M. 1976. "A separated and reattached flow on a blunt flat plate," J. Fluids Engineering (ASME) 79-86, March.

Ota, T. and Narita, M. 1978. "Turbulence measurements in a separated and reattached flow over a blunt flat plate," J. Fluids Engineering (ASME) 100, 224-228, June.

Ota, T. and Kon, N. 1974. "Heat transfer in the separated and reattached flow on a blunt flat plate," J. Heat Transfer (ASME) 459-462, Nov.

Perry, A.E., Chong, M.S., and Lim, T.T. 1982. "The vortex-shedding process behind two-dimensional bluff bodies," J. Fluid Mech. 116, 77-90.

Perry, A.E. and Chong, M.S. 1982. "On the mechanism of wall turbulence," J. Fluid Mech. 119, 173-217.

Perry, A.E, Lim, T.T., and Teh, E.W. 1981. "A visual study of turbulent spots," J. Fluid Mech. 104, 387-405.

Perry, A.E. and Lim, T.T. 1978. "Coherent structures in coflowing jets and wakes," J. Fluid Mech. 88, part 3, 451-463.

Perry, A.E., Lim, T.T. and Chong, M.S. 1980. "The instantaneous velocity fields of coherent structures in coflowing jets and wakes," J. Fluid Mech. 101, part 2, 243-256.

Perry, A.E. and Tan, D.K.M. 1984. "Simple three-dimensional vortex motions in coflowing jets and wakes," J. Fluid Mech. 141, 197-231.

Perry, A.E. and Watmuff, J.H. 1981. "The phase-averaged large-scale structures in three-dimensional turbulent wakes," J. Fluid Mech. 103, 35-51.

Pierrehumbert, R.T. and Widnall, S.E. 1982. "The two- and three-dimensional instabilities of a spatially periodic shear layer," J. Fluid Mech. 114, 59-82, Jan.

Prandtl, L. and Tietjens, O.G. 1934. Applied Hydro- and Aerodynamics McGraw-Hill: New York.

Pronchick, S.W. and Kline, S.J. 1983. "An experimental investigation of the structure of a turbulent reattaching flow behind a backward-facing step," Stanford Univ. Report MD-42.

Rayner, J.M.V. 1979. "A vortex theory of animal flight. Part 1. The vortex wake of a hovering animal. Part 2. The forward flight of birds," J. Fluid Mech. 91, part 4, 697-763.

Robinson, A.C. and Saffman, P.G. 1982. "Three-dimensional stability of vortex arrays," J. Fluid Mech. 125, 411-427, Dec.

Roos, F.W. and Kegelman, J.T. 1985. "Control of coherent structures in reattaching laminar and turbulent shear layers," AIAA Shear Flow Control Conf., Boulder, CO; AIAA #85-0554, March.

Roos, F.W. and Kegelman, J.T. 1986. "Influence of excitation on coherent structures in reattaching turbulent shear layers," presented at the AIAA 24th Aerospace Sciences Meeting, Reno, NV, AIAA #86-0112; MDRL paper no. 86-4, Jan.

Roshko, A. 1976. "Structure of turbulent shear flows: A new look," AIAA J. 14, no. 10, 1349-1357, Oct.

Roshko, A. 1955. "On the wake and drag of bluff bodies," J. Aero. Sci. 22, no. 1, 124-132, Feb.

Roshko, A. 1954. "New hodograph for free streamline theory," NACA Tech. Note no. 3168.

Roshko, A. and Thomke, G.J. 1965. "Observations of turbulent reattachment behind an axisymmetric downstream-facing step in supersonic flow," Douglas SM-43069, Apr.

Saffman, P.G. 1980. "Vortex interactions and coherent structures in turbulence," Proc. Symp. on Transition and Turbulence, Academic Press, 149-166.

Savas, O. 1979. "Some measurements in synthetic turbulent boundary layers," Ph.D. Thesis, Calif. Institute of Tech.

Sigurdson, L.W. and Roshko, A. 1984. "The large-scale structure of a turbulent reattaching flow," Bull. Am. Phys. Soc. 29, no. 9, 1542.

Sigurdson, L.W., Cimbala, J.M. and Roshko, A. 1981. "Controlled excitation of a separated flow," Bull. Am. Phys. Soc. 26, no. 9, 1275.

Sigurdson, L.W. and Roshko, A. 1985 "Controlled unsteady excitation of a reattaching flow," AIAA Shear Flow Control Conference, Boulder, CO, AIAA #85-0552, March.

Slaouti, A. and Gerrard, J.H. 1981. "An experimental investigation of the end effects on the wake of a circular cylinder towed through water at low Reynolds numbers," J. Fluid Mech. 112, 297-314.

Smith, A.M.O. 1954. "Improved solutions of the Falkner and Skan boundary layer equation," S.M.F. Fund Paper FF10, Institute of the Aeronautical Sciences, March.

Sutton, E.P., Evans, G.P., McGuinness, M.D. and Svehla, K.M. 1981. "Influence of wall vibrations on a flow with boundary-layer separation at a convex edge," in Unsteady Turbulent Shear Flows, R. Michel et al., eds., IUTAM Symp., Toulouse, France, pp. 285-293.

Taneda, S. 1978. "Visual observations of the flow past a sphere at Reynolds numbers between 10^4 and 10^6," J. Fluid Mech. 85, part 1, 187-192.

Taneda, S. 1965. "Experimental investigation of vortex streets," J. Physical Soc. Japan, 20, no. 9, 1714-1721, Sept.

Taneda, S. 1956. "Experimental investigation of the wakes behind cylinders and plates at low Reynolds numbers," J. Phys. Soc. Japan, 11, no. 3, 302-307, March.

Taneda, S. 1959. "Downstream development of the wakes behind cylinders," J. Phys. Soc. Japan, 14, no. 6, 843-848, June.

Taneda, S. 1983. "Visual observations of amplification of artificial disturbances in turbulent shear flows," Phys. Fluids 26, no. 10, 2801-2806, Oct.

Tani, I. 1982. "Three-dimensional aspects of boundary-layer transition," in Surveys in Fluid Mechanics, R. Narasimha and S. M. Deshpande, eds. Indian Academy of Sciences: Bangalore, pp. 125-144.

Theodorsen, T. 1955. "The structure of turbulence," 50 Jahre Grenschichtsforschung.

Thomas, A.S.W. 1983. "The control of boundary-layer transition using a wave-superposition principle," J. Fluid Mech. 137.

Tritton, D.J. 1977. Physical Fluid Dynamics, Van Nostrand Reinhold: pp. 234.

Troutt, T.R., Scheelke, B., and Norman, T.R. 1984. "Organized structures in a reattaching separated flow field," J. Fluid Mech. 143, 413-427.

Uberoi, M.S. and Singh, P.I. 1975. "Turbulent mixing in a two-dimensional jet," Phys. Fluids 18, no. 7, 764-769.

Van Dyke, M. 1982. An Album of Fluid Motion, Parabolic Press: Stanford, CA.

Von Karman, T. and Rubach, H. 1912. "The mechanism of fluid and air drag," Physikalische Zeitschrift 13, no. 2, Jan.

Welsh, M.C. and Gibson, D.C. 1979. "Interaction of sound with flow past a square leading edged plate in a duct," J. Sound and Vibration 67, no. 4, 501-511.

Westphal, R.V. and Johnston, J.P. 1983. "Reattaching turbulent shear layers with perturbed structure," AIAA paper no. 83-0603.

White, F.M. 1974. Viscous Fluid Flow, McGraw-Hill.

Willmarth, W.W. 1975. "Structure of turbulence in boundary layers," Adv. Appl. Mech. 15, 159-254.

Winant, C.D. and Browand, F.K. 1974. "Vortex pairing: The mechanism of turbulent mixing layer growth at moderate Reynolds number," J. Fluid Mech. 63, 237-255.

Yule, A.J. 1978. "Large-scale structure in the mixing layer of a round jet," J. Fluid Mech. 89, part 3, 413-432.

TABLES

TABLE I. NON-DIMENSIONALIZED "SHEDDING" FREQUENCIES

GEOMETRY	FD/U_∞	Fh/U_s	REFERENCE
Free Bubbles:			
Circular cylinder	0.21	0.08	Roshko (1955)
90-degree wedge	0.18	0.08	Roshko (1955)
Bluff flat plate	0.14	0.08	Roshko (1955)
Wall Bounded Bubbles:			
Axisymmetric cylinder	0.4-0.5	0.07-0.09	present result
Blunt flat plate	0.14	0.06	Cherry et al. (1983)
Backward-facing step	$Fh/U_\infty = 0.07$	0.07	Eaton et al. (1980)
Miscellaneous review	FX_r/U_∞ = 0.5-0.8	Fh/U_∞ = 0.07-0.11	Mabey (1972)
Forced wedge	$F_{ex}h/U_\infty = 0.075$	$\approx$0.075	Koga et al. (1984)

TABLE II. EXPERIMENTAL CONDITIONS FOR ACOUSTIC FORCING

Experiment Number	u' (m/s)	U_∞ (m/s)	u'/U_∞ (%)	Re_D
1	0.47	12.0	3.9	126,599
2	0.47	8.0	5.9	84,399
3	0.94	12.0	7.8	127,254
4	0.94	8.0	11.8	84,366
5	0.47	4.0	11.8	42,195
6	0.94	4.0	23.6	42,430

TABLE III. MAXIMUM EFFECTS

Quantity	Magnitude
ΔC_{p_s}	-48%
ΔX_r	-58%
ΔU_s	13%
Δh	-48%
ΔCd_f	-15%
ΔSt_h	-53%

FIGURES

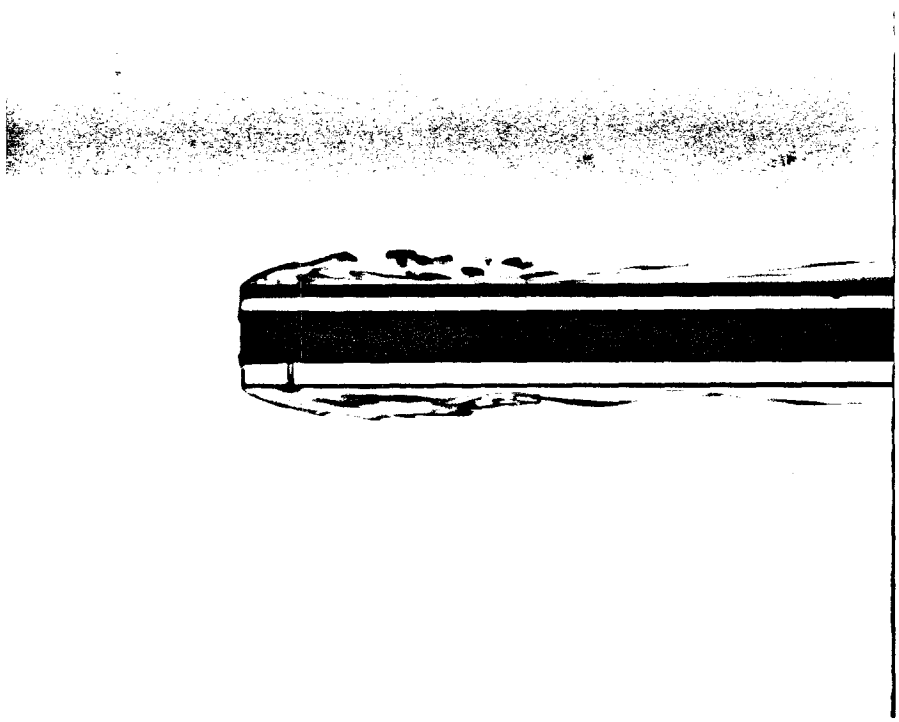

I.2.1.1 Single-port dye visualization

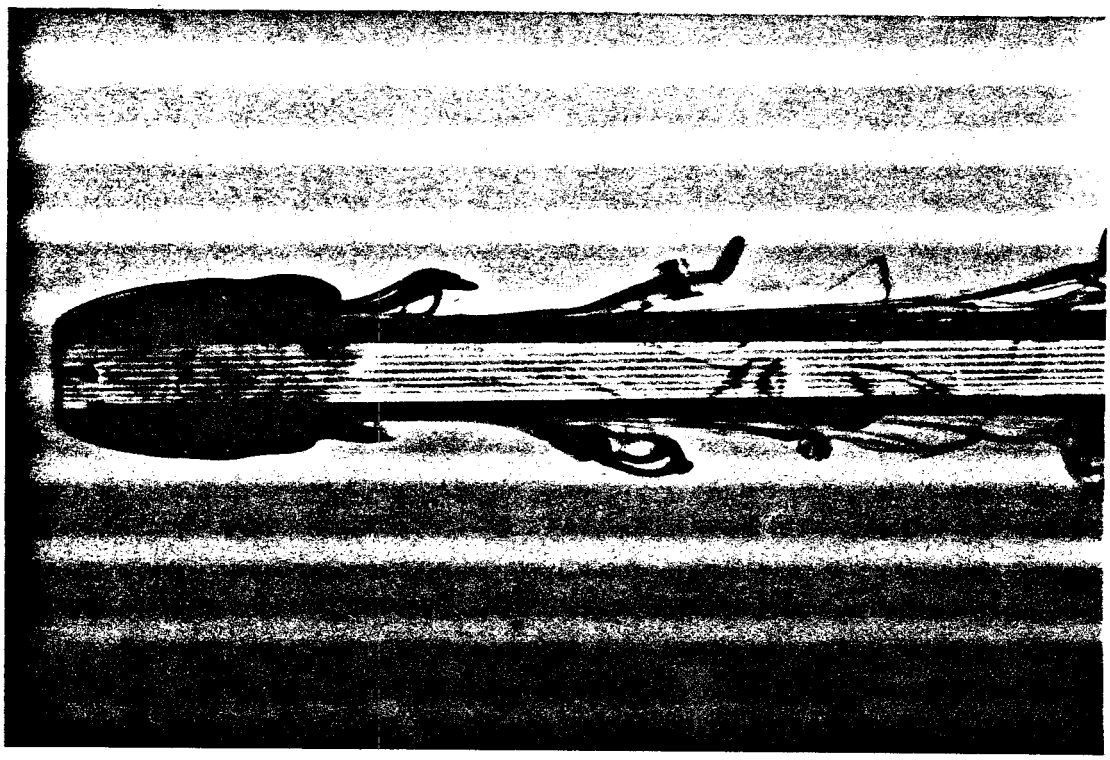

I.2.3.1 Loop structure, Re_D = 1097

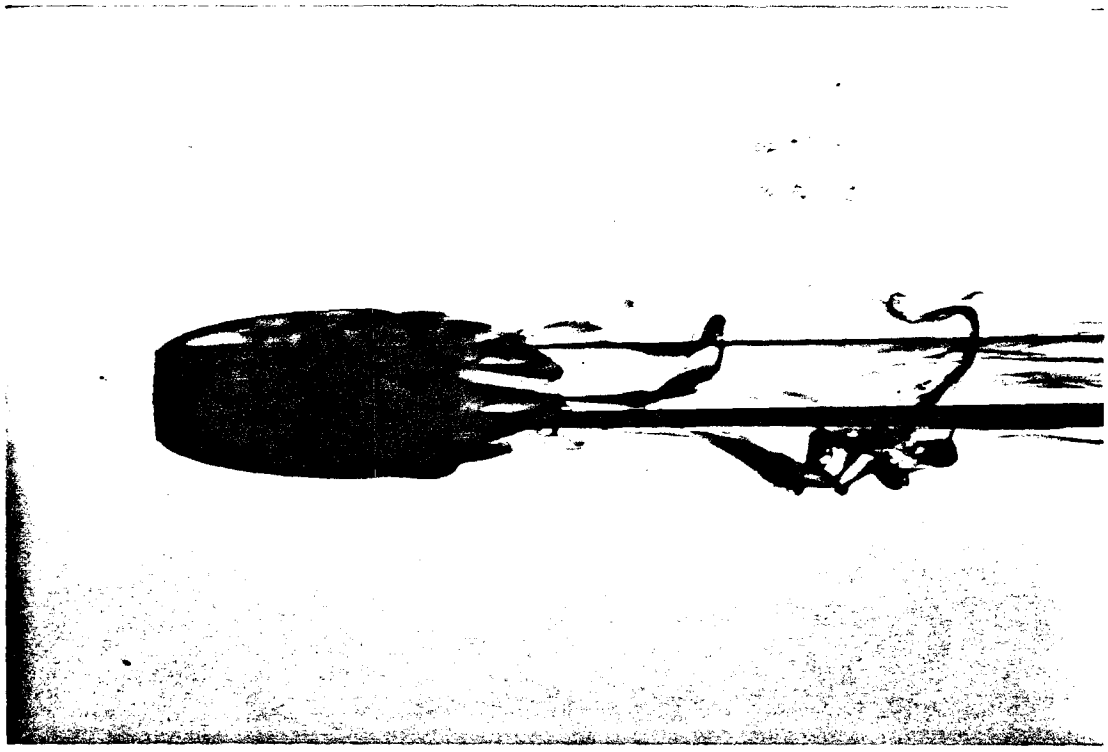

I.2.3.2 Circumferential dye injection

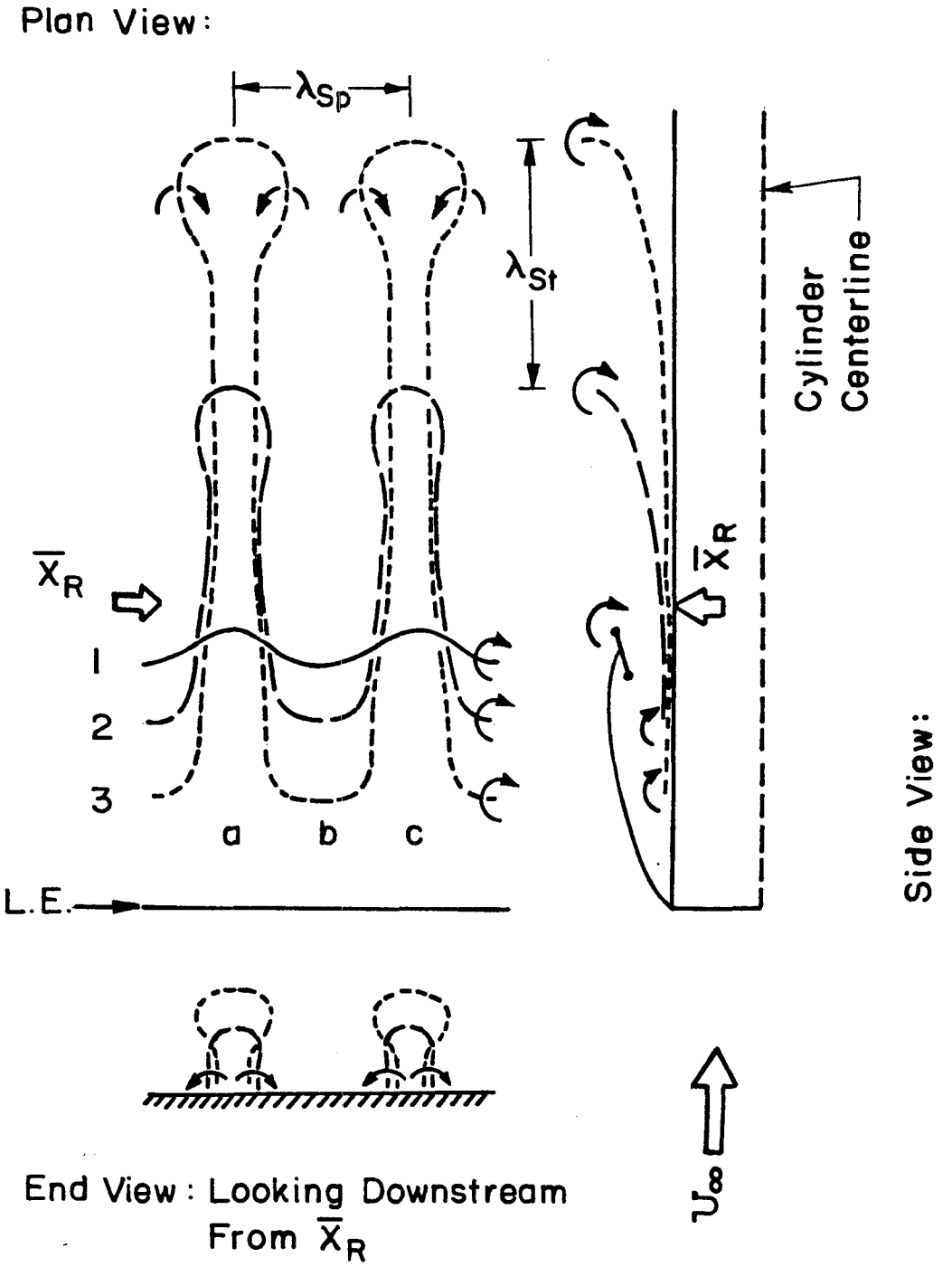

I.2.3.3 **Mode I spanwise phase-matched interaction**

I.2.4.1 Wavy initial instability, Re_D = 2750

I.2.4.2 Mode II loop arrangement, $Re_D = 2750$

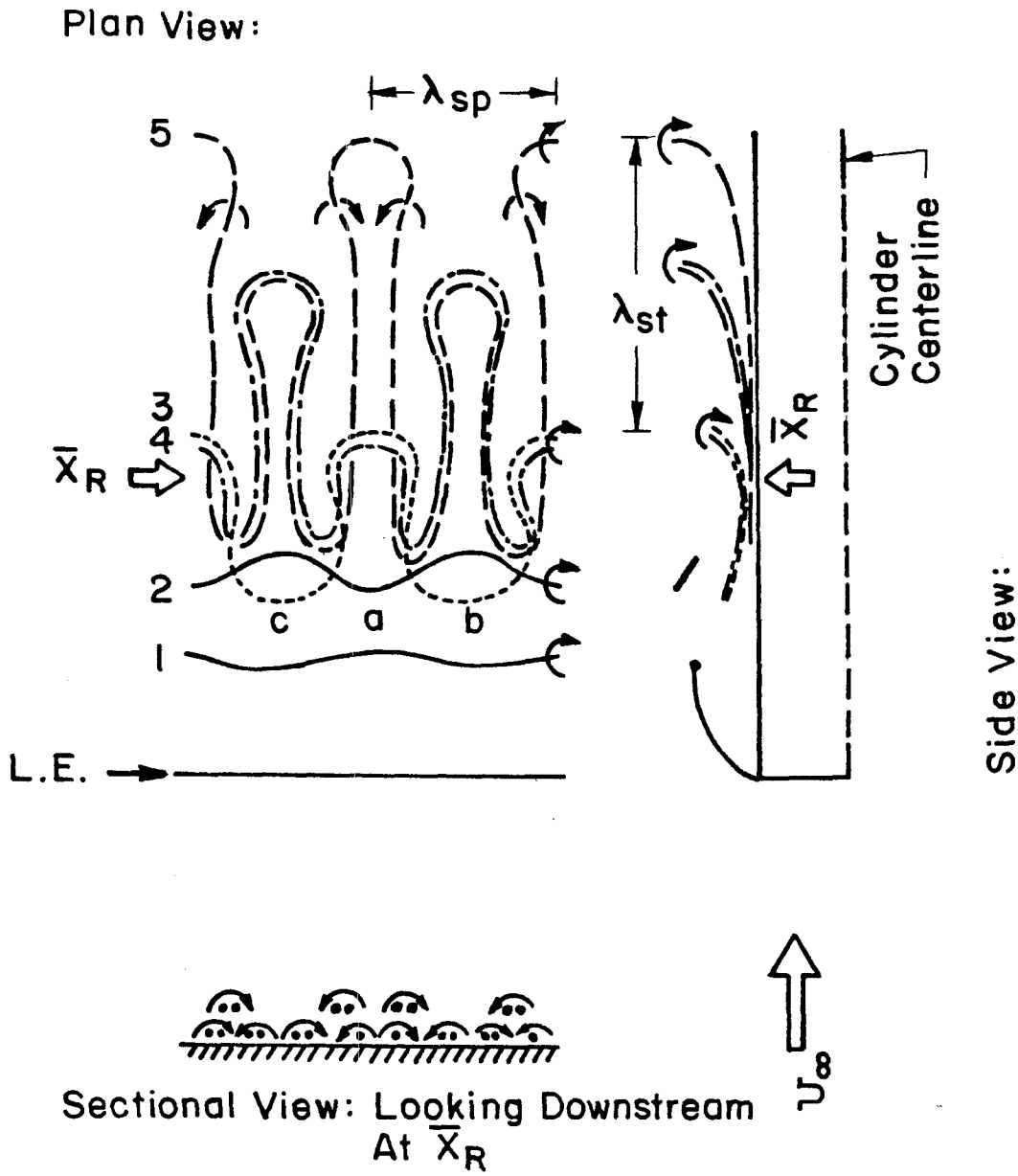

I.2.4.3 **Mode II spanwise phase offset interaction**

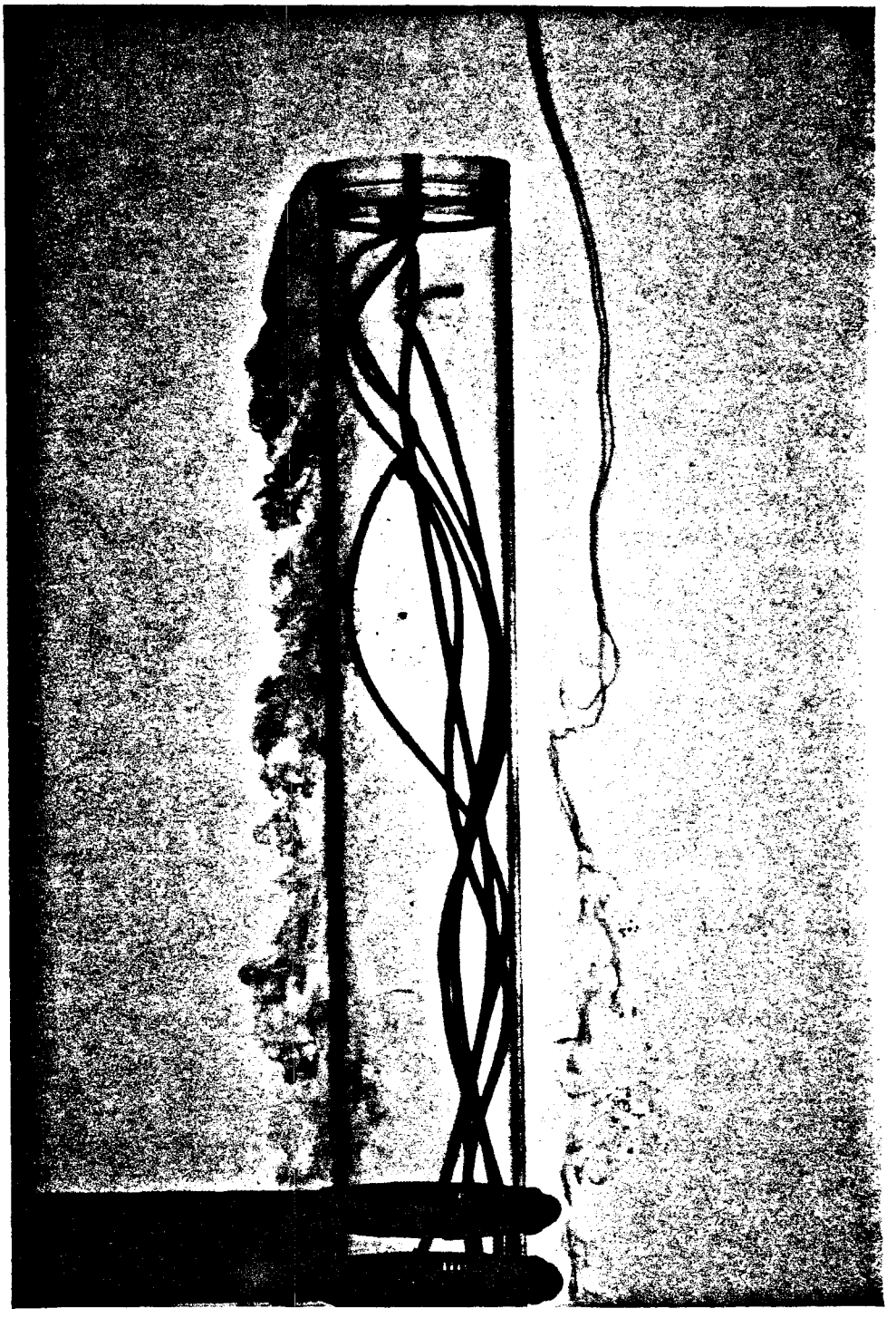

I.2.5.1a Combination of dye injection Re_D = 6300

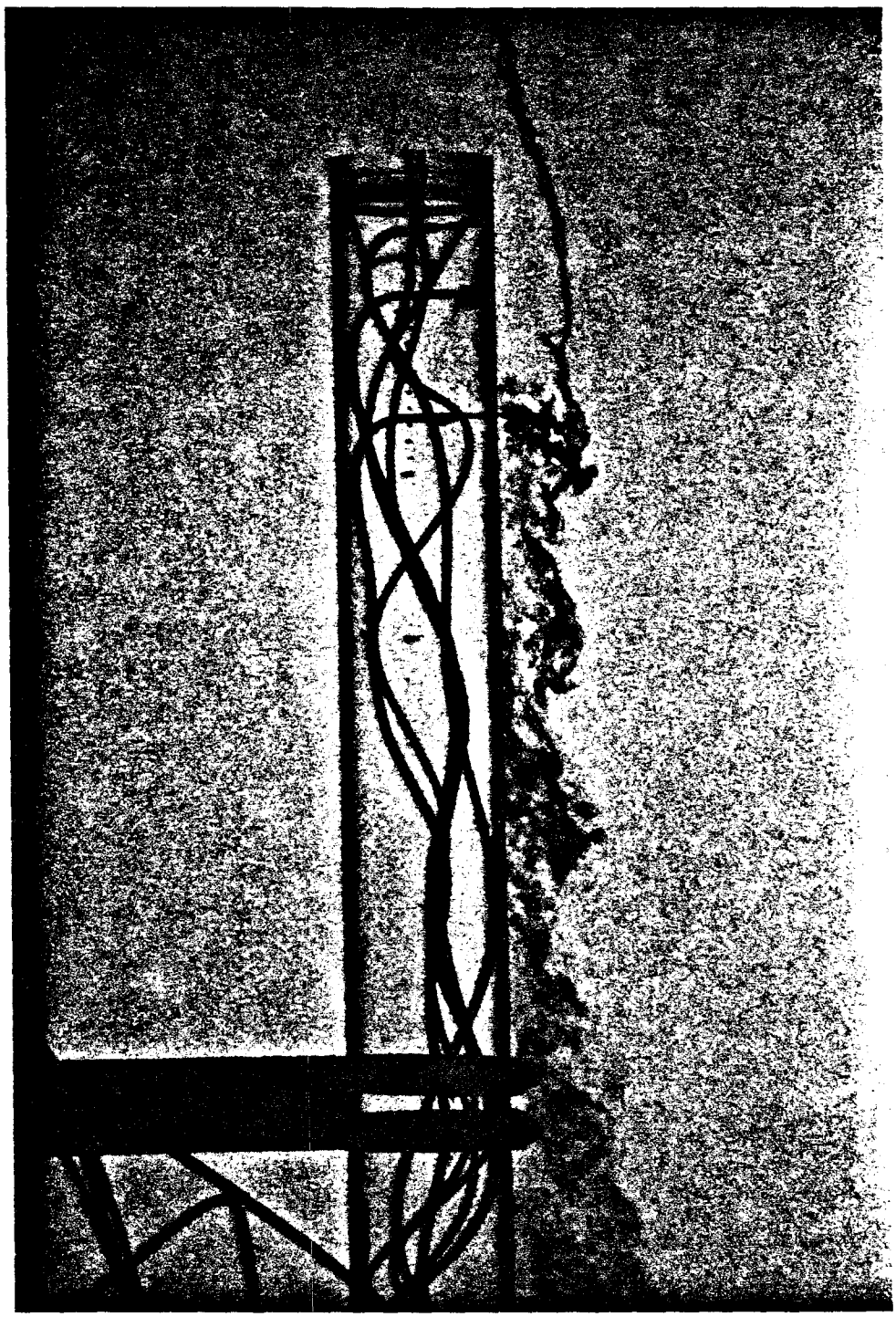

I.2.5.1b Combination of dye injection Re_D = 6300

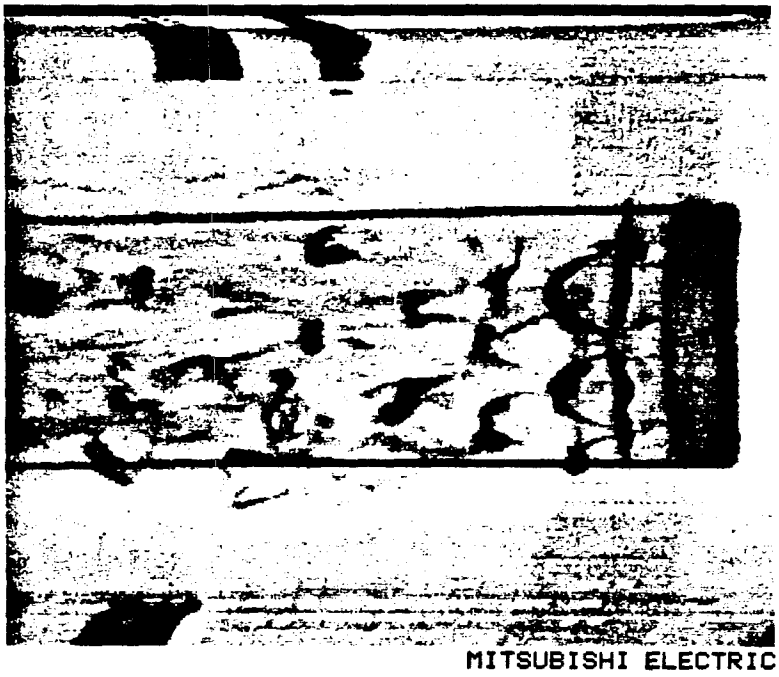

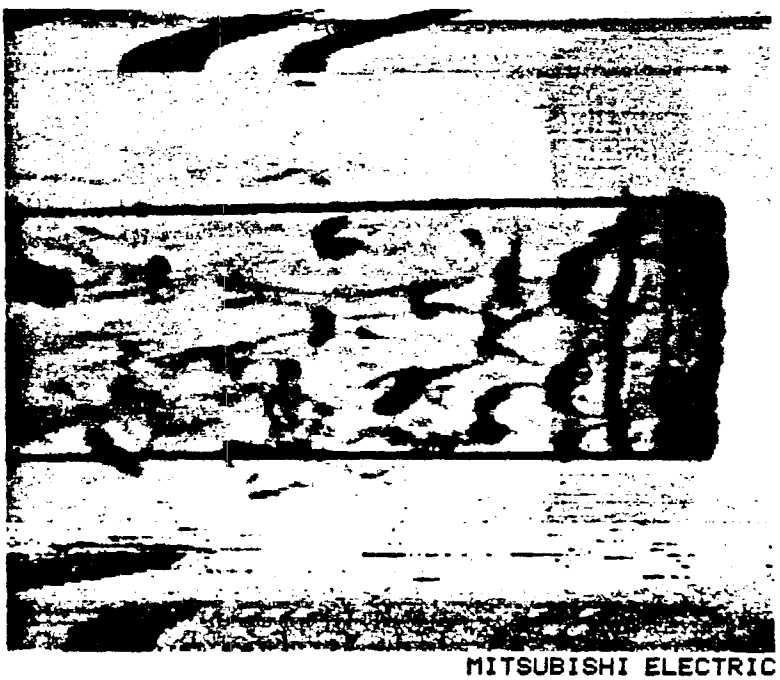

I.2.2.2.1 **Video frames of the blunt flat plate**

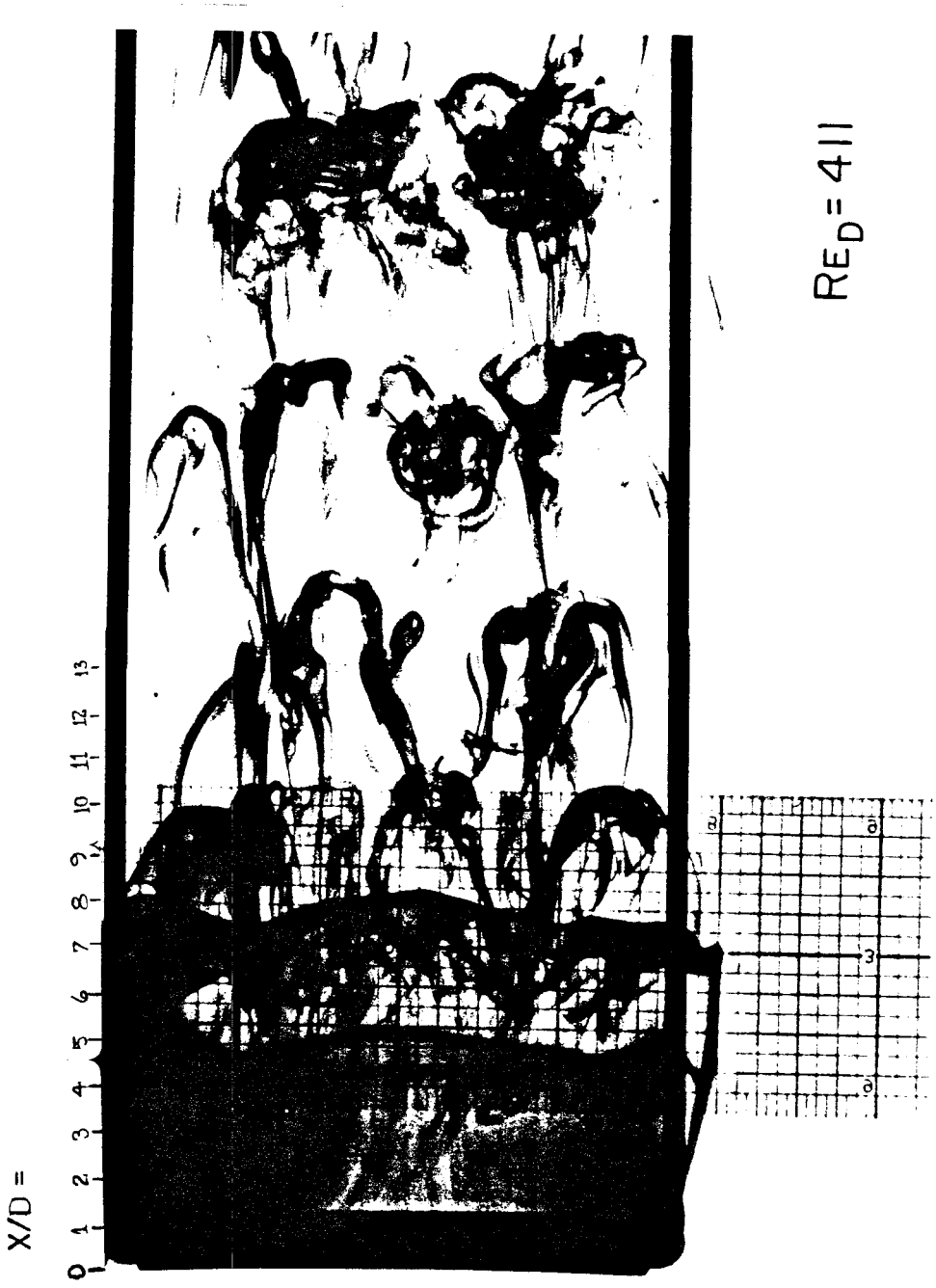

I.2.2.2.2 **Photograph of the blunt flat plate**

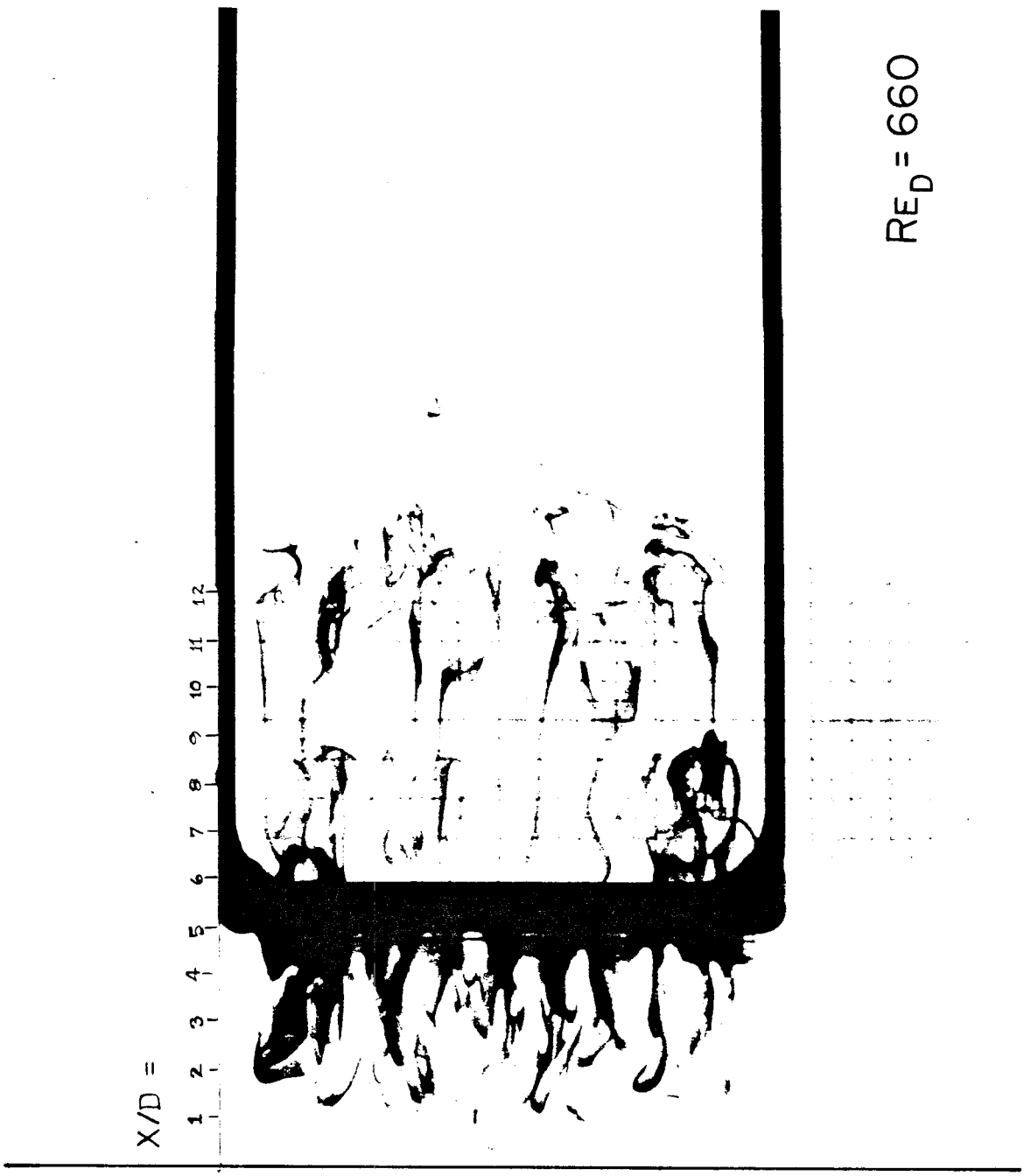

I.2.2.2.1.1 **Counter-rotating vortex pairs**

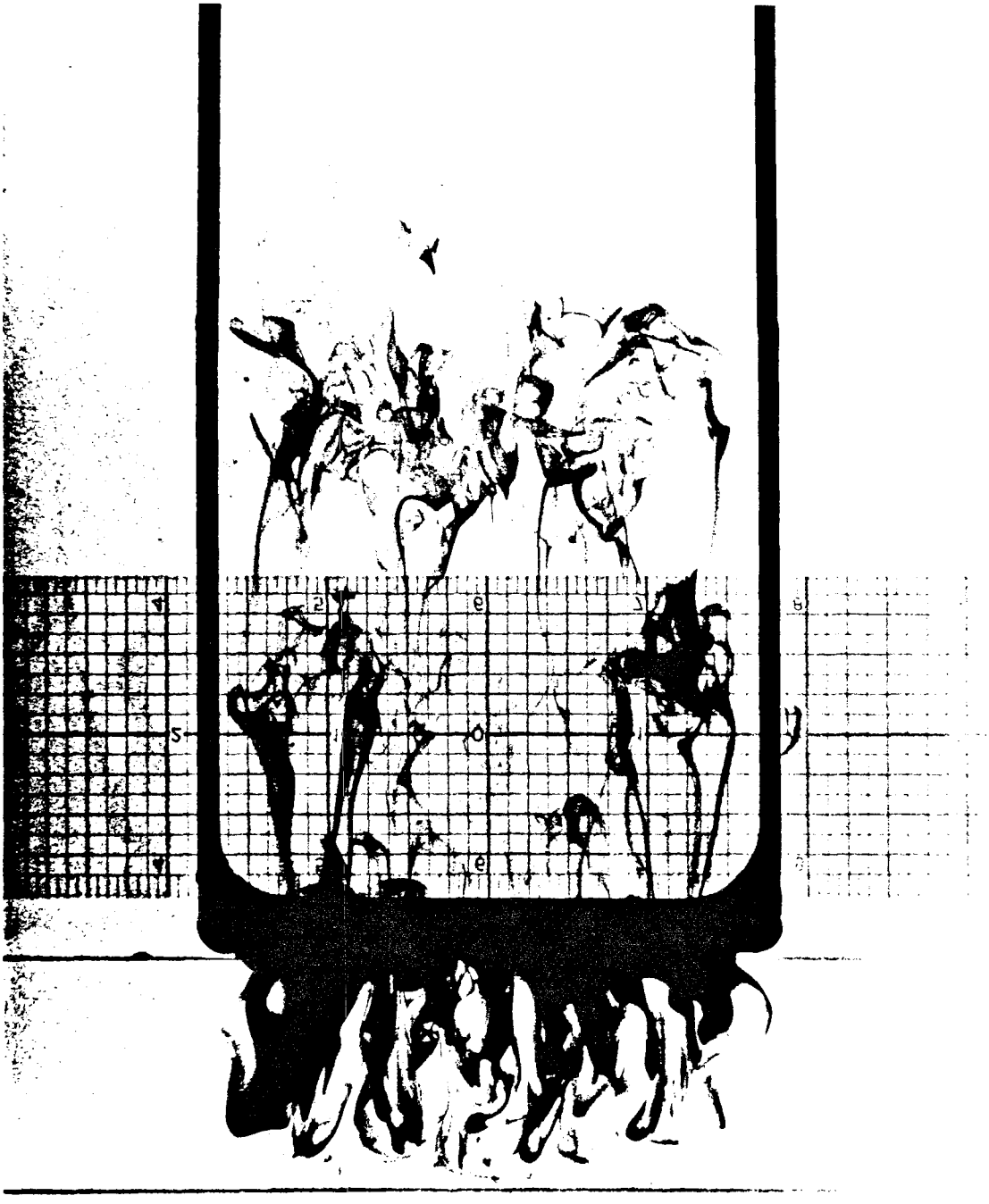

I.2.2.2.1.2 **Counter-rotating vortex pairs**

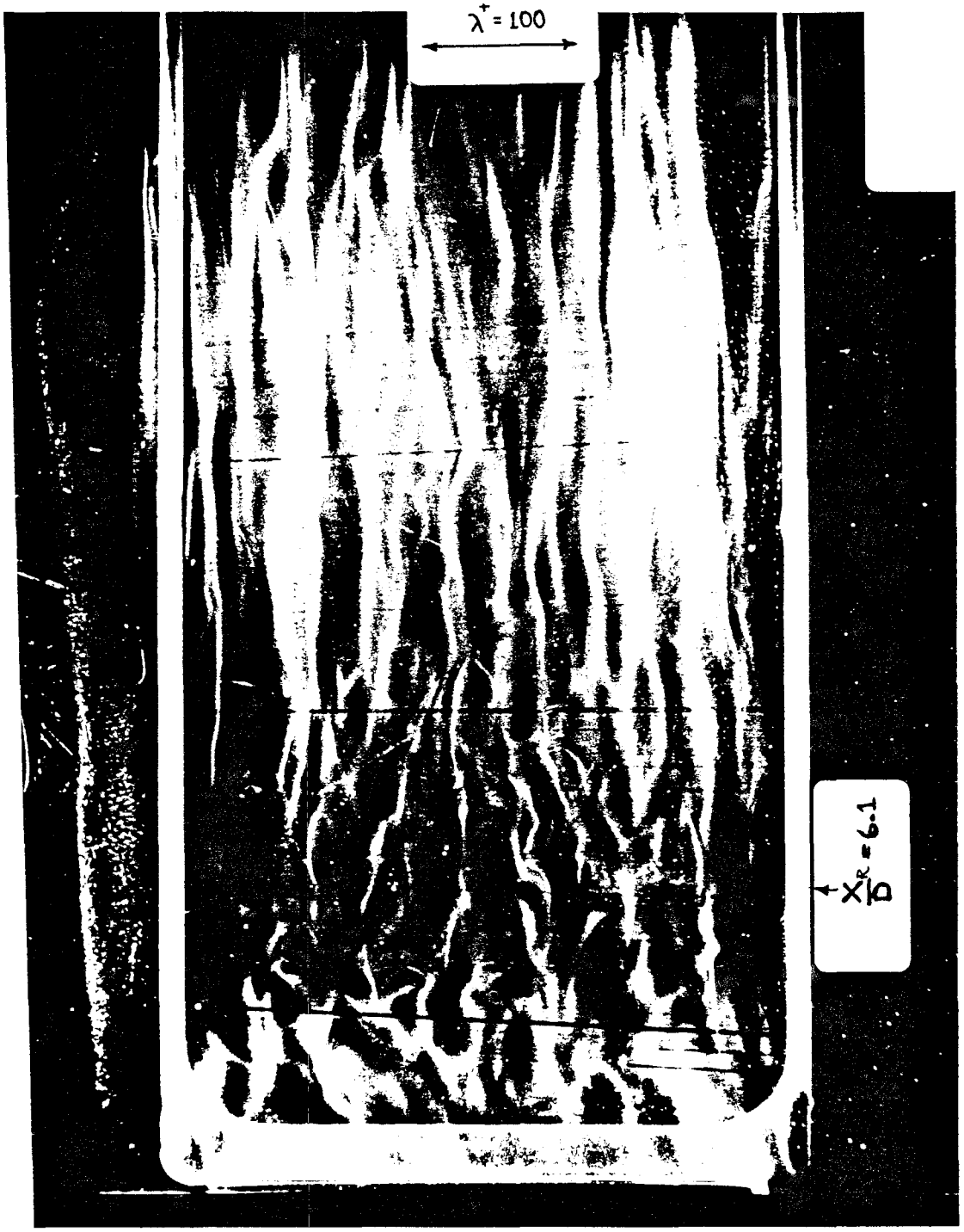

I.2.2.2.2.1 LIF near plate surface $Re_D = 852$

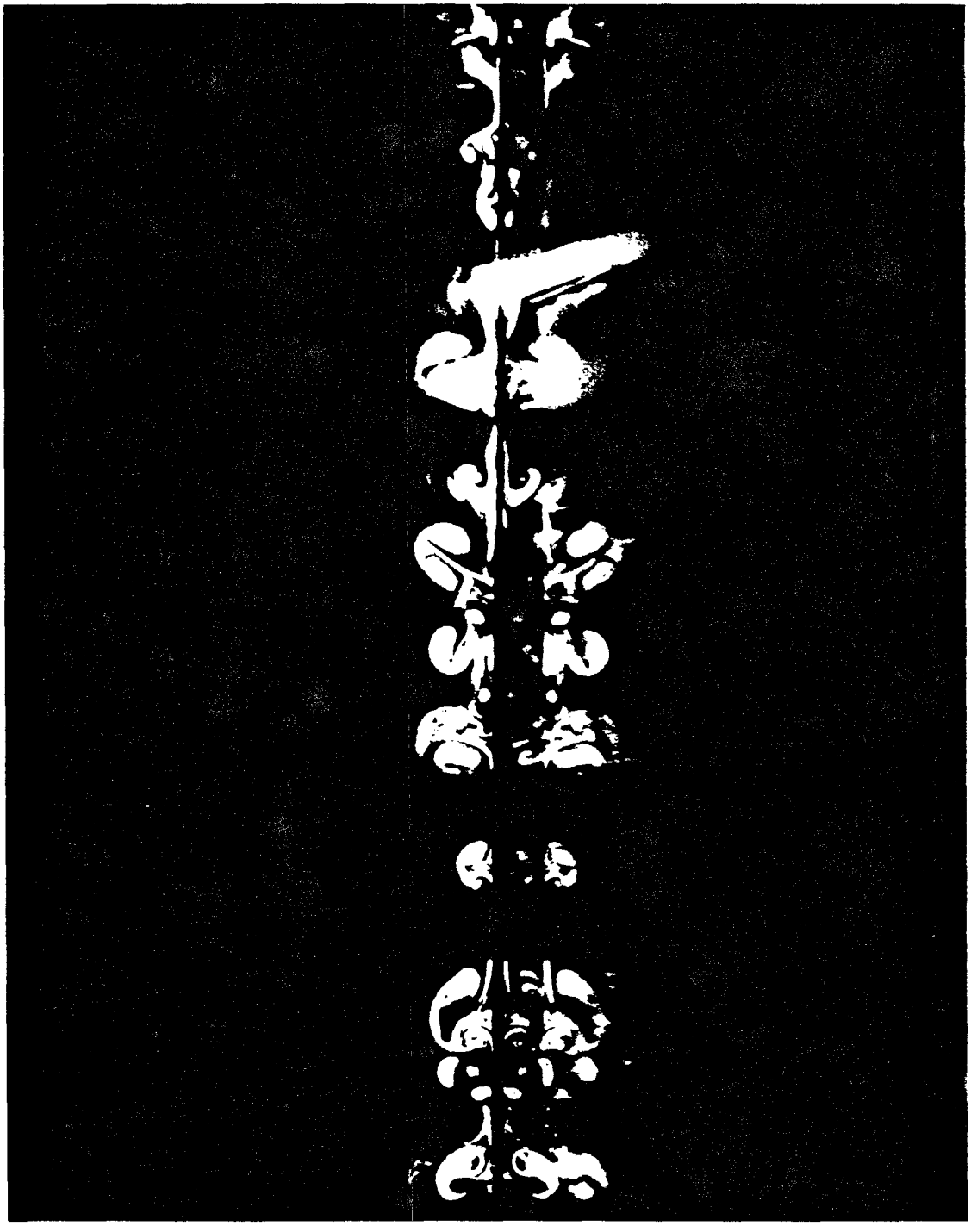

I.2.2.2.2.2.2 LIF upstream view, X/D = 8.3

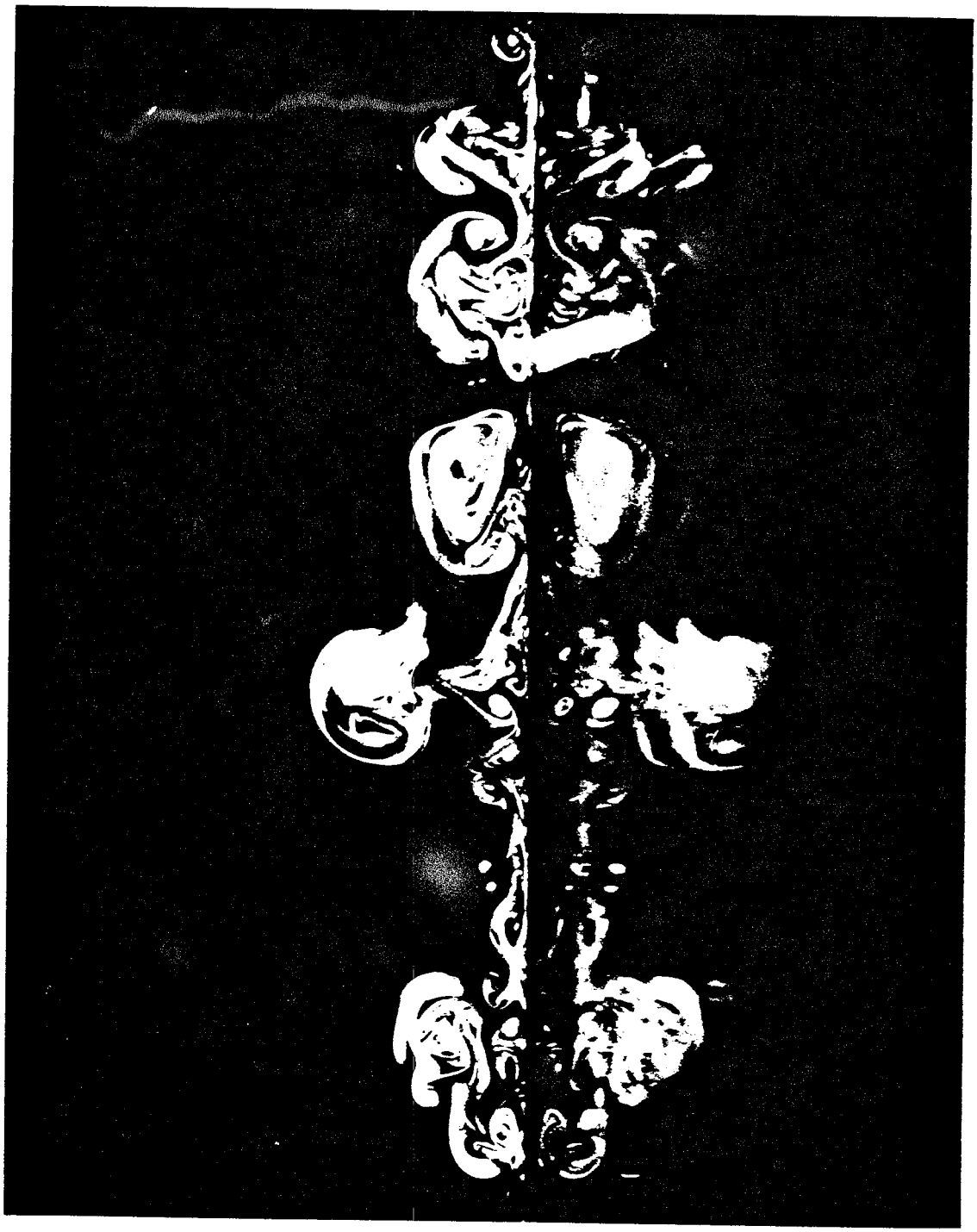

I.2.2.2.2.3 LIF upstream view, X/D = 16.6

I.2.2.2.2.4 LIF plan view, Y/D = 0.9

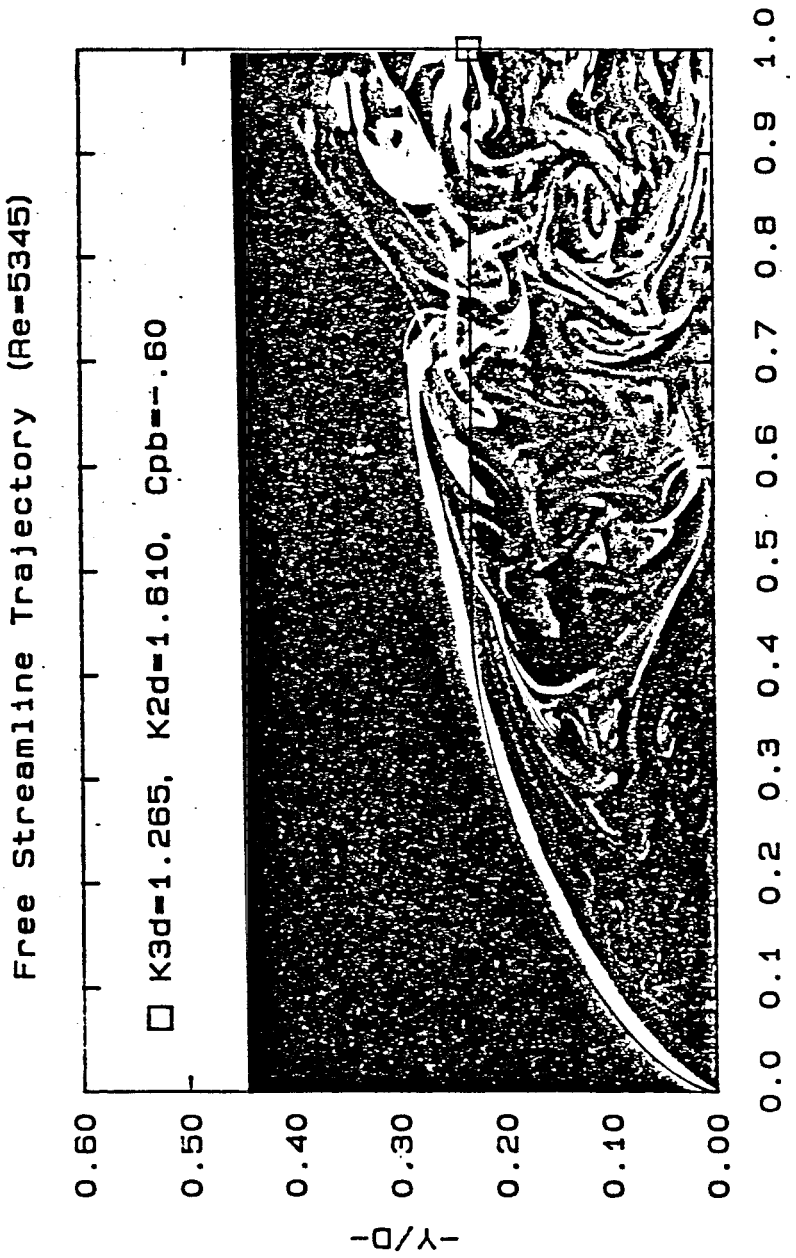

I.4.2.2.1 Free streamline trajectory over a LIF photo

Re_D = 5345

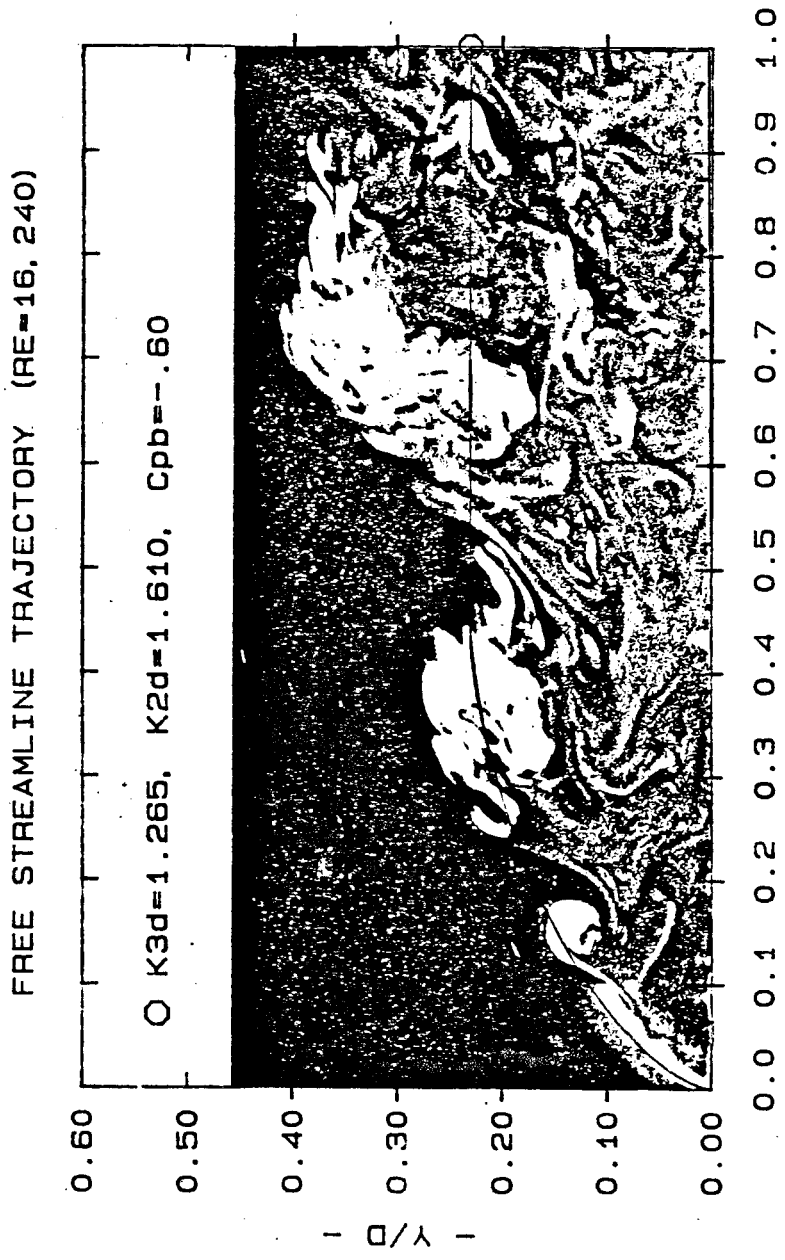

I.4.2.2.2 **Free streamline trajectory over a LIF photo**

Re_D = 16,240

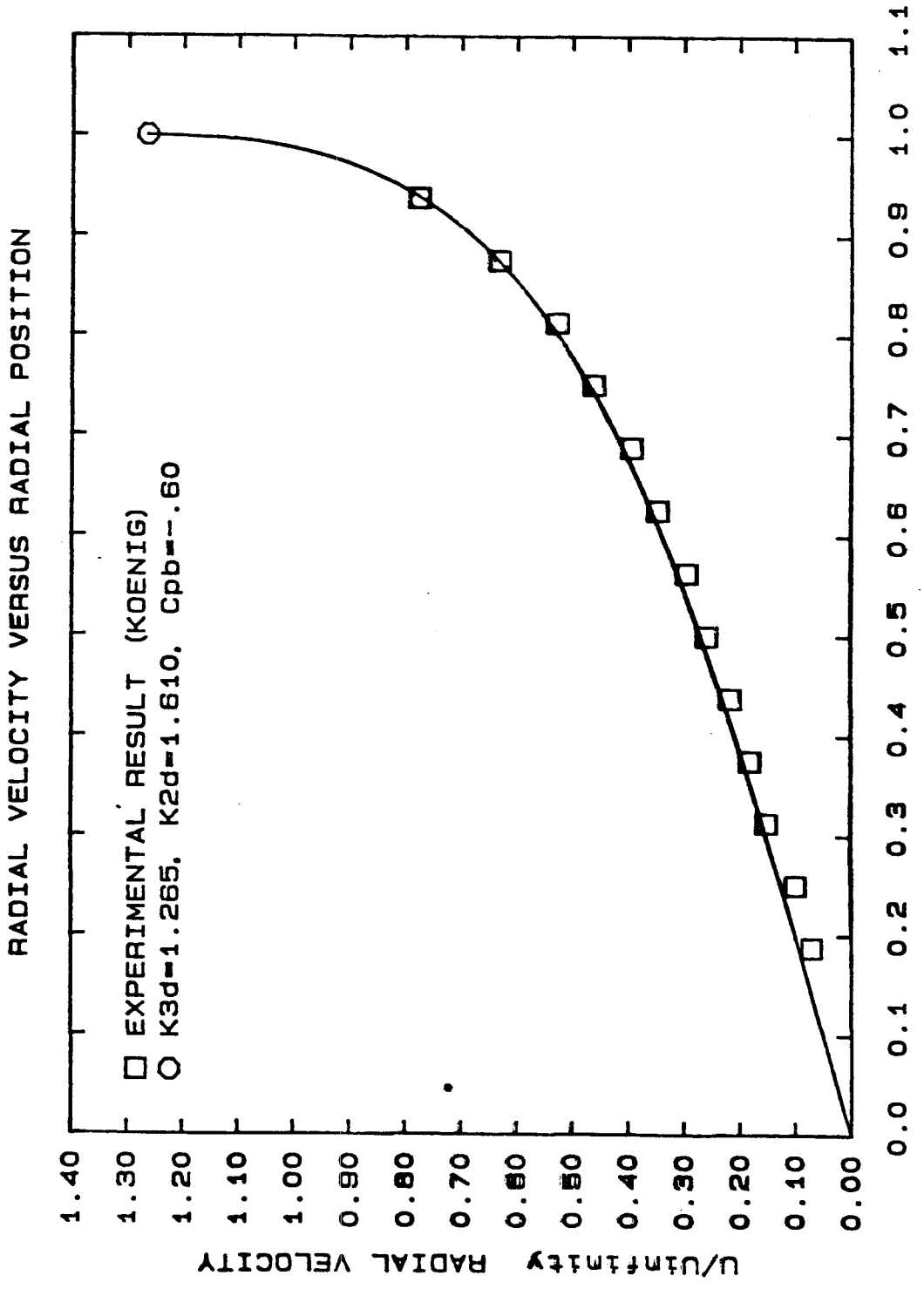

I.4.2.2.3 Radial velocity versus radial position

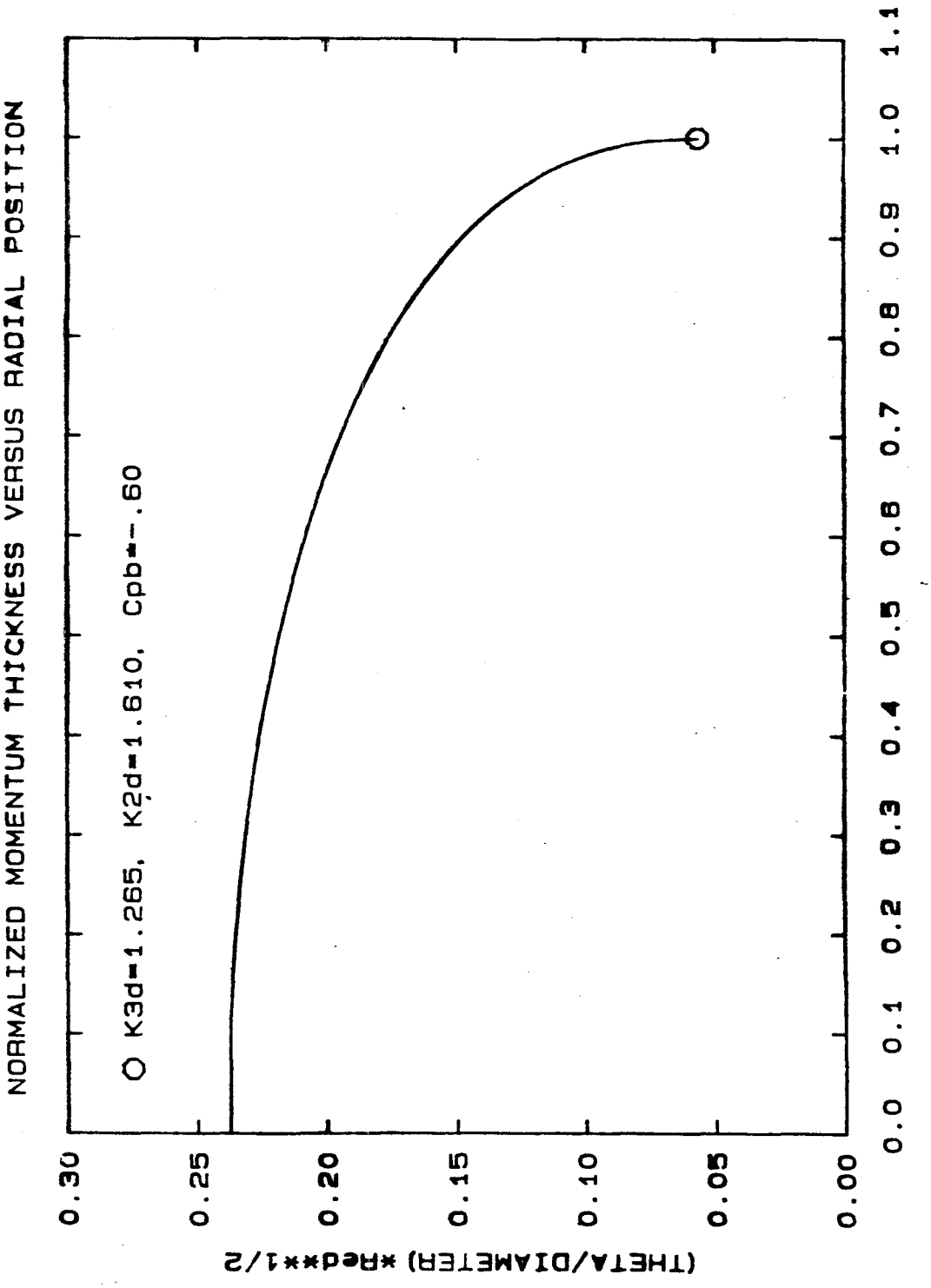

I.4.3.1 Boundary layer thickness on cylinder face

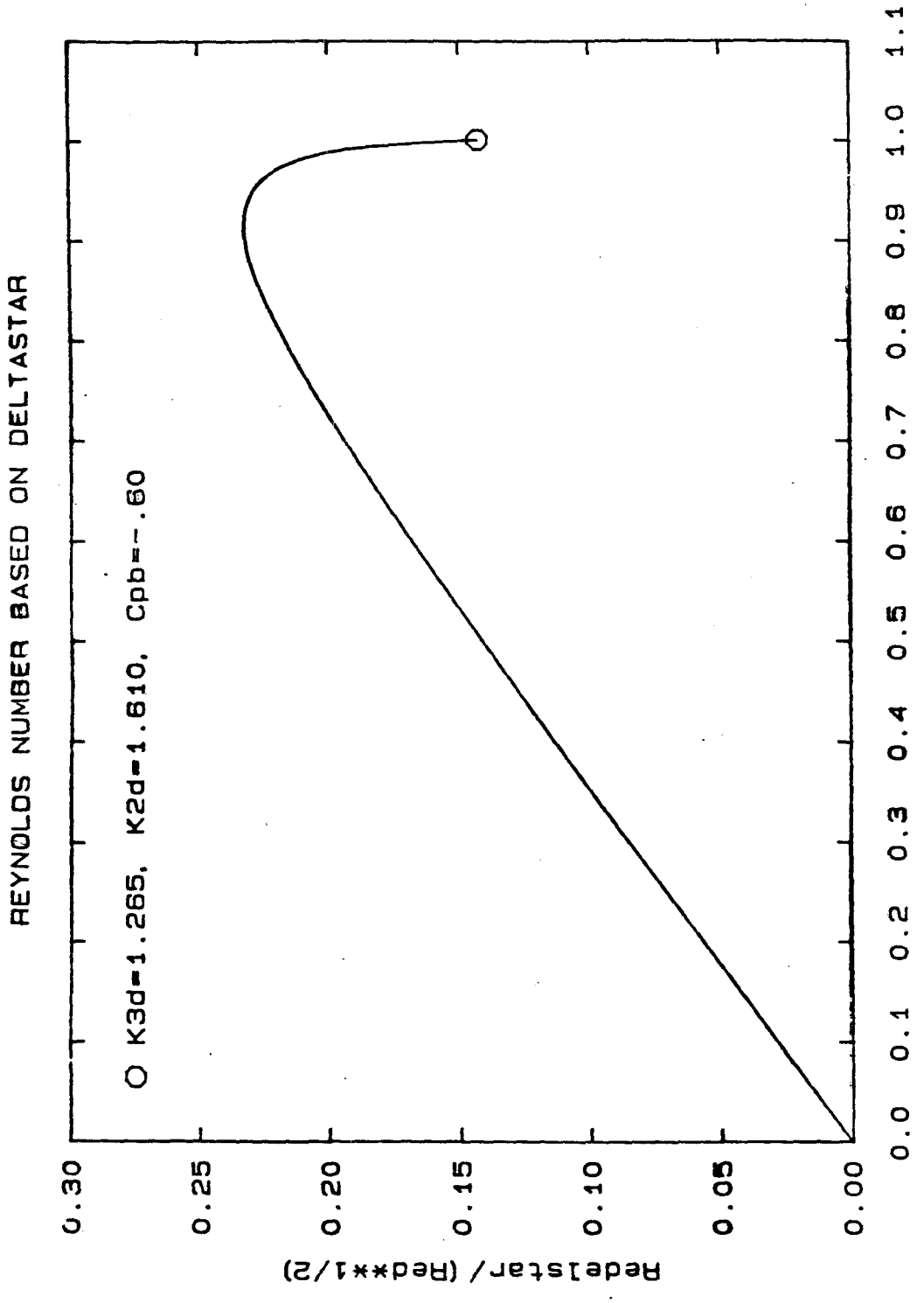
REYNOLDS NUMBER BASED ON DELTASTAR
O K3d=1.265, K2d=1.610, Cpb=-.60
Redelstar/ (Red**1/2)
0.30
0.25
0.20
0.15
0.10
0.05
0.00
0.0 0.1 0.2 0.3 0.4 0.5 0.6 0.7 0.8 0.9 1.0 1.1
r/R RADIAL POSITION
I.4.3.2 Re based on δ*

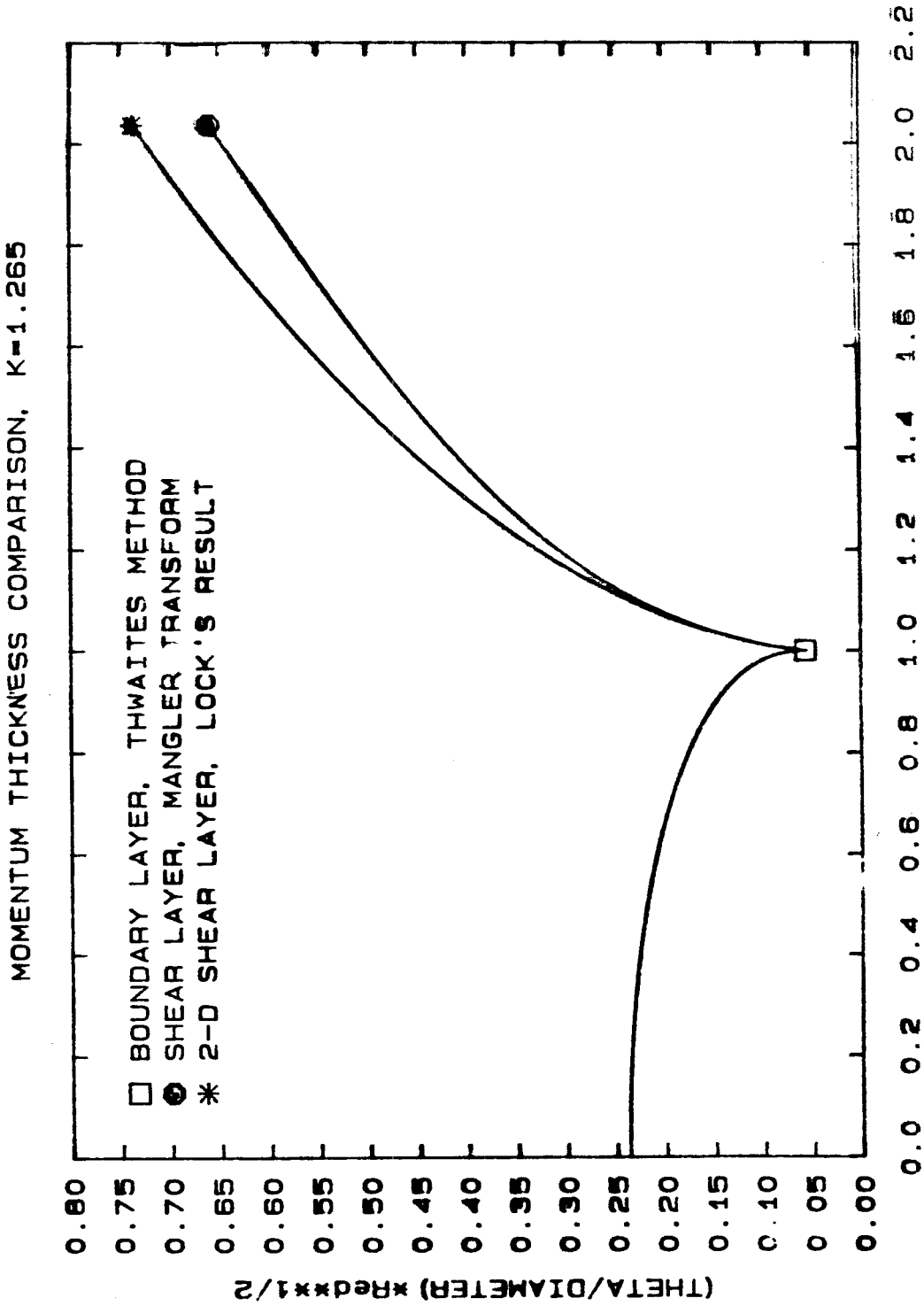

I.4.4.1 Momentum thickness comparison, k = 1.265

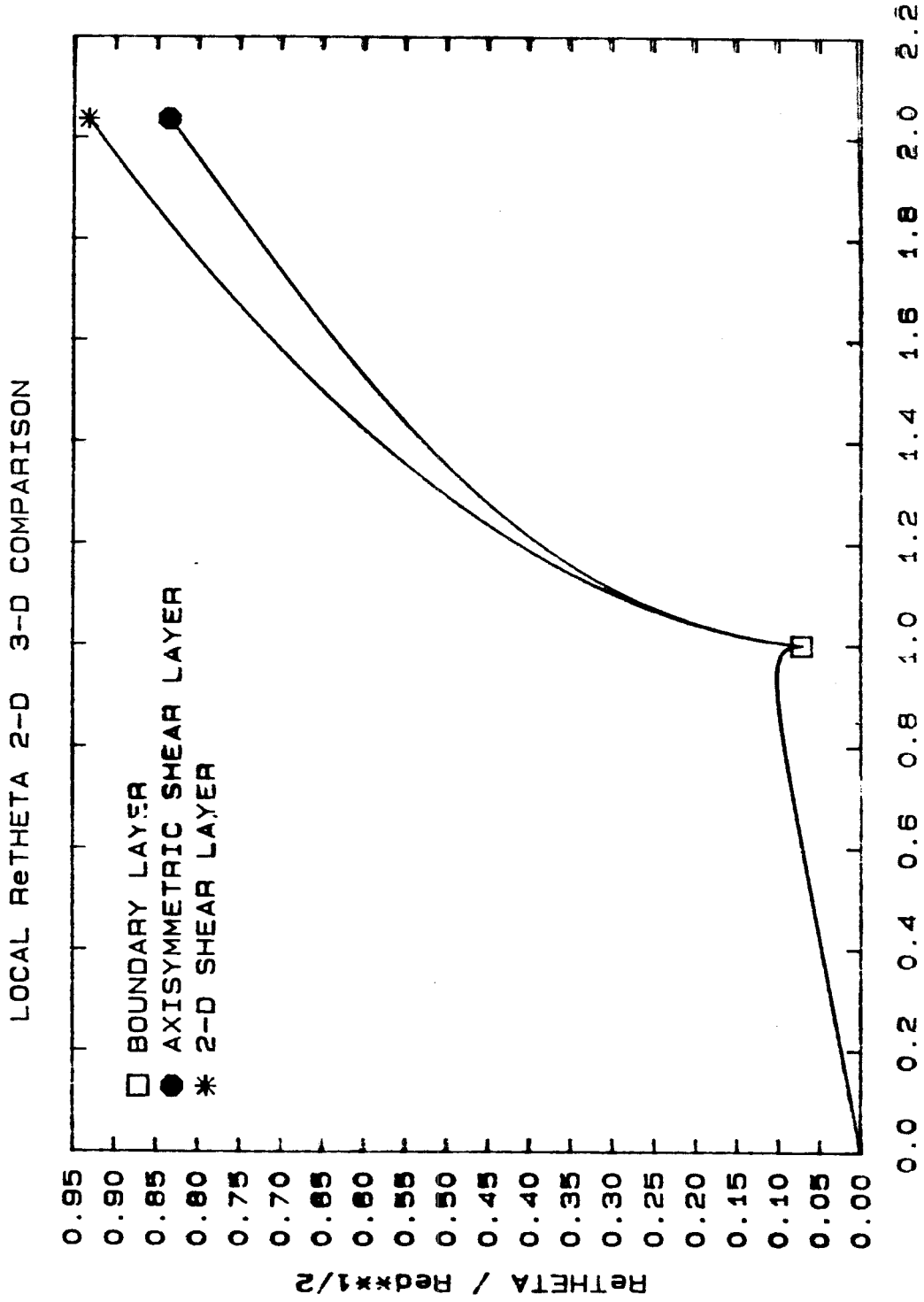

I.4.4.2 Local Re comparison, k = 1.265

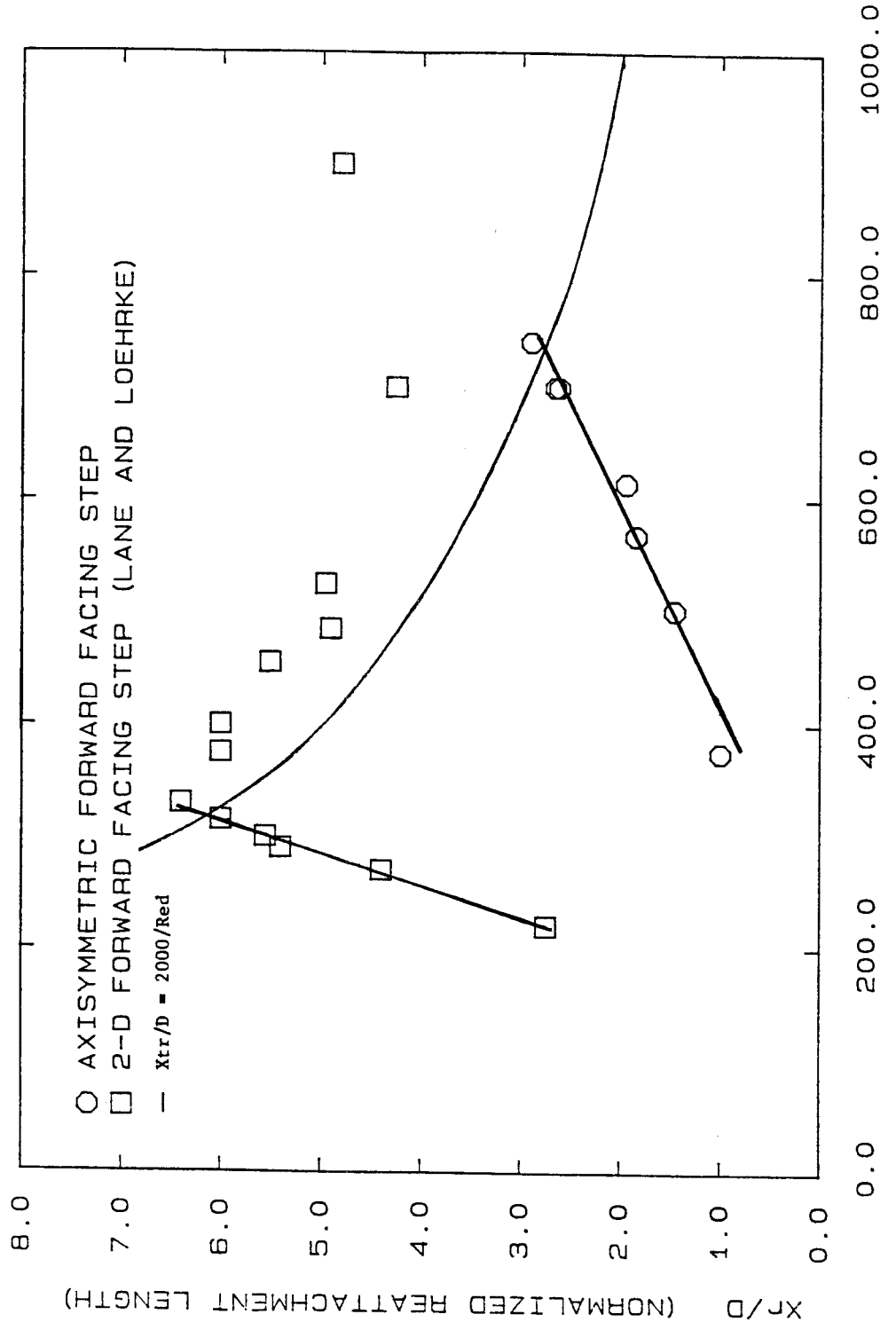

I.4.5.1 Reattachment length versus Re

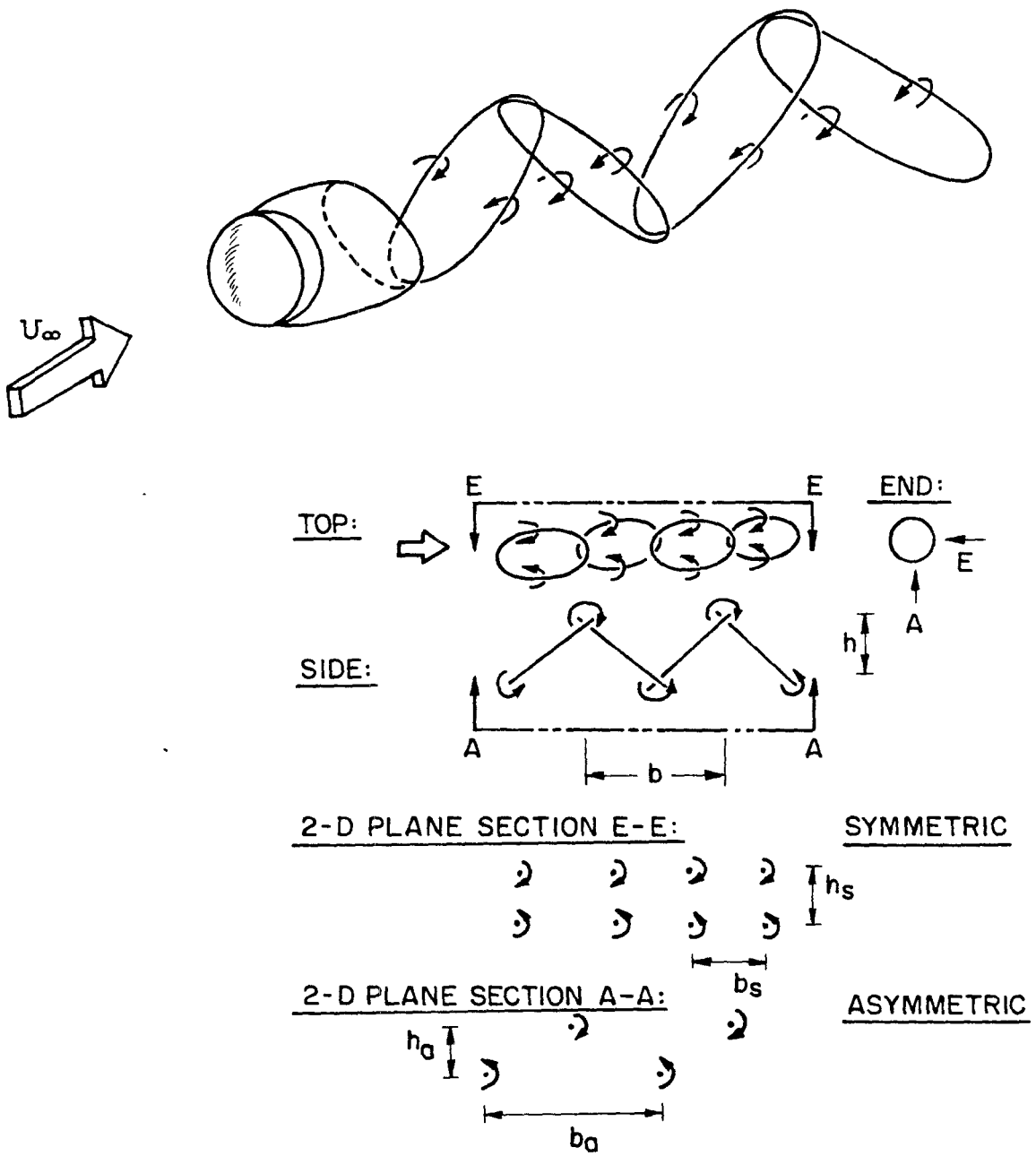

I.5.2.2.1.1 STRUCTURE OF SPHERE SHEDDING

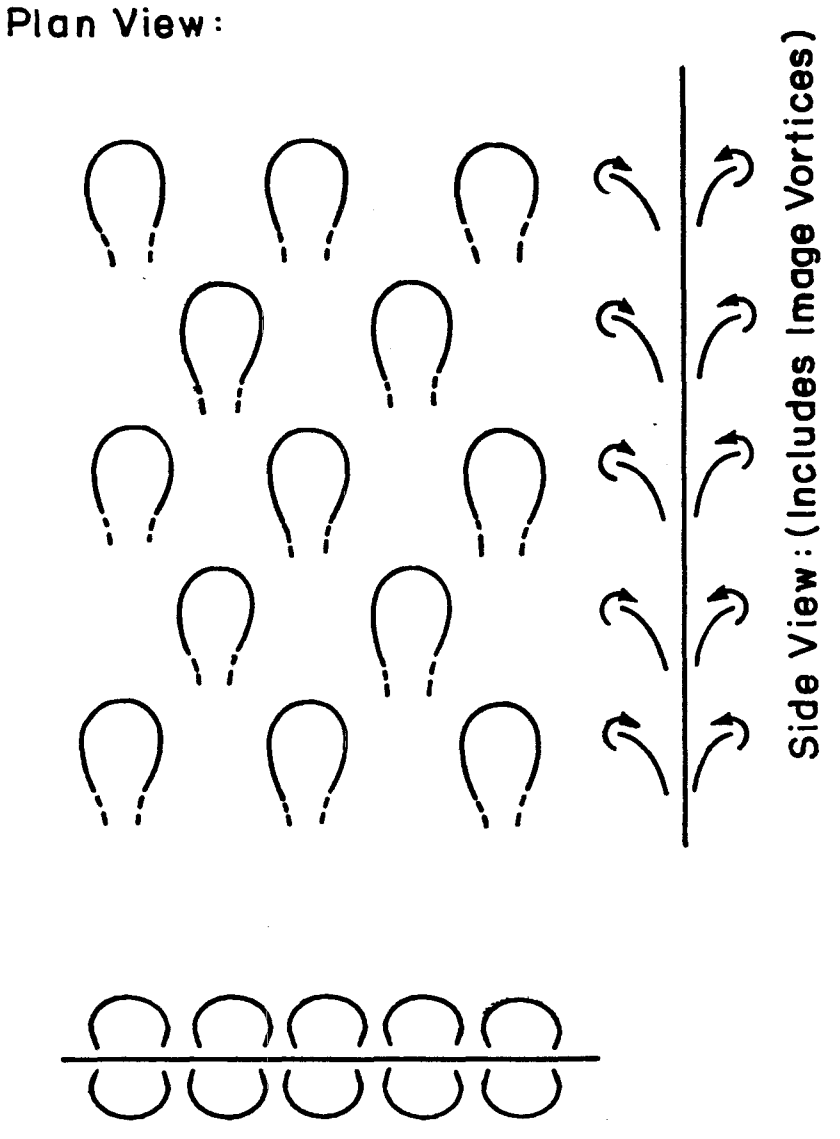

I.5.2.3.1.1 Loops and their images

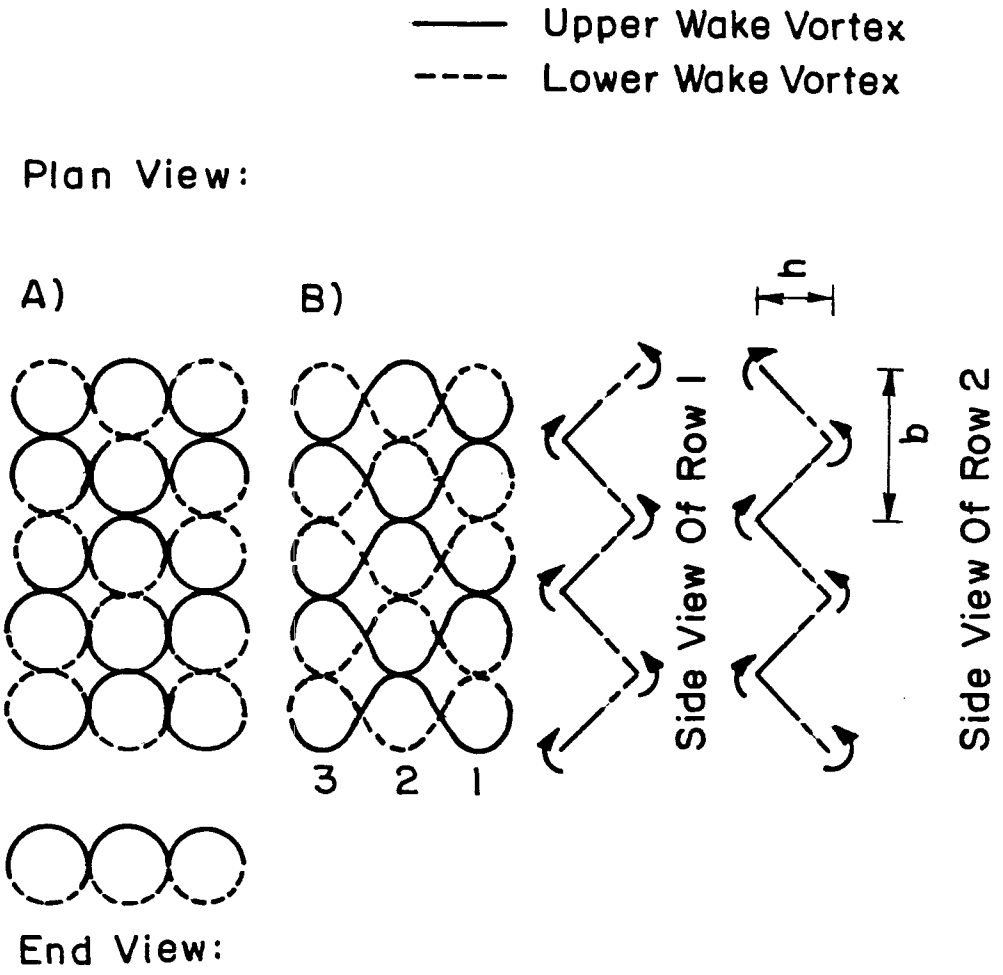

I.5.2.3.2.1 Vortex structure of cylinder wake

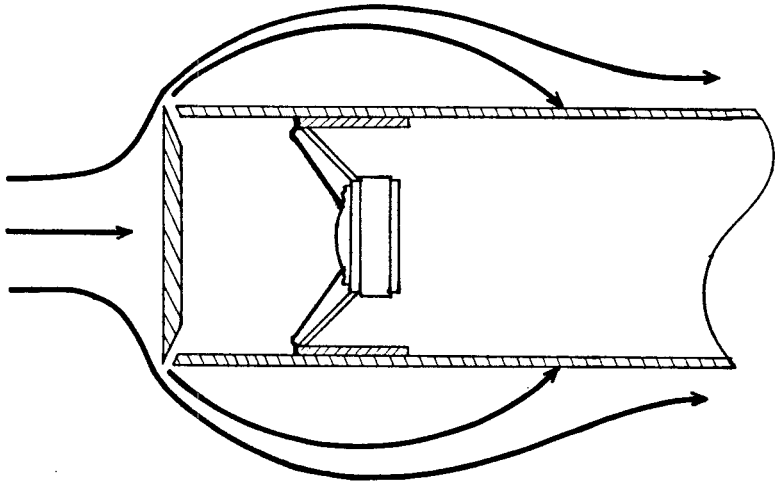

II.1.1 Cross-sectional view of the cylinder.

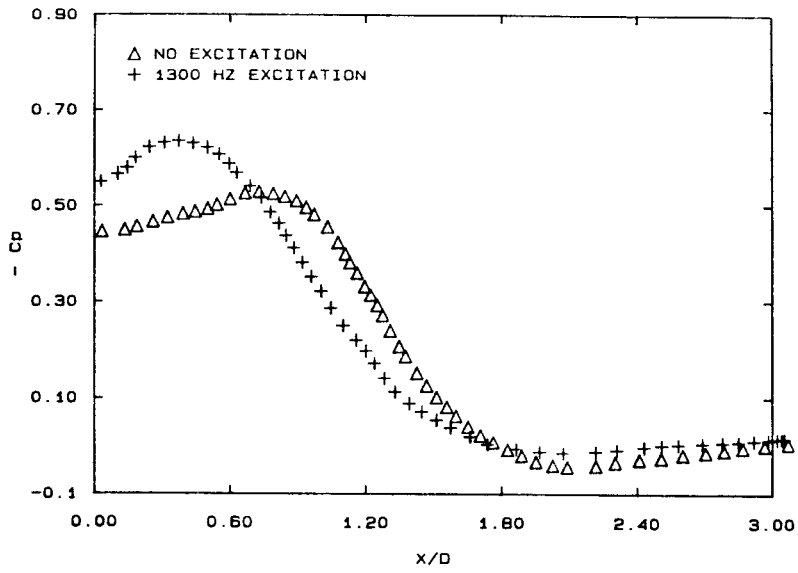

II.3.1 Pressure on the cylinder surface as a function of downstream distance.

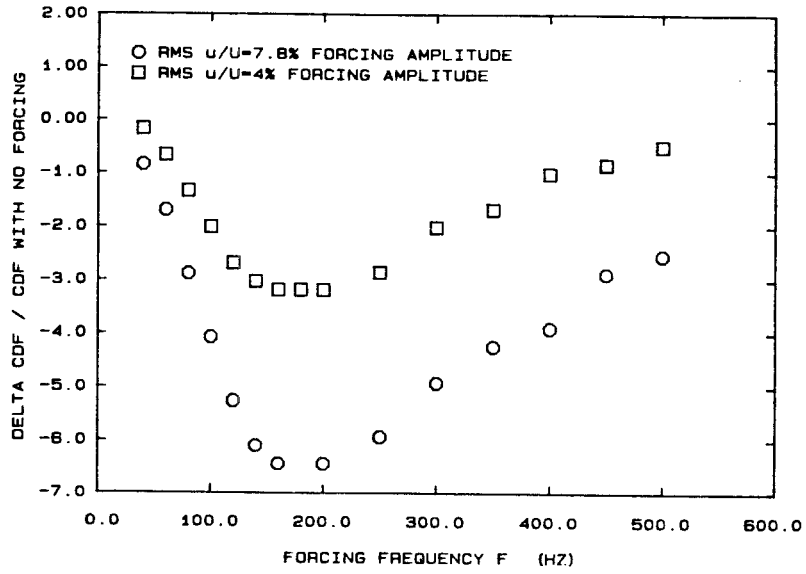

II.3.2 Percent change in pressure drag versus forcing frequency.

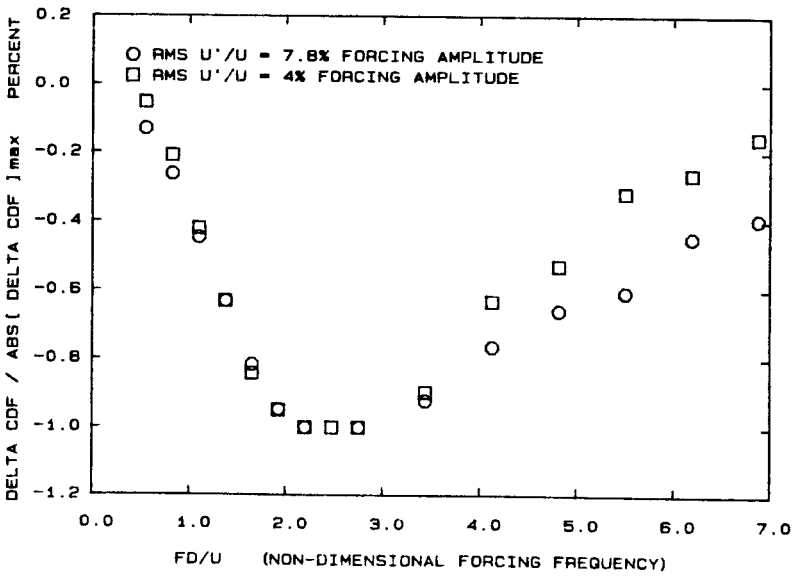

II.3.3 Normalized percent change in pressure drag versus forcing frequency.

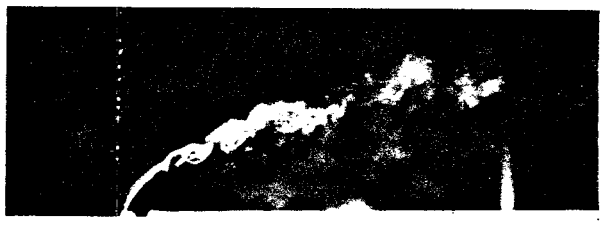

a. $F_{ex}D/U_\infty$ = 0, No excitation.

b. $F_{ex}D/U_\infty$ = 20

c. $F_{ex}D/U_\infty$ = 12

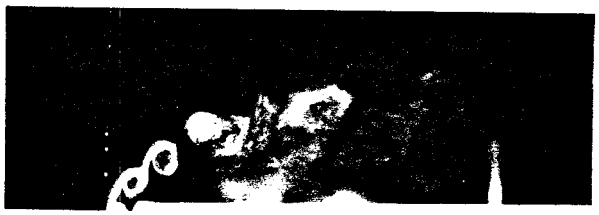

d. $F_{ex}D/U_\infty$ = 8

e. $F_{ex}D/U_\infty$ = 4 ⟵ D/2 ⟶

II.3.2.1 Smoke-wire visualization with varying forcing frequency.
Re_D = 42,400, u'/U_∞ = 23%

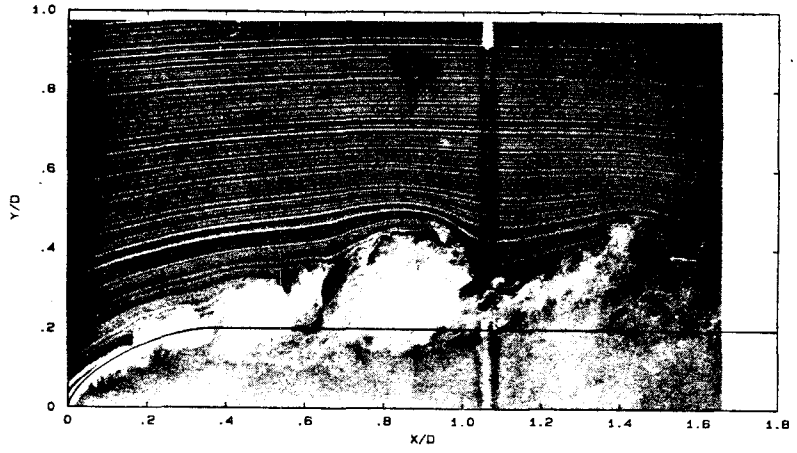

II.3.2.2 Smoke-wire flow visualization, Re_D = 22,000.
a. Unforced.

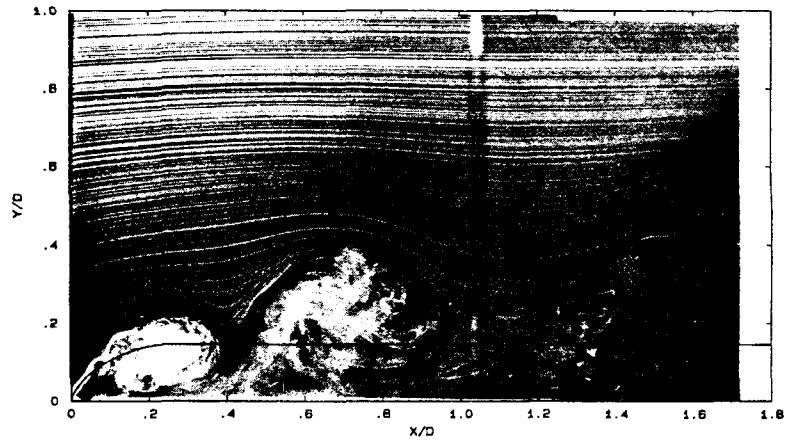

b. Forced, $F_{ex}D/U_\infty$ = 1.64, u'/U_∞ = 12%, $F_{ex}h/U_s$ = .16.

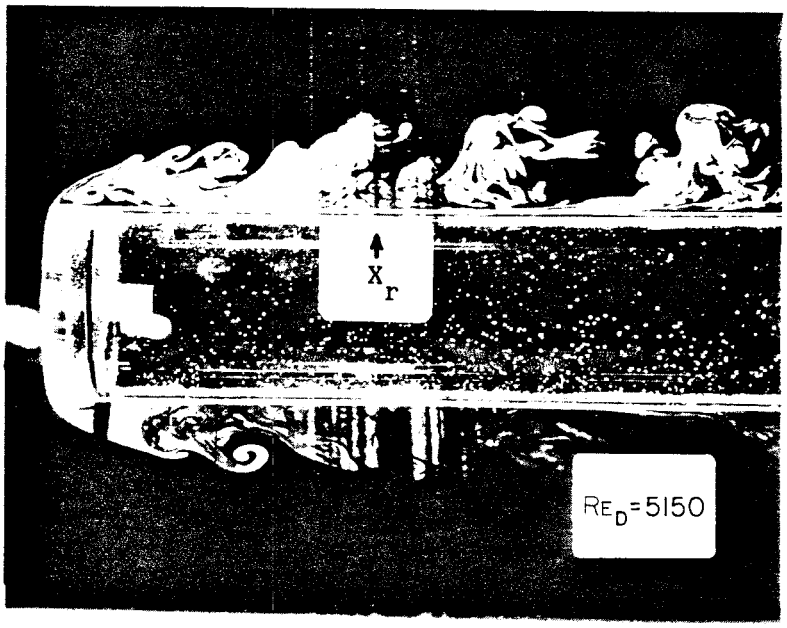

II.4.1.1 Laser induced fluorescence visualization in water, unforced flow.

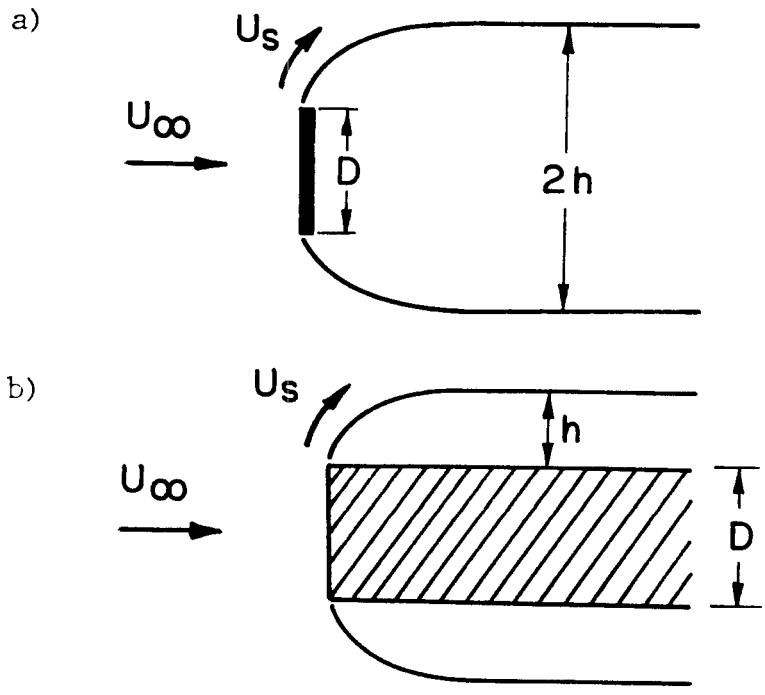

II.4.4.1 Schematic of the free-streamline technique.

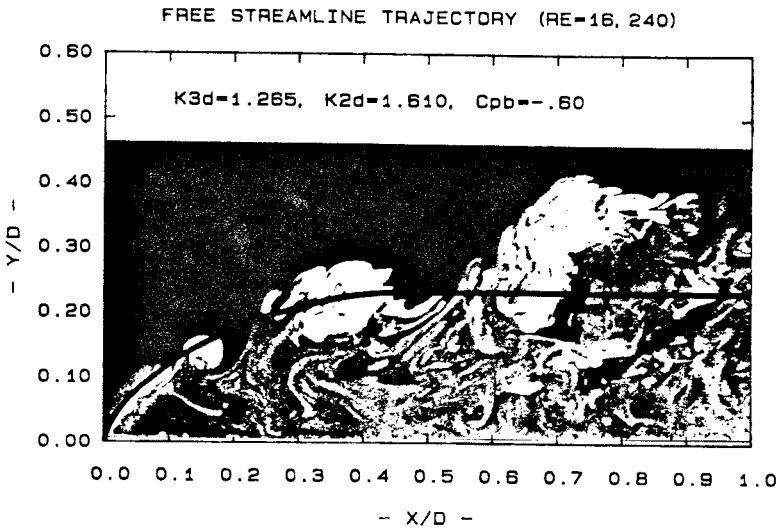

II.4.4.2 Superimposed free-streamline

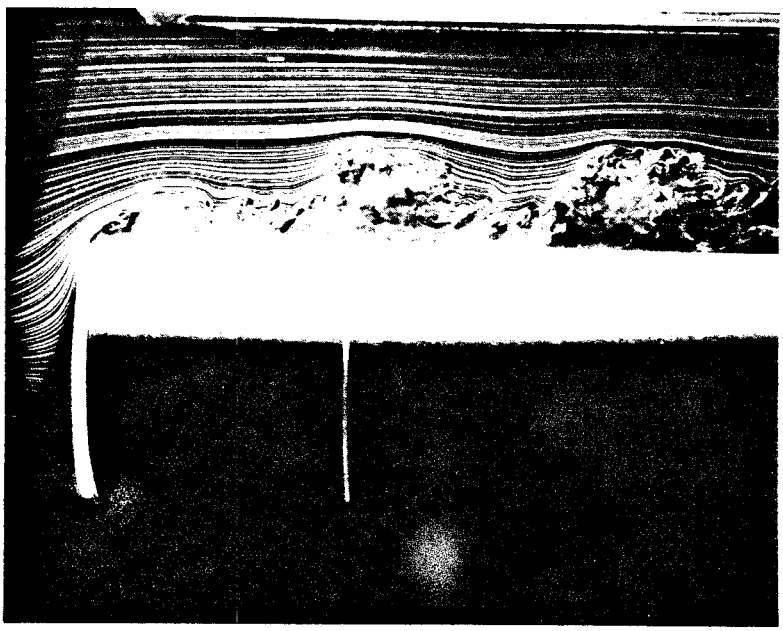

II.4.5.1 Forced case, Re_D = 22,000, $F_{ex}D/U_\infty$ = 1.6, u'/U_∞ = 21%

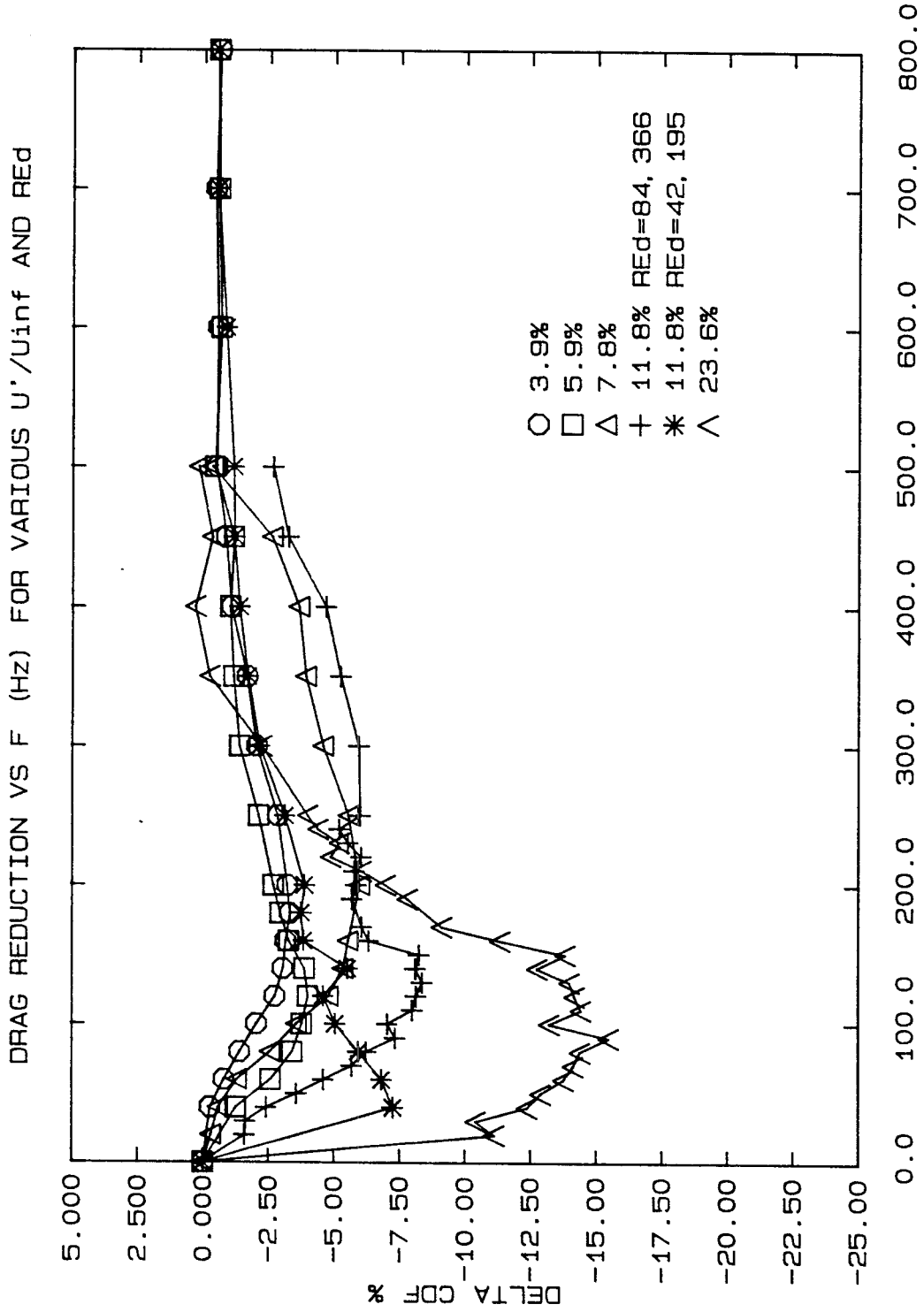

II.4.6.1 **Drag reduction versus F_{ex}**

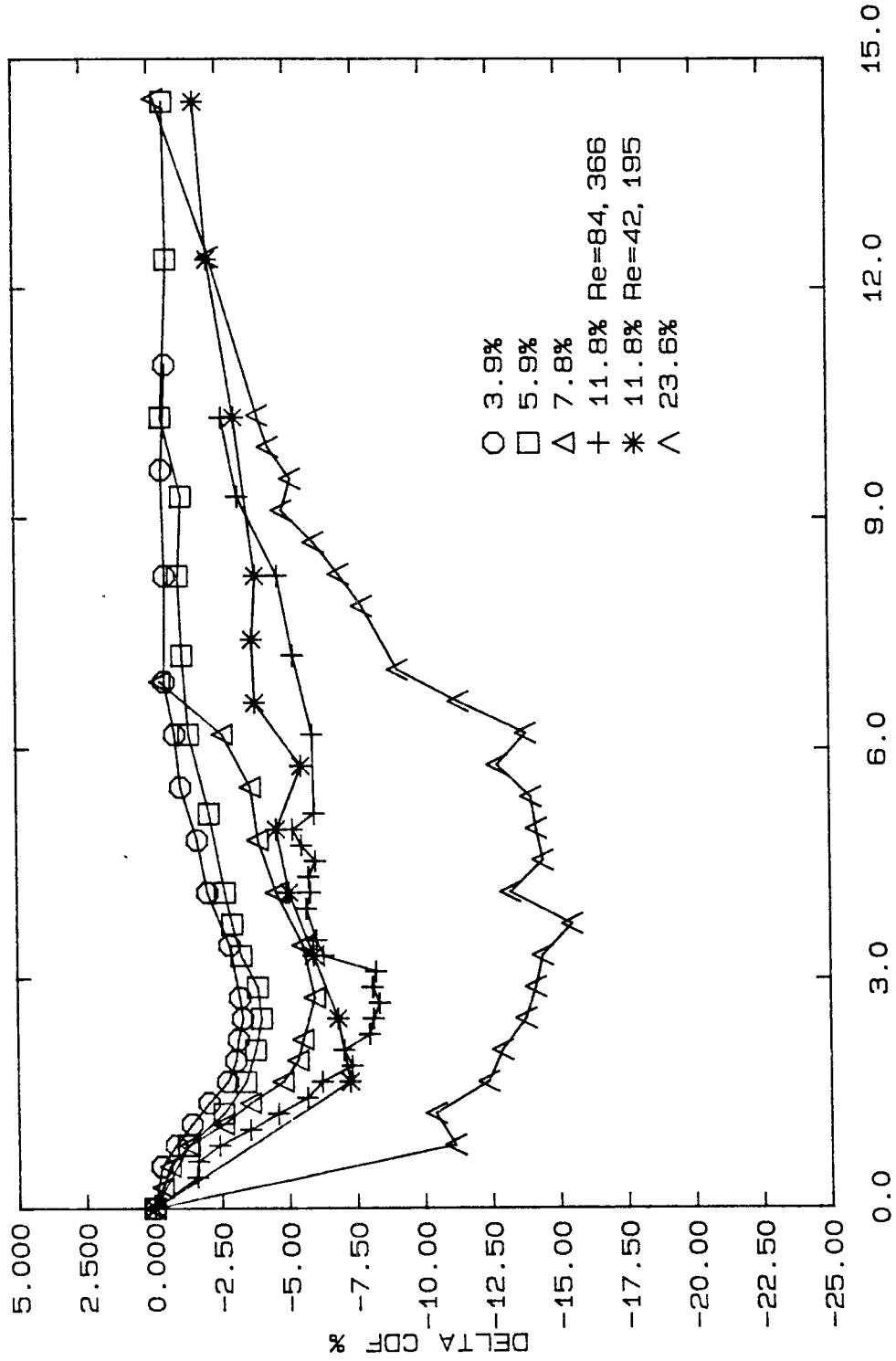

II.4.6.2 **Drag reduction versus $F_{ex}D/U_{\infty}$**

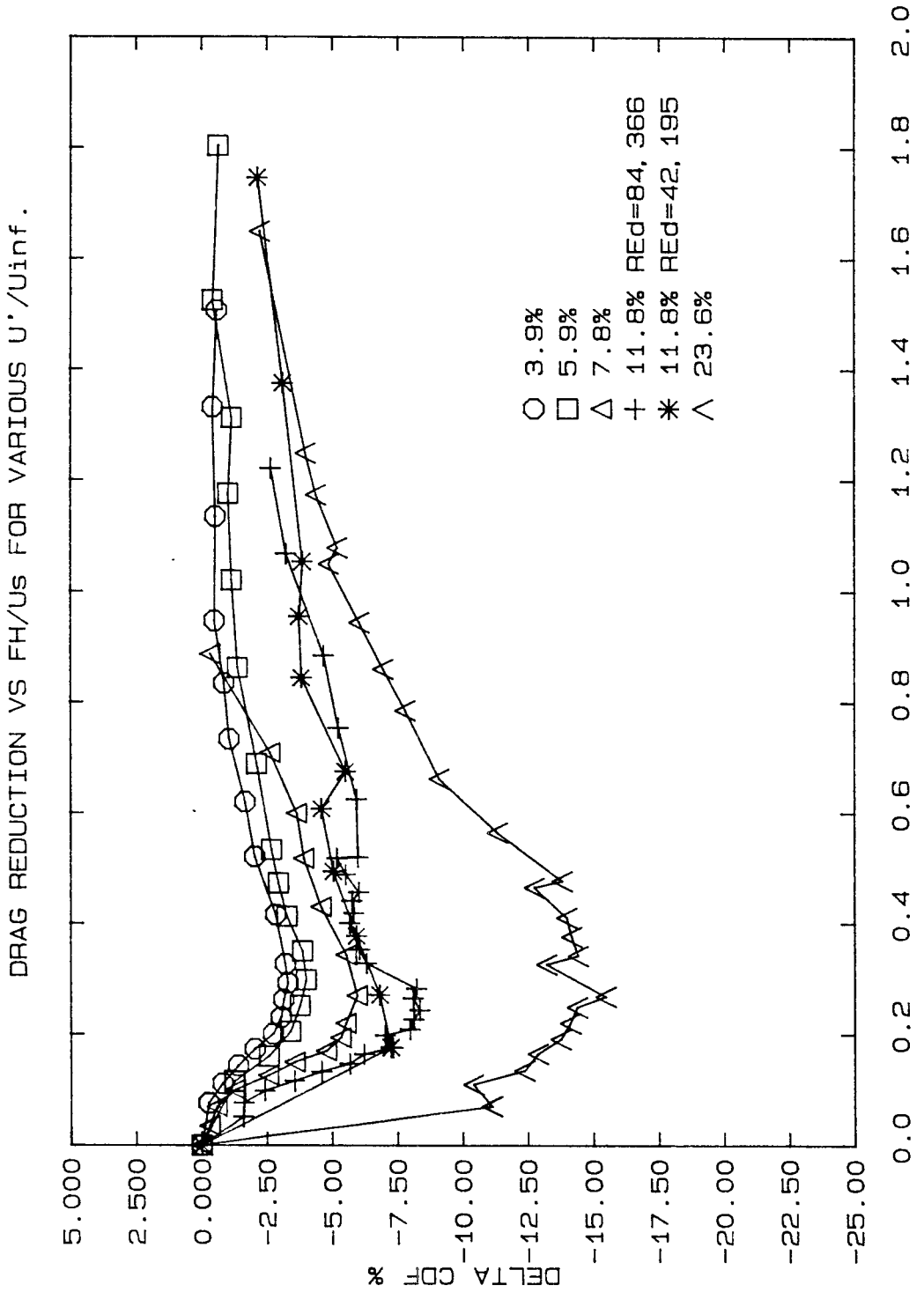

II.4.6.3 Drag reduction versus Fh/U_s

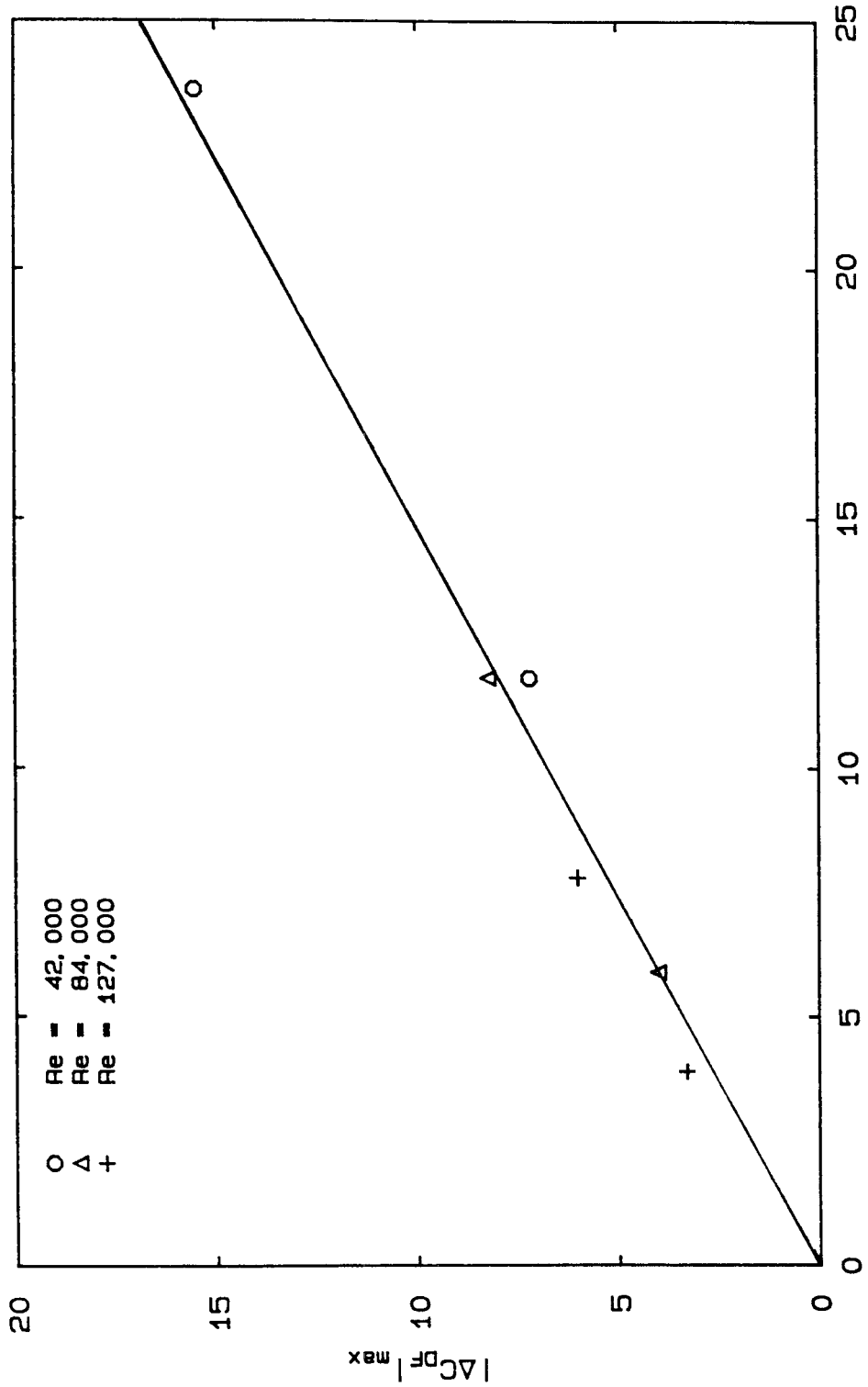

II.4.6.4 Maximum drag reduction versus u'/U_∞

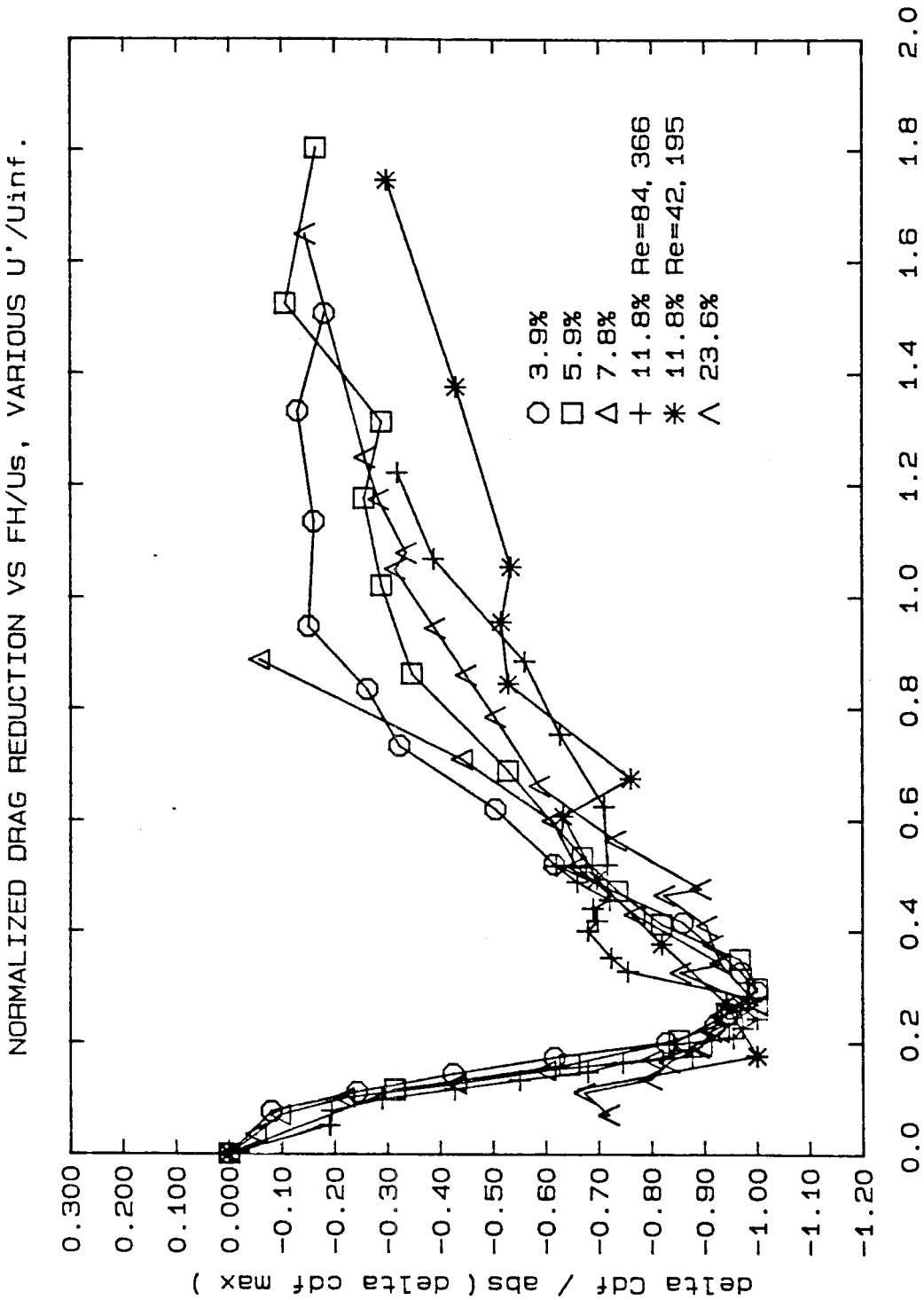

II.4.6.5 **Normalized drag reduction versus Fh/U_s**

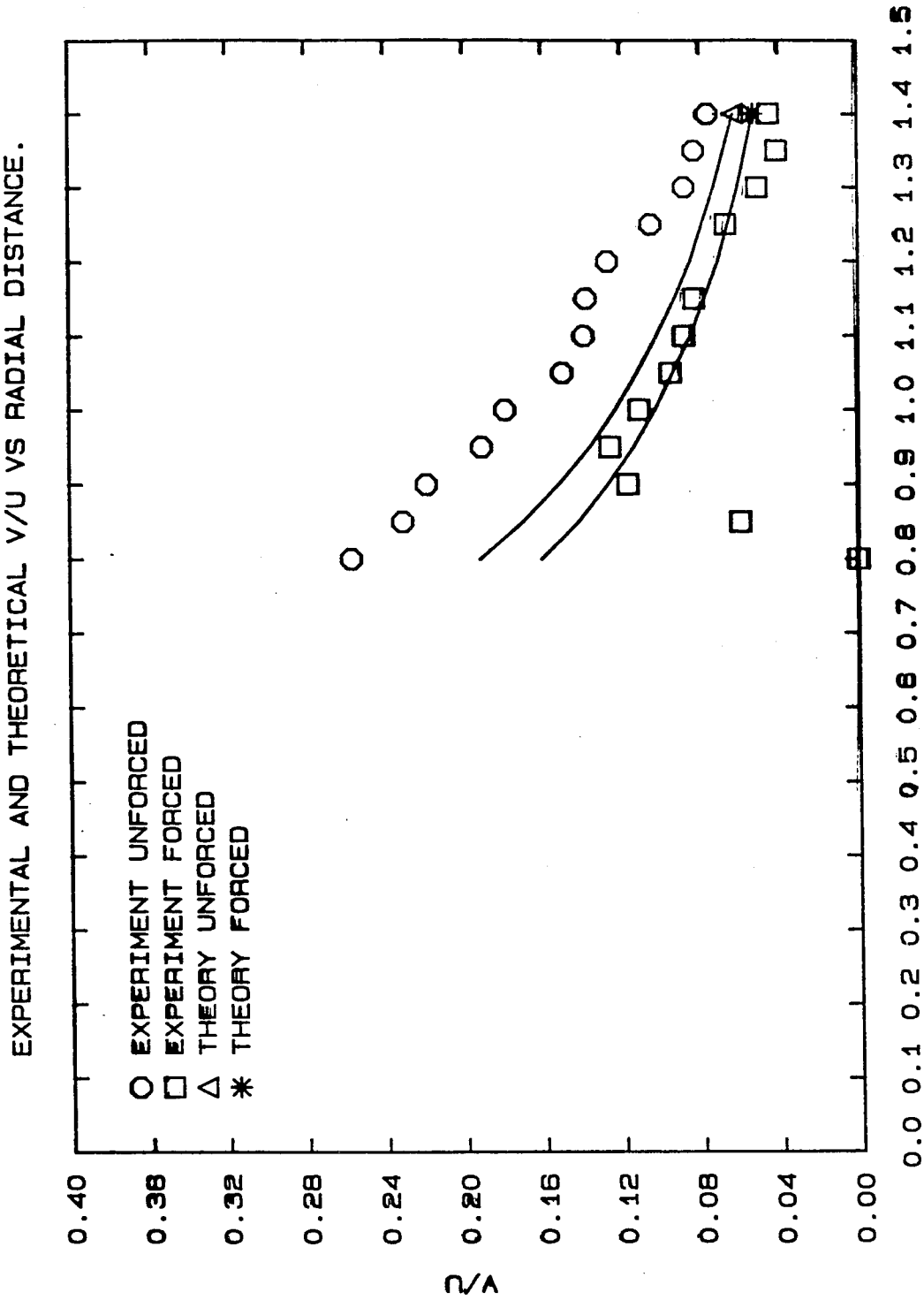

II.4.11.1 v/u versus radial distance